ACKNOWLEDGEMENTS

First and foremost I feel always indebted to ***ALLAH****, the most generous and most merciful.*

I would like to express my deepest gratitude and appreciation to ***Dr. Hassan Ibrahim****, for his kind supervision, continuous encouragement, help, and continuous guidance and for giving me generously of his time.*

Also I would like to thank him for his valuable advices that guided me throughout this work. Most sincere thanks to all members in electric engineering department in the ***Arab academy for science, technology and maritime transport; for their sincere cooperation and assistance.***

Abstract

Solar photovoltaic (PV) systems are distributed energy sources that are an environmentally friendly and renewable source of energy. However, solar PV power fluctuates due to variations in radiation and temperature levels. Furthermore, when the solar panel is directly connected to the load, the power that is delivered is not optimal. A maximum power point tracking (MPPT) is therefore necessary for maximum efficiency.

This thesis presents a study of MPPT for PV system. The study includes discussion of various MPPT algorithms and performs comparative tests of the two MPPT algorithms fuzzy logic controller (FLC) algorithm and the perturbation and observation (P&O) algorithm under varying irradiation and temperature conditions. Some important applications of the MPPT for different loads are described; first the PV system with resistive load is discussed, the modeling and the simulation of the PV module and the DC/DC converter is carried out using MATLAB software.

After that a study of PV water pumping system has been undertaken using DC motor coupling with a centrifugal pump. A comparison between the performance of those systems with and without MPPT in terms of PV total power produced is carried out. Results show that MPPT can very significantly improve the performance of PV system. FLC technique gives better and more reliable control for this application.

Table of Contents Page

Acknowledgements..... I

Abstract..... II

Table of contents..... III

List of tables..... VII

List of figure..... VIII

Nomenclatures..... XII

Chapter (1) Introduction..... 1

1.1 General..... 2

1.2 Overall Trends in Installations and Market..... 3

1.3 Photovoltaic History..... 4

1.4 Architecture of Photovoltaic System..... 5

1.4.1 Advantage and Disadvantage of Photovoltaic System..... 6

1.4.2 Theory of Operation..... 6

1.4.3 Types of Solar cell..... 7

1.4.3.1 Monocrystalline Solar Panels..... 7

1.4.3.2 Polycrystalline Solar Panels..... 8

1.4.3.3 Thin film Panels..... 8

1.4.4 Balance of Systems (BOS)..... 8

1.4.5 Types of Connection Photovoltaic System..... 8

1.4.6 Photovoltaic Array Characteristics..... 10

1.5 MPPT System 10

1.6 Literature Review of MPPT Control Algorithms..... 11

1.6.1 Fractional Open Circuit Voltage..... 12

1.6.2 Fractional Short Circuit Current..... 13

1.6.3 Neural Networks..... 13

1.6.4 Current Sweep..... 14

1.6.5 Array Reconfiguration Method..... 14

1.6.6 β Method..... 15

1.6.7 Look-up Table Method..... 15

1.6.8 Maximum power point current and voltage computation..... 15

1.6.9 Incremental Conductance..... 16

1.6.10 P&O Method..... 16

Table of Contents (Cont'd)

1.6.11 FLC Method..... 16

1.7 Scope of Thesis..... 18

1.8 Organization of Thesis..... 18

Chapter (2) Modeling of Photovoltaic..... 19

2.1 Introduction..... 20

2.2 Solar Cell Modeling..... 20

2.2.1 Simplest Model..... 20

2.2.2 More Accurate Model..... 22

2.2.2.1 PV Series Resistance..... 22

2.2.2.2 PV Parallel Resistance..... 23

2.2.2.2 Recombination..... 23

2.3 PV Module Modeling..... 25

2.4 PV Array Modeling..... 25

2.5 Modeling a PV Module by MATLAB..... 26

2.5.1 The light-generated current..... 27

2.5.2 Diode reverses saturation current..... 28

2.5.3 Series and parallel resistance..... 28

2.6 Factors Affecting the Photovoltaic characteristic..... 30

2.6.1 Temperature effect..... 30

2.6.2 Irradiance effect..... 30

2.6.3 Shading effect..... 31

2.6.4 Reflection effect..... 32

2.7 KC200GTS PV Module and Array Electrical Characteristics..... 32

Chapter (3) Maximum Power Point Tracker..... 37

3.1 Introduction..... 38

3.2 Direct coupling of PV system..... 39

3.2.1 Resistive-Load Connection..... 39

3.3 DC/DC Converter..... 41

3.3.1 Boost Converter..... 41

3.3.2 Steady State Analysis..... 44

3.3.3 Continuous and discontinuous current mode..... 46

3.4 Mechanism of Load Matching..... 46

Table of Contents (Cont'd)

3.5 Pulse Width Modulation..... 48

3.6 PV Water Pumping System..... 48

3.6.1 System Configuration..... 49

3.6.2 DC motor & pump characteristic..... 50

Chapter (4) Fuzzy and P&O Algorithms..... 51

4.1 Introduction..... 52

4.2 Advantage and Disadvantage of Use Fuzzy Logic..... 52

4.3 Fuzzy logic Application Areas..... 53

4.4 Classical Sets versus Fuzzy Sets..... 53

4.4.1 Membership Function..... 54

4.5 Basic Operations..... 56

4.5.1 Complement (NOT)..... 56

4.5.2 Intersection (AND)..... 56

4.5.3 Union (OR)..... 57

4.6 linguistic variables..... 57

4.7 FLC Structure..... 58

4.7.1 FUZZIFICATION..... 58

4.7.2 Fuzzy Rule Base..... 59

4.7.1.2 Fuzzy Inference Engine..... 61

4.7.3 Defuzzification..... 63

4.7.3.1 Centroid Method..... 63

4.8 FLC MPPT..... 64

4.8.1 FUZZIFICATION MPPT..... 65

4.8.2 Fuzzy Inference Engine MPPT..... 66

4.8.3 Defuzzification MPPT..... 66

4.9 P&O MPPT..... 67

Chapter (5) Simulation and Results..... 70

5.1 Simulation results..... 71

5.2 Simulation of Resistive load under Varying Irradiance..... 72

5.3 Simulation of Resistive load under Varying Temperature..... 76

5.4 Simulation of DC Motor Pump under Varying Irradiance..... 79

5.5 Simulation of DC Motor Pump under Varying Temperature..... 84

Table of Contents (Cont'd)

Chapter (6) Conclusion and Future Scope..... 88

6.1 Conclusion..... 89

6.2 Future work..... 90

Publication..... 91

Reference..... 92

Appendix..... 96

List of Tables

Table No.	Title	Page
1.1	Major characteristics of different MPPT techniques	17
4.1	The canonical form for a fuzzy rule base	59
4.2	FLC Rules base	66

List of Figures

Figure No.	Caption	Page
1.1	solar PV existing world capacity 1996-2011	4
1.2	Illustrated photovoltaic system	5
1.3	PV cell showing hole-electron pairs created by photons	7
1.4	Classification of PV systems	9
1.5	I-V, P-V characteristics of photovoltaic cell	10
1.6	MPPT system	11
2.1	equivalent circuit for simplest PV cell	21
2.2	PV are I_{sc} and V_{oc} connection	21
2.3	Equivalent Circuit for Double Exponential PV model	23
2.4	Equivalent Circuit Single Exponential PV model	24
2.5	(a) Array of Nser modules connected in series, (b) Array of Npar modules connected in parallel, (c) Array composed of Nser x Npar modules	26
2.6	Picture of KC200GTS PV module	27
2.7	Circuit model of the photovoltaic module by MATLAB	29
2.8	Circuit model of the photovoltaic array by MATLAB	29
2.9	an array with 6 modules with bypass diodes	31
2.10	I-V Characteristics of PV module at constant temperature and varying irradiance	33
2.11	P-V Characteristics of PV module at constant temperature and varying irradiance	33
2.12	P-V Characteristics of PV module at varying temperature and constant irradiance	34
2.13	I-V Characteristics of PV module at varying temperature and constant irradiance	34
2.14	I-V Characteristics of PV array at constant temperature and varying irradiance	35
2.15	P-V Characteristics of PV array at constant temperature and varying irradiance	35
2.16	P-V Characteristics of PV array at varying temperature and constant irradiance	36

List of Figures (Cont'd)

2.17	I-V Characteristics of PV array at varying temperature and constant irradiance	36
3.1	sun tracking PV panel	38
3.2	intersection point of the I-V curves for the load and PV	39
3.3	direct connection of PV to variable resistive load	40
3.4	PV system operating points with varying resistive loads	40
3.5	fixed load connected to PV at varying irradiance	41
3.6	switching period	42
3.7	circuit diagram of boost converter	42
3.8	boost converter when switch is on	43
3.9	boost converter when switch is off	43
3.10	output waveform of boost converter	45
3.11	the impedance seen by PV is R_{in} that is adjustable by duty cycle	47
3.12	load resistance with and without boost converter	47
3.13	PWM diagram	48
3.14	water pumping system with MPPT	49
4.1	fuzzy and classical sets	54
4.2	Different shapes of membership functions (a) triangular, b) Trapezoidal, (c) Gaussian, (d) Generalized bell	55
4.3	Complement of fuzzy sets A	56
4.4	Intersection of fuzzy sets A and B	56
4.5	Union of fuzzy sets A and B	57
4.6	Universe of discourse for linguistic variable: temperature	57
4.7	Basic parts of a Fuzzy Controller	58
4.8	max-min Mamdani Model Example	62
4.9	example of Centroid Method	63
4.10	fuzzy MPPT input and output variables	64
4.11	Membership function of E, CE	65
4.12	Membership function U	66
4.13	P-V curve of KC200GTS PV module at 1000 W/m^2 and 25^oC	67
4.14	P&O flowchart	68
4.15	Divergence P&O from MPP	69

List of Figures (Cont'd)

5.1	simulink of PV array direct coupled to Dc motor pump load	71
5.2	simulink of PV MPPT system with DC motor pump load	72
5.3	changing irradiance at 25^{o}C for resistive load	72
5.4	PV output power under changing irradiance at 25^{o}C for resistive load	73
5.5	performance of MPPT of PV output power under fixed irradiance at 25^{o}C for resistive load	74
5.6	duty cycle of converter under changing irradiance at 25^{o}C for resistive load	74
5.7	resistive load voltage under changing irradiance at 25^{o}C	75
5.8	resistive load current under changing irradiance at 25^{o}C	75
5.9	changing temperature at 800 W/m^2 for resistive load	76
5.10	PV output power under changing temperature at 800 W/m^2 for resistive load	76
5.11	performance of MPPT of PV output power under fixed temperature at 800 W/m^2 for resistive load	77
5.12	duty cycle of converter under changing temperature at 800 W/m^2 for resistive load	77
5.13	resistive load voltage under changing temperature at 800 W/m^2	78
5.14	resistive load current under changing temperature at 800 W/m^2	78
5.15	changing irradiance at 25^{o}C for DC motor pump	79
5.16	PV output power under changing irradiance at 25^{o}C for DC motor pump	80
5.17	performance of MPPT of PV output power fixed irradiance at 25^{o}C for DC motor pump.	81
5.18	duty cycle of converter under changing irradiance at 25^{o}C for DC motor pump	82
5.19	DC motor voltage under changing irradiance at 25^{o}C	82
5.20	DC motor current under changing irradiance at 25^{o}C	83
5.21	DC motor speed under changing irradiance at 25^{o}C	83
5.22	performance of MPPT of motor speed under fixed irradiance at 25^{o}C for DC motor pump	84

List of Figures (Cont'd)

5.23	changing temperature at 400 W/m^2 for DC motor pump	84
5.24	PV output power under changing temperature at 400 W/m^2 for DC motor pump load	84
5.25	performance of MPPT of PV output power under fixed temperature at 400 W/m^2 for DC motor pump	85
5.26	duty cycle of converter under changing temperature at 400 W/m^2 for DC pump load	85
5.27	DC motor voltage under changing temperature at 400 W/m^2	86
5.28	DC motor current under changing temperature at 400 W/m^2	86
5.29	DC motor speed under changing temperature at 400 W/m^2	87
5.30	performance of MPPT of motor speed under fixed temperature at 400 W/m^2 for DC motor pump	87

List of Nomenclatures

Symbols	Nomenclatures	Units
a, a_2	diode ideality constant	
AC	alternative current	
A_1	load friction	Nm
A_3	motor friction	Nm
BOS	balance of systems	
B_1	damping	$Nm.s.rad^{-1}$
C	boost capacitor	Farad
CCM	continuous conducting mode	
CdTe	cadmium telluride	
CE	change of error	
CIS	copper indium diselenide	
C_{min}	minimum value capacitance	farad
C_1	diode constant	
D	duty cycle	
DCM	discontinuous mode	
E	error	
FLC	fuzzy logic controller	
f_s	switching frequency	Hertz
G	irradiance	W/m^2
G_n	nominal solar irradiation	W/m^2
I	PV current	A
I_a	output current of boost converter	A
I_d	diode current	A
I_m	current source	
I_{mo}	armature current	A
I_{mp}	current at MPP	A
I_n	nominal PV cell output current	A
I_o, I_{o2}	reverse diode saturation current	A
I_{pv}	photon current	A
I_s	input current of boost converter	A
$I_{sc,n}$	nominal short-circuit current at STC	A

List of Nomenclatures (Cont'd)

I_{sc}	short circuit current	A
I-V	current-voltage	
J	rotor inertia	$Kg.m^2$
K	boltzmann's constant	J/K
KCL	Kirchhoff's current law	
K_I	Temperature Coefficient of I_{sc}	A/C
K_V	Temperature Coefficient of V_{oc}	V/C
K_1	fractional open circuit voltage constant	
K_2	fractional short circuit current constant	
K_3	back emf constant	$Nm.A^{-1}$
L	boost inductor	henry
L_a	armature inductance	henry
L_{min}	minimum value of inductor	henry
MPP	Maximum power point	
MPPT	maximum power point tracking	
NB	Negative big	
NN	neural network	
NS	Negative small	
N_p	number of parallel PV cells	
N_{par}	number of parallel PV module	
N_s	number of series PV cells	
N_{ser}	number of series PV module	
PB	Positive big	
PS	Positive small	
PV	Photovoltaic	
PWM	pulse width modulation	
P-V	power-voltage	
P&O	Perturb and Observe	
P_{mp}	power at MPP	Watt
$P_{max,e}$	max experimental peak output power	watt
q	electron charge	C
R	variable resistive load	ohm

List of Nomenclatures (Cont'd)

R_a	armature resistance	ohm
R_{in}	input impedance of boost converter	ohm
R_{load}	load impedance	ohm
R_{opt}	optimal resistance	ohm
R_p	parallel resistance	ohm
R_s	series resistance	ohm
STC	Standard Test Conditions	
T	cell temperature	Kelvin
T_n	nominal temperatures	Kelvin
T_{off}	switch off time	sec
T_{on}	switch on time	sec
T_s	switching period	sec
V	PV voltage	V
V_a	output voltage of boost converter	V
V_d	voltage across diode	V
V_{mo}	armature voltage	V
V_{mp}	voltage at MPP	V
V_{oc}	open circuit voltage	V
$V_{oc,n}$	nominal open-circuit voltage at STC	V
V_s	input voltage of boost converter	V
W	rotor speed	rpm
ZE	Zero	
$\in$	load torque constant	$Nm.s.rad^{-1}$

CHAPTER (1)

INTRODUCTION

CHAPTER (1)

INTRODUCTION

1.1 General

It is well established that energy production and use based on consumption of fossil fuels can have deleterious environmental and human health impacts, including the potential of global warming of the earth through changes in the atmosphere's concentration of carbon dioxide. The worldwide conventional energy sources are rapidly depleting. The increasing of the world energy demand, due to modern industrial society and population growth, is motivating a lot of investments in renewable energy source since it is clean, pollution-free and inexhaustible. PV energy is now becoming one of the fastest growing renewable energy technologies due to continuous cost reduction and technological progress. The PV technology has many advantages in which it incurring no fuel costs, not being polluting, requiring little maintenance, emitting no noise and feasible to install in remote location, but their main drawbacks are high fabrication cost, low energy conversion efficiency, and nonlinear characteristics.

A PV is a non-linear power source. There is a unique point on the power-voltage (P-V) curve, called the maximum power point (MPP), at which the PV array produces maximum output power. As it is well known, the MPP of a PV power generation system depends on array temperature, solar irradiation, and load impedance, so it is necessary to constantly track the MPP [1,2] of the solar array. Therefore MPPT techniques are needed to maintain the PV array's operating point at its MPP.

For years, research has focused on various MPP control algorithms to track the maximum power of the PV array. These techniques include methods using neural networks (NN), P&O methods, Fractional Open Circuit Voltage method, fractional short circuit current method and computational methods [3,4]. One of the computational methods which have demonstrated fine performances under different environmental operating conditions is the fuzzy based MPPT technique. In recent years, FLC has been widely used for industrial processes owing to their heuristic nature associated with simplicity and effectiveness for both linear and nonlinear systems. However, in a number of cases, such as those, when parameter variations take place, or when disturbances are present, or when there is no

simple mathematical model, fuzzy logic based control systems have shown superior performance to those obtained by conventional control algorithms. The main advantages of FLC over the conventional controllers are: they do not need accurate mathematical model, they can work with imprecise inputs, they can handle nonlinearity and they are more robust than conventional nonlinear controllers.

One of the most important applications of PV which haven been presented is standalone systems for water pumping, particularly in regions that have a considerable amount of solar radiation and have no access to national grids. PV pumping systems usually utilize low power pumps ranging from 200-2000W. They are widely used in domestic and livestock water supplies and small-scale irrigation systems, especially those employed for water and energy conservation such as low head drip irrigation systems. Over 50,000 PV pumping systems made up of different configurations had been installed worldwide by 2007 with an increasing potential for the use of PV pumping systems in large-scale irrigation schemes [5].

In this thesis, intelligent control technique using FLC is associated to an MPPT controller been compared with P&O method as one of the most widely conventional method used in this area due to its simple and easily implementation in order to improve energy conversion efficiency and then compared with direct coupling. Simulation and analysis are presented using Matlab Simulink under varying conditions.

1.2 Overall Trends in Installations and Market

Almost 30 GW of new solar PV capacity came into operation worldwide in 2011, increasing the global total by 74% to almost 70 GW as shown in figure (1.1). Solar PV capacity in operation at 2011 was about 10 times the global total just five years earlier, and the average annual growth rate exceeded 58% for the period from the end of 2006 through 2011 [6].

While the market surpassed all previous records, PV-related production ramped up even faster, resulting in a significant oversupply of modules in 2011. Approximately 33.1 GW of crystalline silicon cells and 34.8 GW of modules were produced, up from 21.2 GW and

20.5 GW in 2010. Thin film's actual production increased by an estimated 21% to 4.6 GW. Polysilicon output more than doubled between 2008 and 2010 [6].

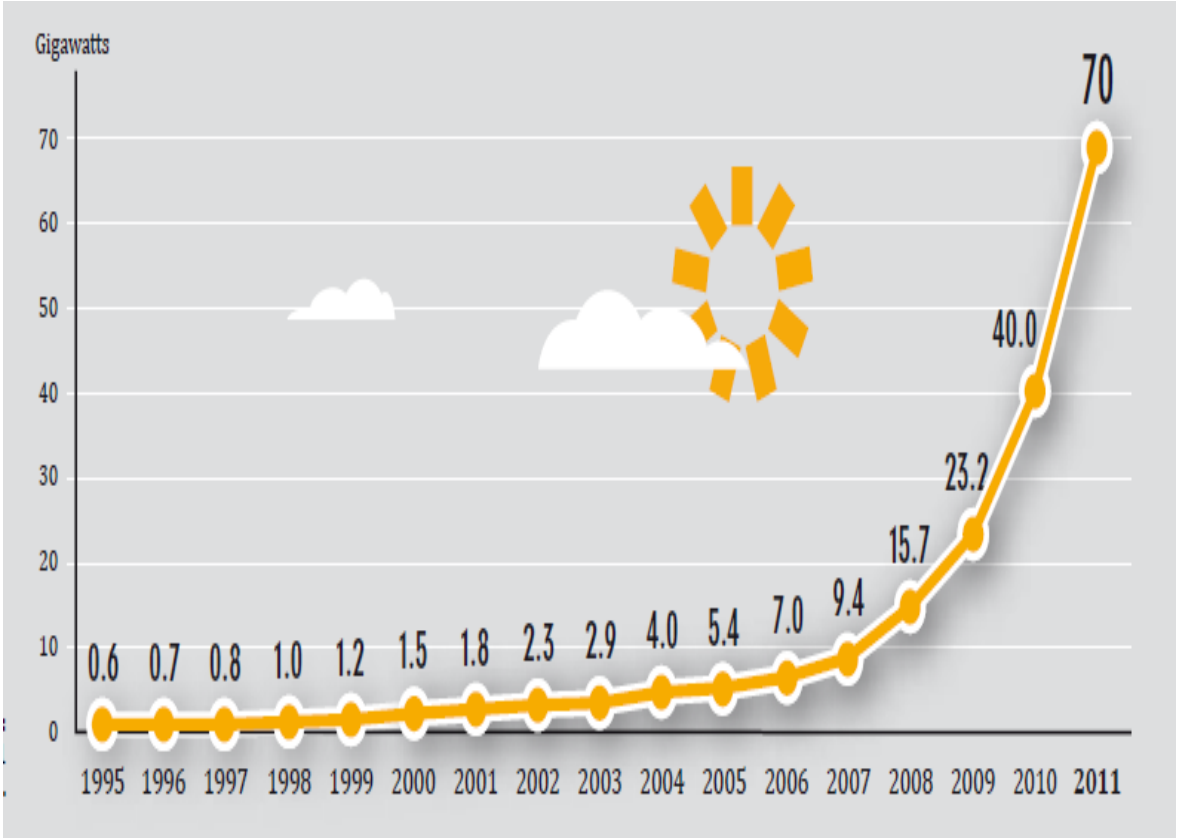

Figure (1.1) solar PV existing world capacity 1996-2011

1.3 Photovoltaic History

The history of PV dates was in 1839 when a French physicist, Edmund Becquerel, discovered the photovoltaic effect while experimenting with an electrolytic cell made up of two metal electrodes placed in an electricity-conducting solution-generation increased when exposed to light, Almost 40 years later, Adams and Day were the first to study the photovoltaic effect in solid selenium and were able to built solid cells with 1~2% efficiency. By the 1950s, the Czochralski began to process the first generation of single-crystal silicon photovoltaic.

The real appearance of PVs in practical was in 1958 when they were used in space for the Vanguard I satellite. Today, the production of PV cells is following a rapidly growing curve since technological advancement of late '80s that has started to rapidly improve efficiency and reduce cost. The word of photovoltaic divided into two words, Photo means light, and Voltaic means electricity, photovoltaic means getting electricity from light (sun)

[7,8]. PV power conversion technologies has been around for many years, and have been implemented for military, space, commercial and residential applications by taking advantage of the abundant solar energy given off by the sun.

1.4 Architecture of PV system

The fundamental power conversion unit of a PV system is the solar cell. Over the past decades, silicon has been almost the only material used for manufacturing solar cells, although other materials have been developed. Progress in manufacture of solar cells are moving so rapidly, In general, cells can be classified as either wafer-based crystalline (single crystal or Polycrystalline) or thin film [9,10].

The power produced by a single solar cell is not enough for general use since it produce an output voltage less than 1V; cells must be connected in series-parallel configurations to produce enough power for high-power applications. They are usually assembled into modules. However, there are different sizes of PV modules commercially available; the most commonly used module is 36 to 72 solar cells connected in series to produce enough voltage. For higher power requirement, the modules are interconnected in series/parallel to form arrays as shown in figure (1.2) [11].

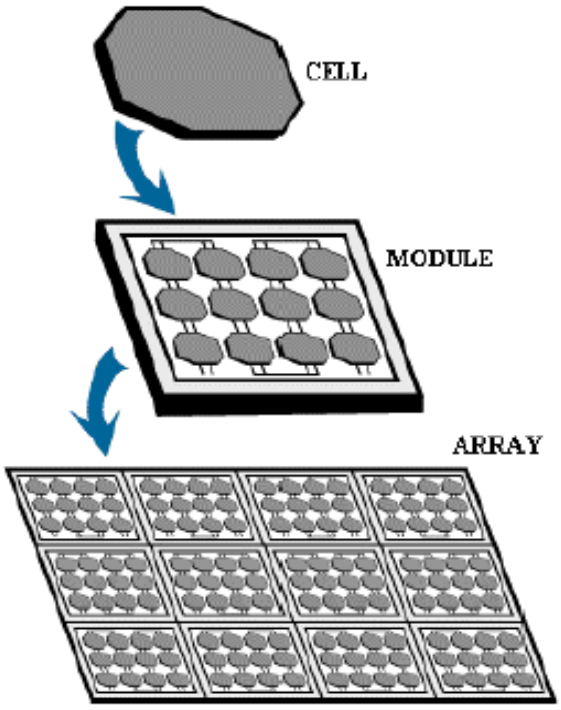

Figure (1.2) Illustrated photovoltaic system

In order to be able to compare different PV modules uniform conditions are usually specified for determining the electrical characteristics. These conditions known as standard test conditions (STC) where parameters obtained from the testing are usually provided on the manufacturer's datasheet. These conditions are [10]:

- Irradiance on cell surface is 1000 W/m^2.
- Operating temperature of 25^oC.
- A specified light spectral distribution with an air mass =1.5.

1.4.1 Advantage and Disadvantage of PV System

PV systems offer substantial advantages over conventional power sources [12]:

- It is free and inexhaustible.
- Reliability.
- Low Maintenance Cost.
- Long lifetime, it can produce power for 25 years.
- No Fuel Cost. Since no fuel source is required, there are no costs associated with purchasing, storing, or transporting fuel.

PV has some disadvantages when compared to conventional power systems [12]:

- A high initial cost.
- Low power conversion efficiency.
- The non-linear current-voltage (I-V) characteristic exhibited by a PV cell due variations in cell temperature and solar irradiation.
- Energy Storage. Some PV systems use batteries for storing energy, increasing the size and cost.

1.4.2 Theory of operation

Solar cell is basically a p-n junction. It relies on the process known as the “photovoltaic effect” to produce electricity. This phenomenon happens when the energy produced by the photons from sunlight on the exposed solar cell is greater than the band energy of the semiconductor. Thus, electron-hole pairs are created by the breakage and loss of the atoms in the material. The existing electric field of p-n junction of solar cells separate the created charge carriers in the depletion region and lead to a forward bias of the p-n junction, so that a voltage potential is built up. This will cause a current proportional to the incident

radiation to flow through the load once it is connected to the cell as shown in figure (1.3) [9,13].

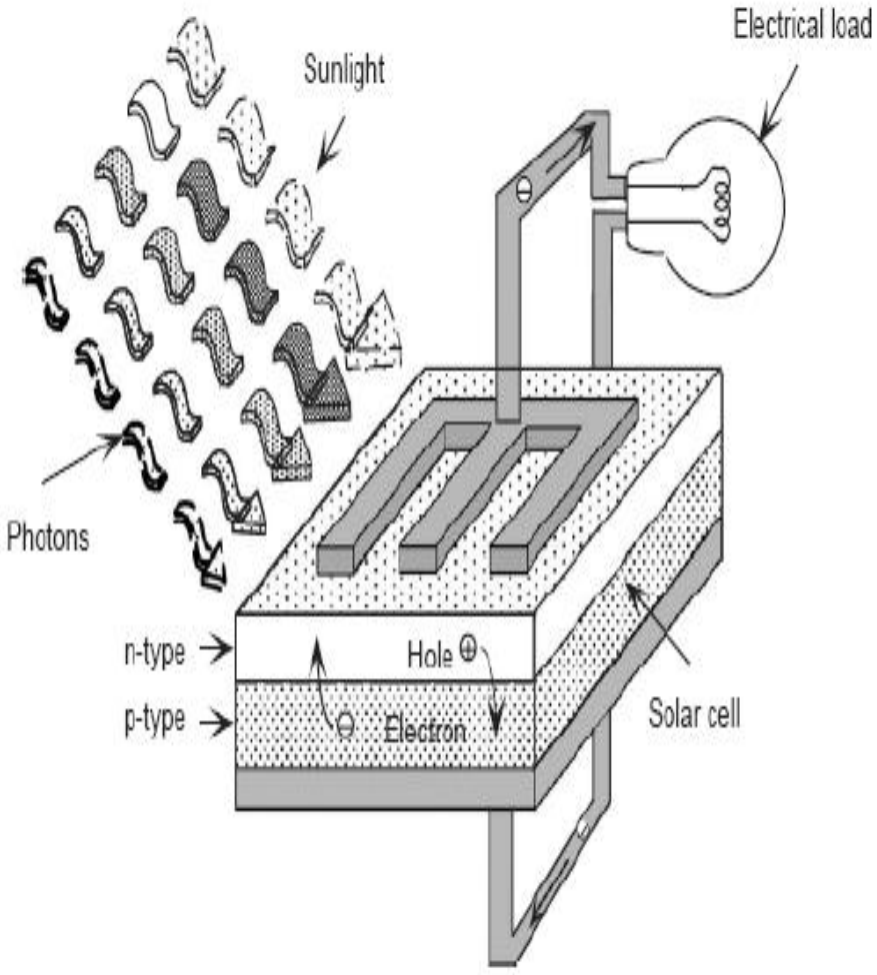

Figure (1.3) PV cell showing hole-electron pairs created by photons

1.4.3 Types of Solar cell

There are different types of solar panels which differ in their material, price, and efficiency [10].

1.4.3.1 Monocrystalline Solar cell

It has efficiency approximately 18%. They are made from a large crystal of silicon. These types of solar panels are the most efficient panels; however they are the most

expensive. They do somewhat better in lower light conditions than the other types of solar panels.

1.4.3.2 Polycrystalline Solar cell

It has efficiency approximately 16%. Instead of one large crystal, this type of solar panel consists of multiple amounts of smaller silicon crystals; they are the most common type of solar panels on the market today. They look a lot like shattered glass. They are slightly less efficient than the monocrystalline solar panels and less expensive to produce.

1.4.3.3 Thin film Solar cell

It has efficiency approximately 7%.Amorphous silicon, copper indium diselenide (CIS) and cadmium telluride (CdTe) are used as semiconductor materials. These types of solar panels have lower efficiency than the other two types of solar panels, and the cheapest to produce.

1.4.4 Balance of Systems (BOS)

BOS are the components which added to the PV array to be able to integrate with systems. These components can be classified into [12]:

- Wiring components which includes distribution panel, junction box and miscellaneous connectors, lighting protectors, grounding connections, fuse box.
- Batteries and Battery charge controller: Stand-alone PV systems require energy storage to compensate for periods without or within sufficient solar irradiation, such as during the night or during cloudy weather.
- Inverter: it is used to convert the direct current output of the array or the battery into alternating current (AC) to be suitable for AC loads.
- DC/DC converter: it is used to adjust output volt to be suitable for load.
- MPPT controller: used to extract maximum power of PV array to be transfer to the load. It will be explained in more details in chapter 3.

1.4.5 Types of Connection Photovoltaic System

PV systems can be configured generally into stand-alone and grid-connected systems as shown in figure (1.4) [12].

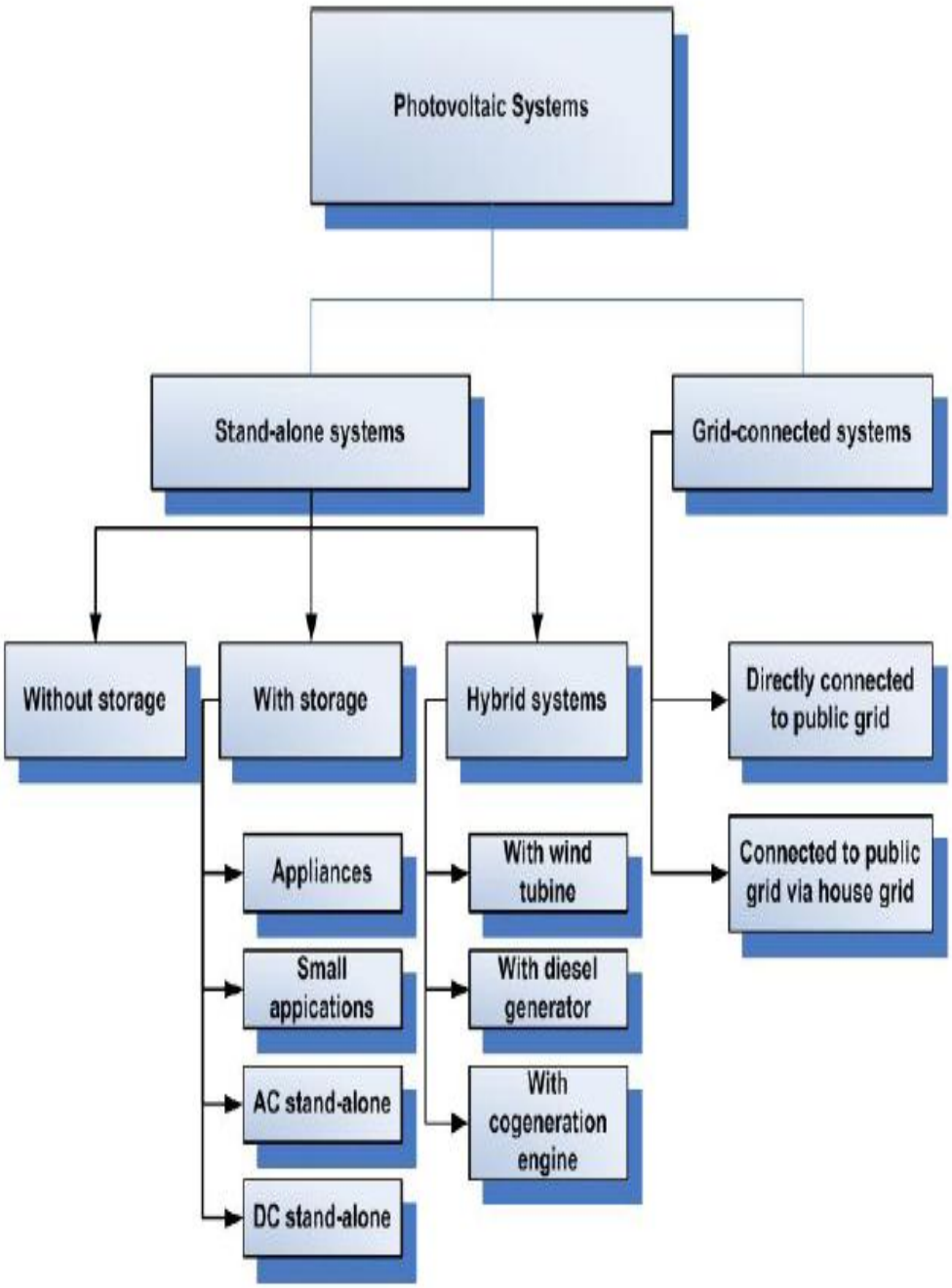

Figure (1.4) Classification of PV systems

An important advantage offered by distributed energy resources such as PV systems is their potential to provide sustainable electrical energy in areas where the conventional power grid is absent. They can be located near loads, providing benefits that bulk power generation cannot. Consumers living in remote areas or townships far from the power grid can run their appliances using PV energy. In the current study, the PV system is used as stand-alone system for water pumping application; which can be useful in remote or rural areas.

1.4.6 Photovoltaic Array Characteristics

The photovoltaic I-V and P-V characteristic is nonlinear and changes with irradiation and temperature. Sample I-V and P-V curves are overlaid on the same graph as shown in figure (1.5) under fixed irradiation and temperature. The formulas standing behind these curves are discussed in Chapter 2 where a detailed literature survey of PV arrays and their operation is included. The main purpose behind introducing figure (1.5) is getting an idea about the notion of the MPP of a PV array. The bending point of the I-V curve and P-V curve is the MPP of the array under a certain temperature and irradiance. Thus when operating a PV array at its MPP, maximum power is extracted and the array is operating at its maximum efficiency.

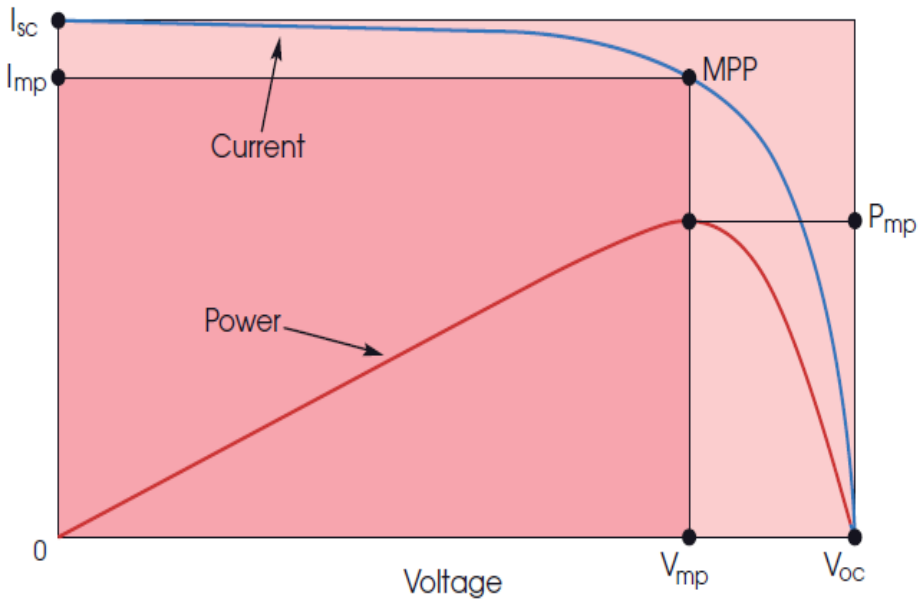

Figure (1.5) I-V, P-V characteristics of photovoltaic cell

1.5 MPPT System

A MPPT system is an electronic system that operates the PV module in a way that it extracts the maximum power from module. The MPPT plays the role of impedance adapter, i.e. it matching the impedance of the load to that of the module. A complete PV system with an MPPT system including a solar module, an MPPT algorithm and a DC/DC converter as shown in figure (1.6), the topology is mathematically modeled and simulated in a Matlab/Simulink environment separately. After all subsystems have been verified one

by one to ensure good functionality and efficiency, they are connected together and combined with a load to assess the overall performance of this residential PV application.

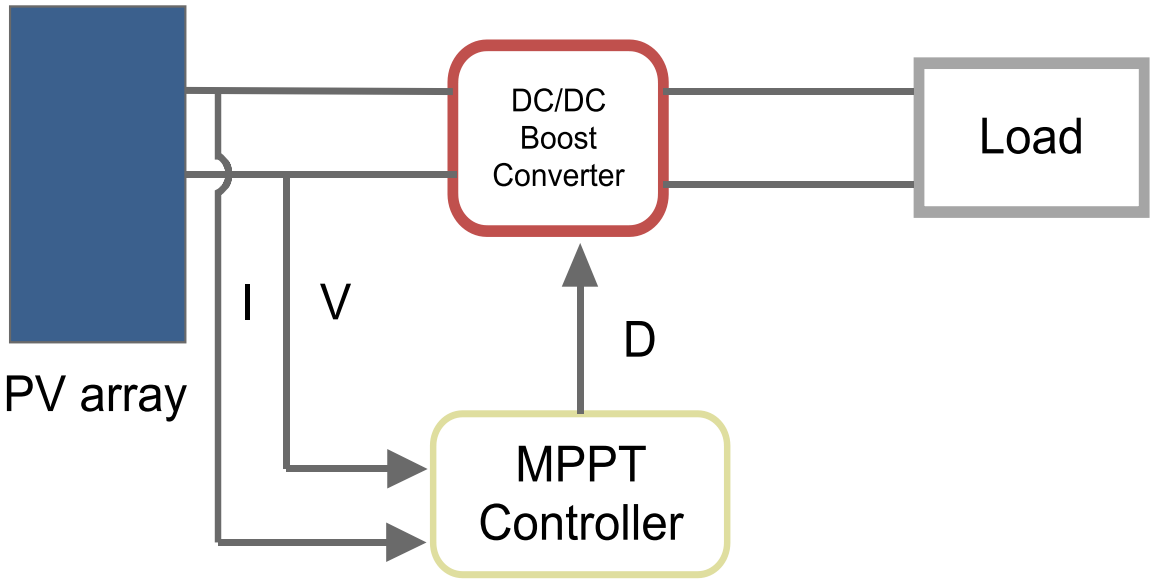

Figure (1.6) MPPT system

1.6 Literature Review of MPPT Control Algorithms

Over the past decades many methods have been developed to find MPP and published. These techniques differ in many aspects such as required sensors, complexity, cost, range of effectiveness, convergence speed, correct tracking when irradiation and/or temperature change and hardware needed for the implementation.

Some of these techniques are [3,14]:

1) Fractional Open Circuit Voltage.
2) Fractional Short Circuit Current.
3) Neural Networks.
4) Current sweep.
5) Array Reconfiguration Method.
6) β method.
7) Look-up Table Method
8) Maximum power point current and voltage computation
9) Incremental Conductance.

10) P&O method.
11) Fuzzy Logic method.

1.6.1 Fractional open circuit voltage

This method uses the approximately linear relationship between the voltage at MPP (V_{mp}) and the open circuit voltage (V_{oc}), which varies with the irradiance and temperature:

$$V_{mp} \approx k_1 V_{OC} \tag{1.1}$$

Where k_1 is a constant depending on the characteristics of the PV array and it has to be determined beforehand by determining the V_{mp} and V_{oc} for different levels of irradiation and different temperatures. According to [15] the constant k_1 has been reported to be between 0.71 and 0.8. Once the constant of proportionality k_1, is known, the V_{mp} can be determined periodically by measuring V_{oc}. To measure V_{oc} the power converter has to be shut down momentarily so in each measurement a loss of power occurs. Another problem of this method is that it is incapable of tracking the MPP under irradiation slopes, because the determination of V_{mp} is not continuous. One more disadvantage is that the MPP reached is not the real one because the relationship is only an approximation.

To overcome these drawbacks, some solutions have been proposed, as is reported in [3]. For example, pilot cells can be used to obtain V_{oc}. They are solar cells that represent the PV array's cells and which are not used to produce electricity but to obtain characteristics parameters such as V_{oc} without interfering with the power converters. These pilot cells have to be carefully chosen and placed to represent the PV array characteristics and the irradiation conditions. One drawback of using these pilot cells is that the cost of the system is increased.

Depending on the application, this technique can be used because it is very easy to implement and it is cheap - it does not require DSP or microcontroller control and just one voltage sensor is used. However, this method is not valid under partial shading of the PV array because the constant k1 changes [14]. To update k1 a voltage sweep is proposed, this obviously adds to the implementation complexity and incurs more power loss.

1.6.2 Fractional short circuit current

Just like in the fractional open circuit voltage method, there is a relationship under varying atmospheric conditions between short circuit current (I_{sc}) and the current at MPP (I_{mp}), as is shown by:

$$I_{mp} \approx k_2 I_{SC} \tag{1.2}$$

The coefficient of proportionality k_2 has to be determined according to each PV array, as in the previous method happened with k_1. According to [15,16] the constant k_2 has been reported to be between 0.78 and 0.92.Measuring the short circuit current while the system is operating is a problem. It usually requires adding an additional switch to the power converter to periodically short the PV array and measure I_{SC}.

One other option a boost converter is used and the switch of the converter is used to short the PV array. Short circuiting the PV array also leads to a loss of power. One last disadvantage is that the real MPP is not reached because the proportional relationship is an approximation. Furthermore, k_2 changes if the PV array is partially shaded, which happens due to shades or surface contamination. To overcome this problem, [16] proposes an online tuning of k_2 and a periodical sweep of the PV voltage from open circuit to short circuit to update k_2 and guarantee that the real MPP is reached in the presence of multiple maxima which obviously increases the complexity of the system. Most of the literature using this MPPT technique uses a DSP as controller.

1.6.3 Neural networks

Another MPPT method well adapted to microcontrollers is NN [3]. They came along with Fuzzy Logic and both are part of the so called Soft Computing. More complicated NN's are built adding more hidden layers. The number of layers and the number of nodes in each layer as well as the function used in each layer vary and depend on the user knowledge. The input variables can be parameters of the PV array such as V_{oc} and I_{sc}, atmospheric data as irradiation and temperature or a combination of these. The output is usually is duty cycle for the converter.

The performance of the NN depends on the functions used by the hidden layer and how well the neural network has been trained. The links between the nodes are all weighted.

The weights are adjusted in the training process. To execute this training process, data of the patterns between inputs and outputs of the NN are recorded over a lengthy period of time, so that the MPP can be tracked accurately.

The main disadvantage of this MPPT technique is the fact that the data needed for the training process has to be specifically acquired for every PV array and location, as the characteristics of the PV array vary depending on the model and the atmospheric conditions depend on the location. These characteristics also change with time, so the neural network has to be periodically trained [14].

1.6.4 Current Sweep

In this method the I-V characteristic curve is obtained using a sweep waveform for the PV array current. The sweep is repeated at fixed time intervals so the I-V curve is updated periodically and the V_{mp} can be determined from it at these same intervals. How the I-V curve is determined and the function chosen for the sweep waveform can be found in [3,14].

With this method the real MPP is obtained. On the other hand, the sweep takes certain time during which the operating point is not the MPP, which implies some loss of available power. Strictly speaking, it is not possible to track the MPP under irradiation slopes, because the MPP varies continuously. Only if the sweep is instantaneous the global MPP could be found, but that is impossible. Furthermore, the implementation complexity is high, the convergence speed is slow and both voltage and current measurements are required.

1.6.5 Array Reconfiguration Method

In this method the PV arrays are arranged in different series and parallel combinations such that the resulting MPPs meet a specific load requirement. This method is time consuming and tracking of the MPP in real time is not obvious [3]. According to the technique suggested to optimize the operation of photovoltaic system; it assumed that the solar array is going to be divided into two modules. The first one represents the basic module, and the second will be divided into sub modules. Three ways of arranging these modules together can be achieved the parallel, series, and parallel-series arrangements.

1.6.6 β Method

The method based on β tracking, has the advantage of fast tracking. The analysis of the I-V characteristics of a PV array, leads to an intermediate variable β, is given by:

$$\beta = \ln(I_o * C_1) \quad (1.10)$$

Where 'I_o' is reverse saturation current and 'C_1' is the diode constant depending on the electronic charge, ideality factor, Boltzmann constant, temperature in Kelvin and the number of series connected cells, respectively. Thus, depends on all of these parameters. It is observed that the value of β remains within a narrow band as the array operating point approaches the MPP. Therefore by tracking β, the operating point can be quickly driven to close proximity of the MPP using large iterative steps [3].

1.6.7 Look-up Table Method

In this case, the measured values of the PV generator's voltage and current are compared with those stored in the controlling system, which correspond to the operation at the maximum point, under predetermined climatologically conditions. In this method, a PI type controller adjusts the duty cycle of the DC-DC converter. The zero error is reached when the current and power of the Photovoltaic generator are equal to the pre-determined values of I_{mp} and power at MPP (P_{mp}). Any change of the irradiance or load, results in a disturbance of the tuned system, and the PI controller again brings the system to its optimum operating point. These algorithms have the disadvantage that a large capacity of memory is required for storage of the data. Moreover, the implementation must be adjusted for a panel PV specific. In addition, it is difficult to record and store all possible system conditions. But it has also some advantages. It is simple and the system is able to perform fast tracking, as all the data regarding maximum point are available [3].

1.6.8 Maximum power point current and voltage computation

I_{mpp} and V_{mpp} are computed from equations involving temperature and irradiance levels, which are not usually easy to measure. Once I_{mpp} or V_{mpp} is obtained, feedback control is used to force the PV array to operate at the MPP. On the other hand, the MPP is correctly tracked even under changing atmospheric conditions [3,14].

1.6.9 Incremental Conductance

This algorithm exploits the fact that the slope of the P-V curve of a PV array is equal to zero at the MPP, positive on the left of the MPP and negative on the right [17,18].

The MPP can thus be tracked by comparing the instantaneous conductance (I/V) to the incremental conductance (ΔI/ΔV). Once the MPP is reached, the operation of the PV array is maintained at this point unless a change in ΔI is noted, indicating a change in atmospheric conditions and the MPP. The algorithm decrements or increments duty cycle for the converter to track the new MPP. The increment size determines how fast the MPP is tracked. Fast tracking can be achieved with bigger increments but the system might not operate exactly at the MPP and oscillate about it instead; so it can be said that the incremental conductance can track rapidly at different conditions with higher accuracy than perturb and observe algorithm but it increases complexity of system.

1.6.10 P&O Method

P&O method has a simple feedback structure and fewer measured parameters. It operates by periodically perturbing (i.e. incrementing or decreasing) the array operating voltage and observing PV output power. If the perturbation leads to an increase (decrease) in array power, the subsequent perturbation is made in the same (opposite) direction. In this manner, the peak power tracker continuously seeks the peak power condition. More details of the P&O are given in chapter 4. Advantages of the P&O include easy of implementation and previous implementations that were tested such as in [16]. Disadvantages include oscillations around the MPP.

1.6.11 FLC Method

The use of fuzzy logic control has become popular over the last decade because it can deal with imprecise inputs, does not need an accurate mathematical model and can handle nonlinearity. Microcontrollers have also helped in the popularization of fuzzy logic control [16].

Fuzzy logic control generally consists of three stages: fuzzification, rule base table lookup, and defuzzification. The inputs to a MPPT fuzzy logic controller are usually an error (E) and a change in error (CE). The error can be chosen by designer, but usually it is

chosen as Δp/Δv because it is zero at the MPP [19,20]. Different inputs has been implemented as in [21,22,23,24]

The output of fuzzy logic converter is the change in the duty cycle of converter, the advantage of controller, beside deal with imprecise inputs, does not need an accurate mathematical model and can handle nonlinearity, are fast convergence and minimal oscillation around MPP, the disadvantage of this method is that their effective depends a lot on the skills of the designer, not on choosing the right error computation, but also coming up with appropriate rule base. More of this method will be later in chapter 4.

Table (1.1) shows major characteristics of different MPPT techniques comparing by each other in their accuracy, implementation, speed, and other fields as shown in Table (1.1) [16,18].

Table (1.1) Major characteristics of different MPPT techniques

MPPT Technique	True MPPT	Analog or Digital	Convergence speed	Implementation complexity	Sensed parameter
Fractional Voc	No	Both	Medium	Low	Voltage
Fractional Isc	No	Both	Medium	Medium	Current
Neural Networks	Yes	Digital	Fast	High	Varies
Current sweep	Yes	digital	slow	High	Current, voltage
Array Reconfiguration Method	No	digital	slow	High	Current, voltage
β method	Yes	digital	Fast	High	Current, voltage
Look-up Table Method	Yes	digital	Fast	Medium	Voltage, Current, Irradiance, Temperature
Imp and Vmp computation	Yes	digital	N/A	Medium	Irradiance, Temperature
Incremental Conductance	Yes	digital	Varies	Medium	Current, voltage
P&O	Yes	Both	varies	Low	Current, voltage
FLC	Yes	digital	Fast	High	Varies

1.7 Scope of Thesis

The aim of the thesis is to study and analyze the MPPT for solar system, by using different analysis techniques. This thesis presents reimplementation of some of the previous techniques. Intelligent control technique using fuzzy logic control is associated to an MPPT controller in order to improve energy conversion efficiency and compared with P&O method as one of the most widely used techniques in MPPT because of its simplicity. Simulation and analysis of P&O and fuzzy logic control are presented.

1.8 Organization of Thesis

Chapter 1 "**Introduction**" Includes the historical background of the photovoltaic, its basic principle and types. It also includes literature survey of the MPPT algorithm.

Chapter 2 "**Modeling of Photovoltaic**" Describes the solar cell, module , array and analyzing its characteristics. Also the modeling of PV cell and array is described and simulating using MATLAB software

Chapter 3 "**Maximum Power Point Tracker**" The MPPT problem is defined and the mechanism of transferring maximum power form Photovoltaic source to the load using DC/DC converter as interface between them is described. Also a PV water Pumping system is discussed.

Chapter 4 "**Fuzzy and P&O Algorithms**" Gives explanation of fuzzy control and analysis of fuzzy and P&O algorithms for extracting MPPT from PV.

Chapter 5 "**Simulation and results**" Simulation using MATLAB software, comparison between with and without MPPT is carried out under different irradiation and temperature for different loads, result of performances of two algorithms is carried out.

Chapter 6 "**Conclusion and Future Scope**" mainly includes the conclusion and future scope of this thesis work.

CHAPTER (2)

MODELING OF PHOTOVOLTAIC

CHAPTER 2

MODELING OF PHOTOVOLTAIC

2.1 Introduction

The philosophy behind digital simulation of solar energy systems is that experiments which normally should be done on real systems under high assembling costs can be done numerically in a short time on a computer, thus saving time and investments.

Digital simulation of these systems serve for the purpose of understanding the operational behavior of the various components of the system and the interaction among them, since by simulating the system performance, one can trace all steps of energy conversion and identify the losses throughout the system in details. Computer simulation allows a wide range of system parameters to be varied, and the operating characteristics of the system to be investigated. Finally, computer simulation permits the extrapolation of a system design to other localities, with different meteorological conditions, and makes it possible to compare different systems. Basis for a computer simulation is a reflection of a real system which is based on theoretical analysis of the various physical processes occurring in a system. Mathematical equations describing quantitatively the system characteristics are formulated from this analysis and translated into computer to be used in the simulation process.

This chapter discusses the modeling of PV cell, module and array according to manufacturer supplied data for a specific module, and then the model is used to study characteristics of PV under different atmospheric conditions.

2.2 Solar Cell Modeling

Different models have been used to represent solar cell varying in there accuracy of modeling, depending on designer need. These models are [8]:

2.2.1 Simplest Model

It consists of an ideal current source in parallel with an ideal diode as shown in figure (2.1). The current source (I_{pv}) represents the current generated by solar cell due to photons received from the sun, and is constant under constant temperature and irradiance.

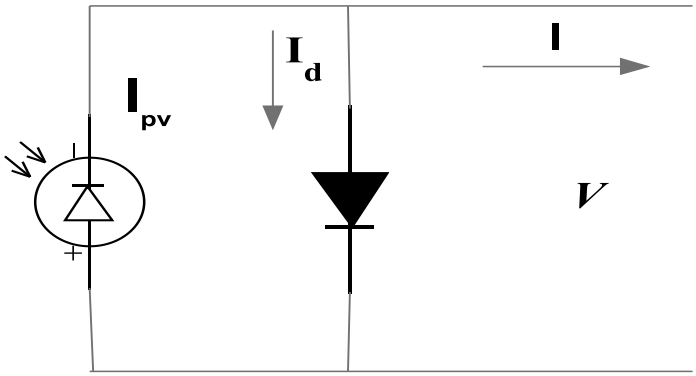

Figure (2.1) equivalent circuit for simplest PV cell

There are two key parameters frequently used to characterize a solar cell. Shorting together the terminals of the cell, as shown in figure (2.2a), the photon generated current will follow out of the cell as a short-circuit current , thus, $I_{pv} = I_{sc}$. And as shown in figure (2.2b), when there is no connection to the solar cell (open-circuit), the photon generated current is shunted internally by the intrinsic p-n junction diode. This gives the open circuit voltage [8]. The PV module or cell manufacturers usually provide the values of these parameters in their datasheets.

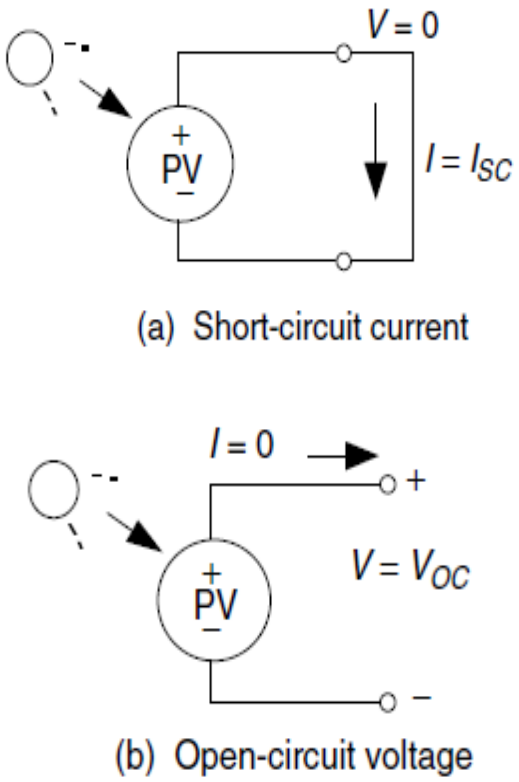

Figure (2.2) PV are I_{sc} and V_{oc} connection

The output current (I) from the solar cell is found by applying the Kirchhoff's current law (KCL) on the equivalent circuit shown in figure (2.1) [25,26].

$$I = I_{pv} - I_d \tag{2.1}$$

Where

- I_d is the current shunted through the intrinsic diode.

The diode current I_d is given by the Shockley's diode equation (2.2):

$$I_d = I_o\left[exp\left(\frac{Vq}{kTa} - 1\right)\right] \tag{2.2}$$

Where

- I_o is the reverse saturation current of diode (A)
- q is the electron charge (1.602×10^{-19} C)
- V is the cell voltage (V).
- k is the Boltzmann's constant (1.381×10^{-23} J/K),
- T is the cell working temperature in Kelvin (K).
- a is the diode ideality constant.

By replacing I_d of the equation (2.2) into equation (2.1), gives the I-V relationship of the solar cell.

$$I = I_{pv} - I_o\left[\exp\left(\frac{Vq}{kTa} - 1\right)\right] \tag{2.3}$$

2.2.2 More Accurate Model

There are a few things that have not been taken into account in the simplest model and it will affect the performance of a PV cell in practice. These include the series resistance, parallel resistance, and recombination factor of solar cell.

2.2.2.1 PV Series Resistance

In a practical PV cell, there is a series resistance in a current path through the semiconductor material, the metal grid, contacts, and current collecting bus [27]. These

resistive losses are lumped together as a series resister (R_s). Its effect becomes very conspicuous in a PV module that consists of many series-connected cells. The series resistance has no effect on the open-circuit voltage, but reduces the short-circuit current [28].

2.2.2.2 PV Parallel Resistance

This is also called shunt resistance. It is a loss associated with a small leakage of current through a resistive path in parallel with the intrinsic device [27]. This can be represented by a parallel resistor (R_p). Its effect is much less conspicuous in a PV module compared to the series resistance, and it will only become noticeable when a number of PV modules are connected in parallel for a larger system. The R_p has no effect on the short circuit current, but reduces the open-circuit voltage [28].

2.2.2.3 Recombination

Recombination at the depletion region of solar cells explains non-ohmic current paths in parallel with the intrinsic solar cell. This is relevant at low voltage bias and can be represented in an equivalent circuit by a second diode term with a saturation density current (I_{o2}) as shown in figure (2.3), which is different from the I_o of the simplest solar cell diode, and given diode ideality constant (a_2) is most often assumed to equal 2 [27].

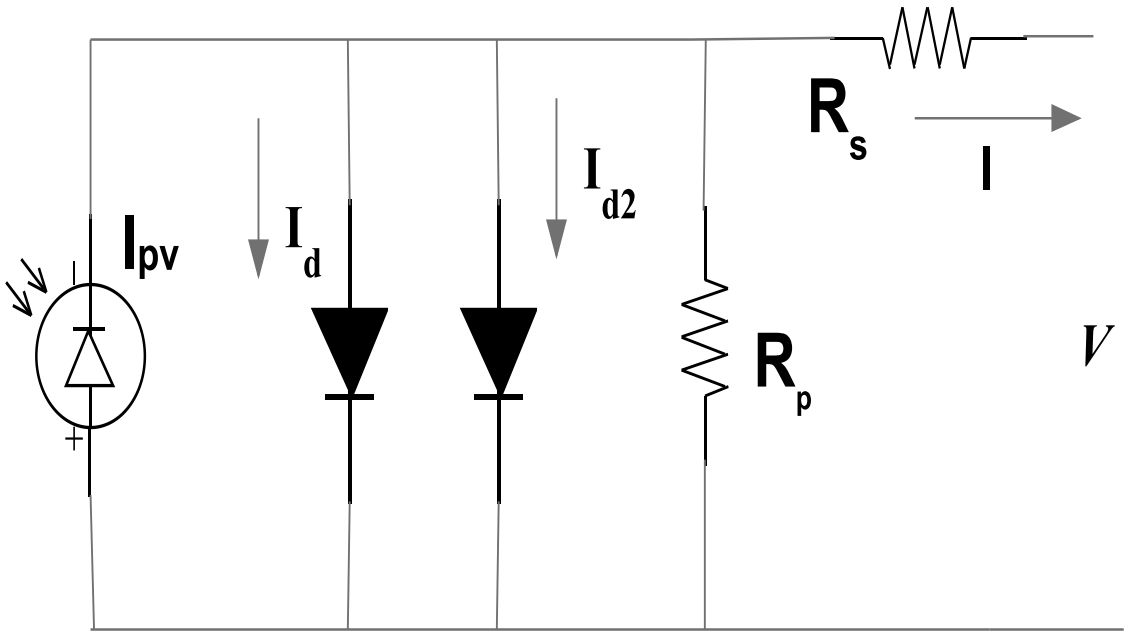

Figure (2.3) Equivalent Circuit for Double Exponential PV model

So the I-V relationship of PV cell instead of equation (2.3) can be written as [29,30]:

$$I = I_{pv} - I_o \left[\exp\left(\frac{q}{kTa}(v + IR_S) - 1\right)\right] - I_{o2}\left[\exp\left(\frac{q}{kTa_2}(v + IR_S) - 1\right)\right] - \frac{(v + IR_s)}{R_p} \quad (2.4)$$

The double exponential model is one of the most accurate models, but it exhibits a high complexity due to its double exponential terms. Therefore, the use of this single Exponential model to describe the static I-V characteristic has been considered widely, the main advantage of using the model with single diode is to simplify the electric circuit and consequently the equation that describes the device operation [31]. Figure (2.4) represent the equivalent circuit of single exponential model.

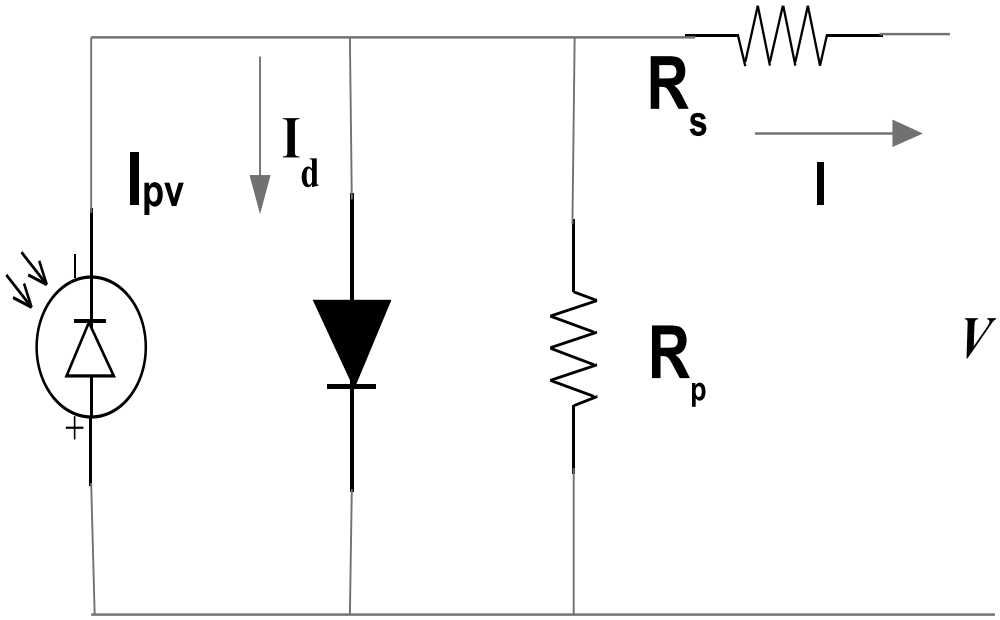

Figure (2.4) Equivalent Circuit Single Exponential PV model

So the I-V relationship of PV cell instead of equation (2.4) can be written as [29,32]:

$$I = I_{pv} - I_o \left[\exp\left(\frac{q(v + IR_S)}{kTa} - 1\right)\right] - \frac{(v + IR_s)}{R_p} \quad (2.5)$$

2.3 PV Module Modeling

The basic equation (2.5) of the solar cell does not represent the I-V characteristic of a practical PV module. PV module is composed of several connected PV cells. The strategy of modeling a PV module is no different from modeling a PV cell. It uses the same PV cell model. The terminal equation for the current and voltage of the module becomes as follows [33,34]:

$$I = I_{pv} - I_o \left[\exp\left(\frac{q(v + IR_S)}{V_t a} - 1 \right) \right] - \frac{(v + IR_s)}{R_p} \tag{2.6}$$

Where $V_t = N_s kT/q$ is the thermal voltage of the module with number of cells connected in series (N_s). Cells connected in series provide greater output voltages while cells connected in parallel (N_p) increase the current. If the module is composed of N_p cells then the PV and saturation currents may be expressed as $I_{pv} = I_{pv,cell} * N_p$, $I_0 = I_{0,cell} * N_p$, where N_p is equal to 1 in our study.

2.4 PV Array Modeling

The PV array is composed of several interconnected photovoltaic modules. The modeling process is the same as the PV module from the PV cells. Figure (2.5) shows a photovoltaic array, which consists of multiple modules, linked in parallel and series. N_{ser} is the total quantity of modules within the series and N_{par} is amount of modules in parallel. The number of modules modifies the value of R_p and R_s. After extending the relation I-V of the PV modules to a PV array, the new relation of I-V of the PV array is calculated by equation (2.7) [33,34]

$$I = I_{pv} N_{par} - I_r N_{par} \left[\exp\left(\left[\frac{v - IR_s \left(\frac{N_{ser}}{N_{par}} \right)}{V_t \, N_{ser}} \right] - 1 \right) - \frac{\left(v + IR_s \left(\frac{N_{ser}}{N_{par}} \right) \right)}{R_p \left(\frac{N_{ser}}{N_{par}} \right)} \right] \tag{2.7}$$

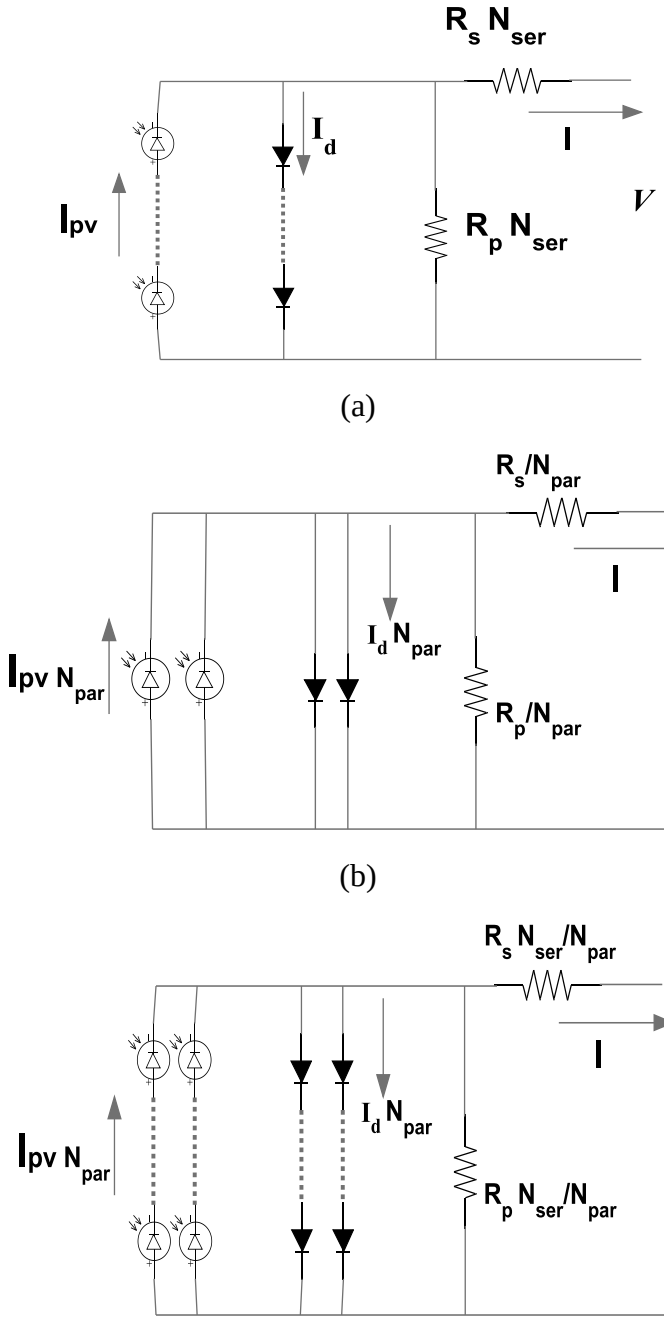

Figure (2.5) (a) Array of N_{ser} modules connected in series, (b) Array of N_{par} modules connected in parallel, and (c)array composed of N_{ser} x N_{par} modules.

2.5 Modeling a PV Module by MATLAB

Manufacturers of PV arrays, provide only a few experimental data about electrical and thermal characteristics, instead of the I–V equation. Unfortunately, some of the parameters required for adjusting PV array models cannot be found in the manufacturer's datasheets, such as I_{pv} or I, R_s, R_p, a, and I_o.

All PV array datasheets bring basically the following information: the nominal open-circuit voltage ($V_{oc,n}$), the nominal short-circuit current ($I_{sc,n}$), V_{mp}, I_{mp}, the open-circuit voltage/temperature coefficient (K_V), the short circuit current/temperature coefficient (K_I), and the maximum experimental peak output power ($P_{max,e}$). This information is always provided with reference to the STC of temperature and solar irradiation. Some manufacturers provide I–V curves for several irradiation and temperature conditions. These curves make easier the adjustment and the validation of the desired mathematical I–V equation. Basically, this is all the information one can get from datasheets of PV arrays.

KC200GTS PV module, pictured in figure (2.6), is chosen for a MATLAB simulation model. The module is made of 54 multi-crystalline silicon solar cells in series and provides 200W of nominal maximum power as shown in datasheet in [35]. The study of work is taken from [36], the single diode model with moderate complexity, and provides fairly accurate results is used, which described by equation (2.6) and (2.7) for simulation. To solve these equations the following parameters must be defined.

Figure (2-6) Picture of KC200GTS PV module

2.5.1 The light-generated current

The amount of incident light directly affects the generation of the current generated by the device. I_{pv} of the elementary cells, without the influence of the series and parallel resistances, is difficult to determine. The assumption $I_{sc} \approx I_{pv}$ is generally used in the modeling of PV devices because in practical devices the series resistance is low and the parallel resistance is high. The I_{pv} of the PV cell depends linearly on the solar irradiation and is also influenced by the temperature according to the following equation (2.8) [36].

$$I_{pv} = (I_n + K_I \Delta T)\frac{G}{G_n} \quad (2.8)$$

Where

- I_n is the nominal PV cell output current (at 25°C and 1000 W/m^2) depending on R_s,R_p and I_{sc}.
- $\Delta T = T - T_n$ (T_n being nominal temperatures [in Kelvin]).
- G_n is the nominal solar irradiation (1000 W/m^2).
- G is solar irradiation (W/m^2)

Note that T, G are inputs parameter can be changed or modified by user in simulation. The value of K_I is relatively small and this makes the cell output current linearly dependent on solar radiation level more than temperature.

2.5.2 Diode reverses saturation current

The I_0 is strongly dependent on the temperature, and it can be expressed in equation (2.9) as shown

$$I_o = \frac{I_{sc,n} + K_I \Delta T}{\exp\left[\left(v_{oc,n} + K_V \Delta T\right)/aV_t\right] - 1} \quad (2.9)$$

Where

- a assumed to be 1.

2.5.3 Series and parallel resistance

The goal is to find the value of R_s and R_p that makes the peak power of the mathematical P–V curve ($P_{max,m}$) coincide with the $P_{max,e}$ at the (V_{mp}, I_{mp}) point. This requires several iterations.

In the iterative process, R_s must be slowly incremented starting from $R_s = 0$. Adjusting the P–V curve to match the experimental data requires finding the curve for several values of R_s and R_p. The value of R_s and R_p are taken from work done by [36].

Finally the PV module can be simulated with an equivalent circuit model based on the PV model of figure (2.7), where it shows a circuit model using one current source (I_m) and two resistors (R_s and R_p). This circuit can be implemented by MATLAB simulator. The value of the model current I_m is calculated by the computational block that has V, I, I_o, and I_{pv} as inputs. I_o is obtained from equation (2.9) and I_{pv} is obtained from equation (2.8). The photovoltaic array can be simulated with the modified I-V equation (2.7). The simulation circuit presented previously must be modified according to the number of associated modules as shown in figure (2.8).

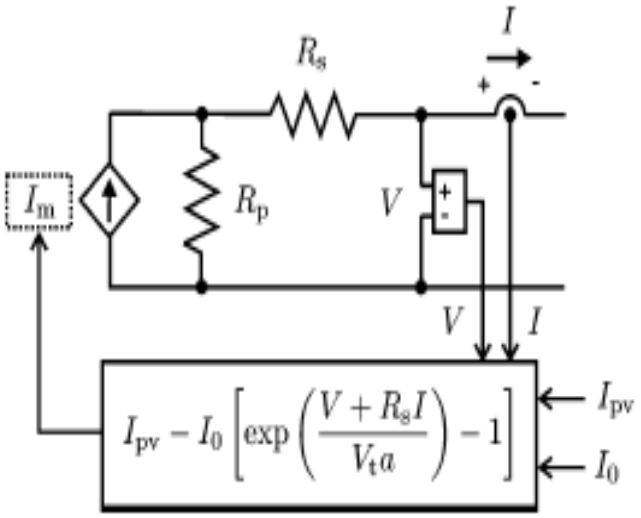

Figure (2.7) Circuit model of the photovoltaic module by MATLAB

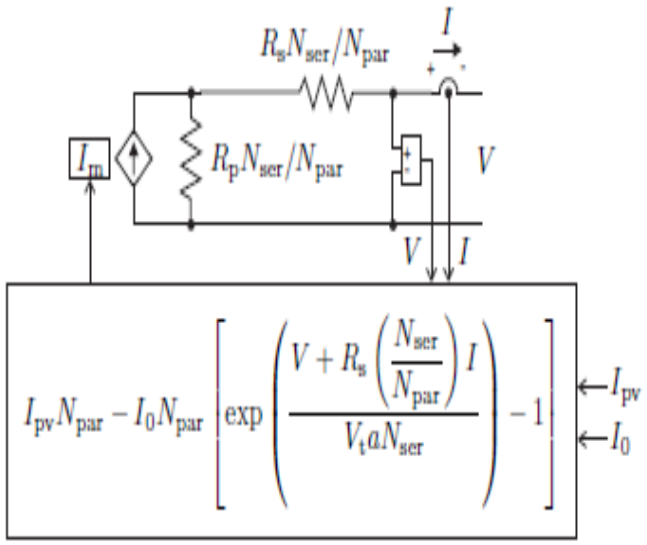

Figure (2.8) Circuit model of the photovoltaic array by MATLAB

2.6 Factors Affecting the PV characteristic

To understand characteristic of photovoltaic, several factors must be taken into considerations which are:

2.6.1 Temperature effect

A PV module's temperature has a great effect on its performance. It is observed that the temperature mainly affects the terminal voltage; it increases with decreasing temperature as. This is somewhat surprising as one would typically expect the PV array to operate more efficient as temperature increases. However, one of the reasons the PV array operates more efficient with decreasing temperature is due to the gap energy of semiconductor materials varies with temperature. An increase in temperature will cause the band gap energy of the material increase. With higher band gap energy, the electrons in the valence band will require more energy from the photons to move to the conduction band. This means that a lot more photons will not have sufficient energy to be absorbed by the electrons in the valence band resulting in fewer electrons moving to the conduction band and a less efficient solar cell [37].

2.6.2 Irradiance effect

PV array are only effective as the amount of energy that can produce. Because PV array rely on conditions that are never constant, the amount of power extracted from a PV module can be very inconsistent. Irradiance is an important changing factor for a solar array performance. It is used to describe the density of the radiation incident on a given surface. In PV system, it is the amount of solar energy that is absorbed by the array over its area. Irradiance is expressed typically in watt per square meter (W/m^2). Given ideal conditions, a PV array should obtain an irradiance of 100 W/m^2 up to 1000 W/m^2. Unfortunately, this value that is obtained by a PV array will vary greatly depending on geographic location, angle of the sun …

The output of PV array is directly proportional to irradiance. This makes sense where by the principle of operation of the solar cell the generated current is proportional to the flux of photons. When the irradiance or light intensity is low, the flux of photon is less. When the sun is bright, the light intensity is high, more current is generated. The change in

voltage is minimal with varying irradiance and for most practical application; the change is considered negligible [9].

2.6.3 Shading effect

Performance of a series connected string of solar cells is adversely affected if all its cells are not equally illuminated (partially shaded). In a PV array spread over vast area, it is likely that shadow may fall over some of its cells due to tree leaves falling over it, birds on the array, shade of a neighboring construction etc. In a series connected string of cells, all the cells carry the same current. Even though a few cells under shade produce less photon current but these cells are also forced to carry the same current as the other fully illuminated cells. The shaded cells may get reverse biased, acting as loads, draining power from fully illuminated cells. If the system is not appropriately protected, hot-spot problem can arise and in several cases, the system can be irreversibly damaged. To overcome this problem a bypass diodes offer an easy current path around any shaded cells. Ideally there would be one bypass diode for each solar cell, but this is rather expensive. Many PV modules therefore incorporate one diode per small group of cells as shown in figure (2.9) [38].

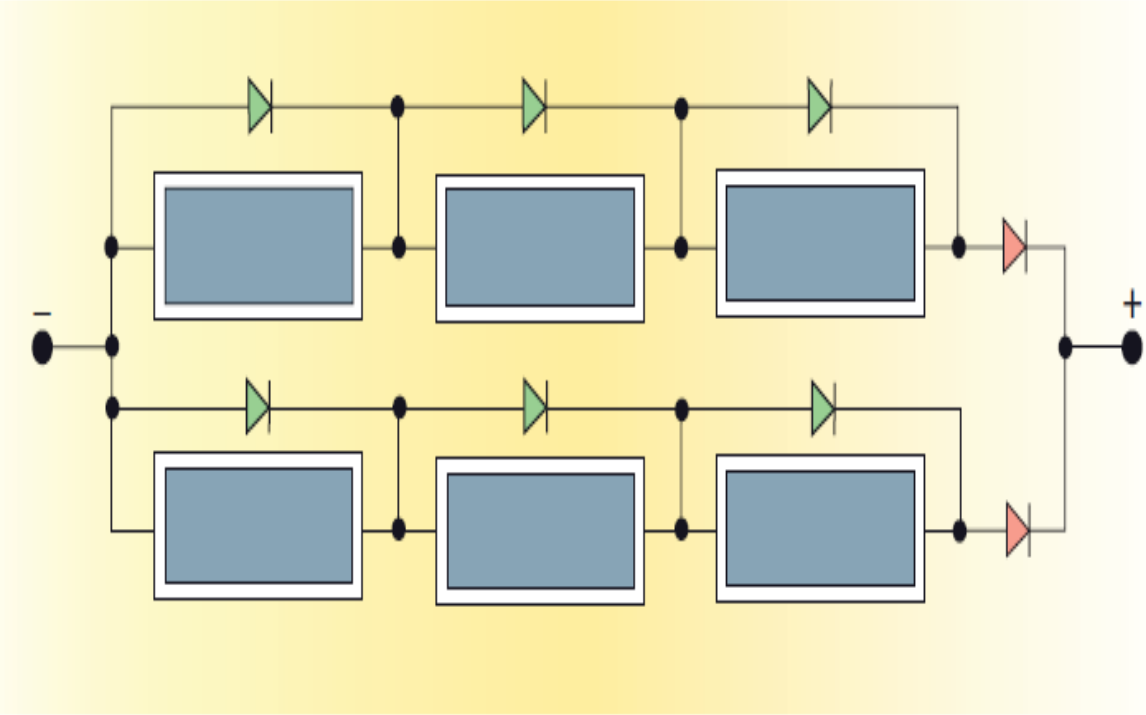

Figure (2.9) an array with 6 modules with bypass diodes

2.6.4 Reflection effect

A photon can be reflected, absorbed or it can pass through a semiconductor. Since only the photons that are absorbed contribute to the electrical energy, it is important to reduce the percentage of photons that are reflected. An anti-reflective coating is usually applied to the surface of the solar cell to decrease the number of photons that are reflected [38].

2.7 KC200GTS PV Module and Array Electrical Characteristics

A simulation is done by Matlab Simulink for PV which shows the effect of solar irradiation and temperature on the characteristics of PV module and array. To investigate the effect of solar irradiation on the currents and voltages of the module, temperature was held constant at 25 °C and the resulting I-V and P-V characteristics were plotted. Figure (2.10), (2.11) shows the I-V, P-V characteristics of the module at different irradiation levels of 200, 400, 600, 800 and 1000 W/m^2 respectively. It is noticed that the output current is directly proportional to the changes in solar irradiation as expected from the model. However, the open circuit voltage does not change significantly.

To find out the effect of temperature on the module performance, solar irradiation level was assumed constant at 1000 W/m^2 while allowing temperature to vary between 10 and 70 °C. The result is shown in figures (2.12) and (2.13) for the I-V and P-V characteristics as temperature was set to 10, 30, 50 and 70 °C respectively. The open circuit voltage of the module decreases as surface temperature increases. Current, on the other hand, increases slightly with temperature. The maximum output power of the module decreases as the surface temperature increases.

The simulated PV array used consists of 2 series and 3 parallel modules. The array I-V and P-V characteristics at five different values of irradiance and temperature are shown in figures (2.14), (2.15), (2.16) and (2.17) respectively.

A locus of MPP at different temperature and irradiation level is shown; it can be observed that MPP is varying and not a fixed point, as PV is working at different condition. So that the MPPT is needed to track the MPP to insure that the maximum power is extracted from the PV module or array all the time.

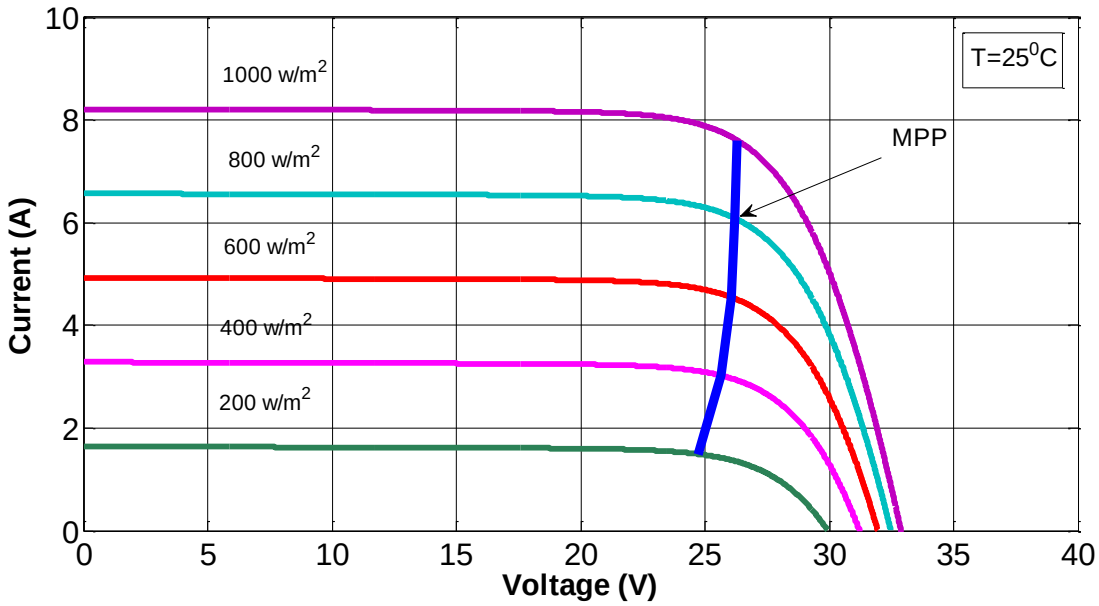

Figure (2.10) I-V Characteristics of PV module at constant temperature and varying irradiance

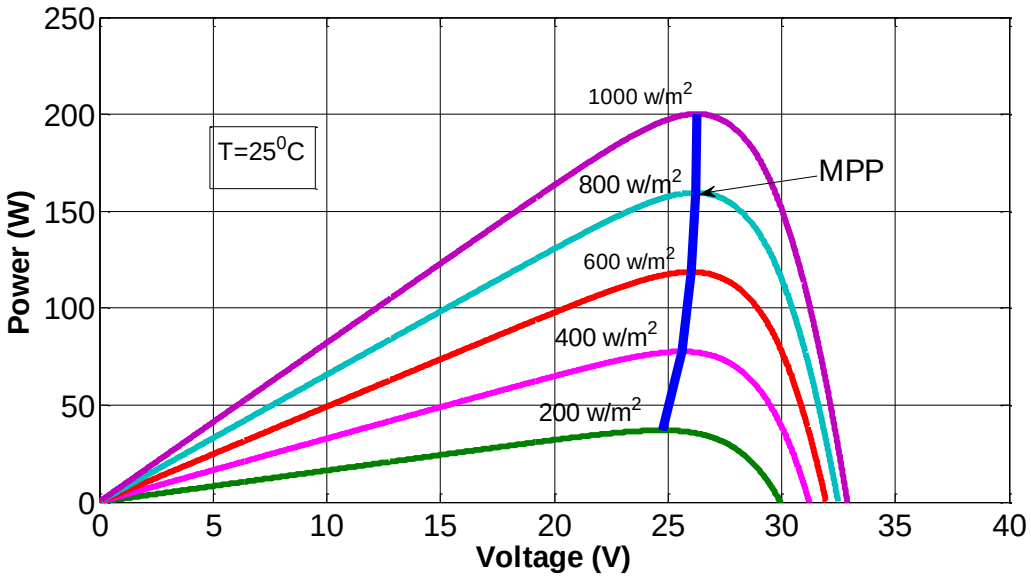

Figure (2.11) P-V Characteristics of PV module at constant temperature and varying irradiance

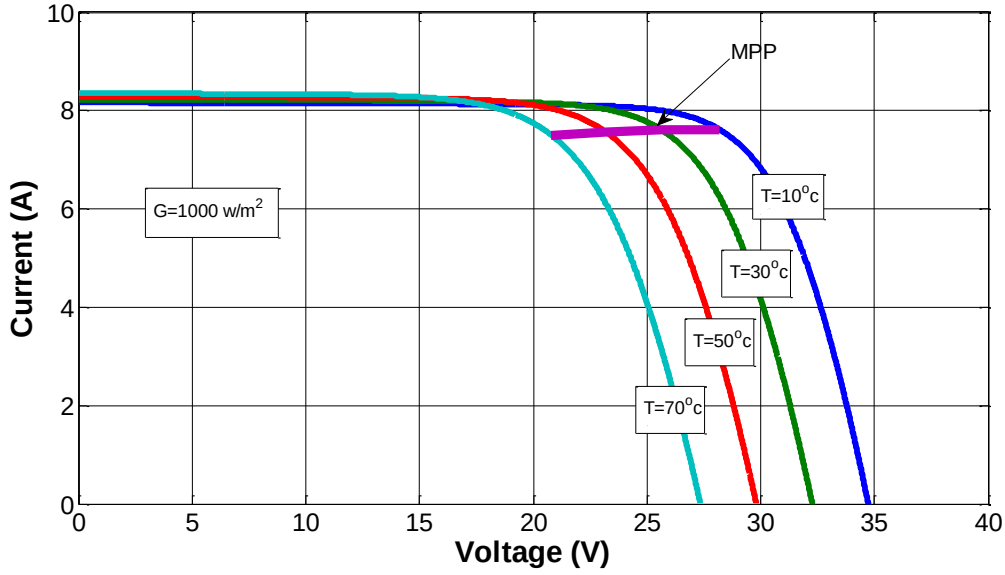

Figure (2.12) I-V Characteristics of PV module at varying temperature and constant irradiance

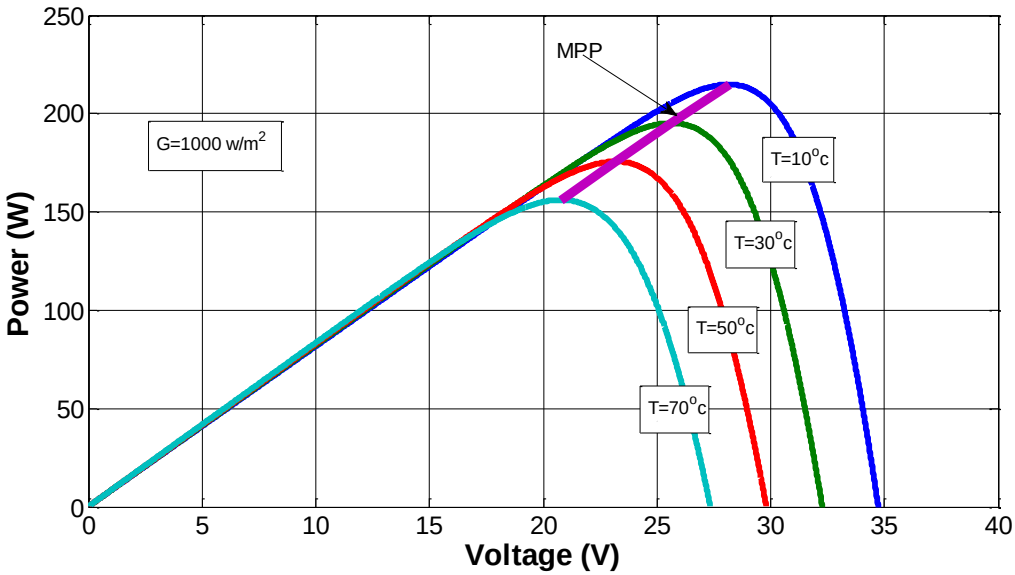

Figure (2.13) P-V Characteristics of PV module at varying temperature and constant irradiance

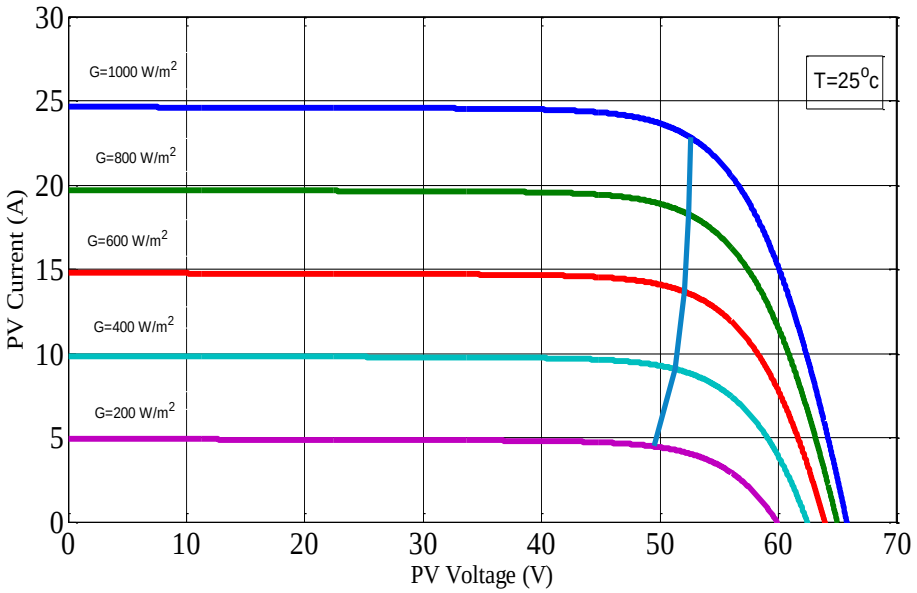

Figure (2.14) I-V Characteristics of PV array at constant temperature and varying irradiance

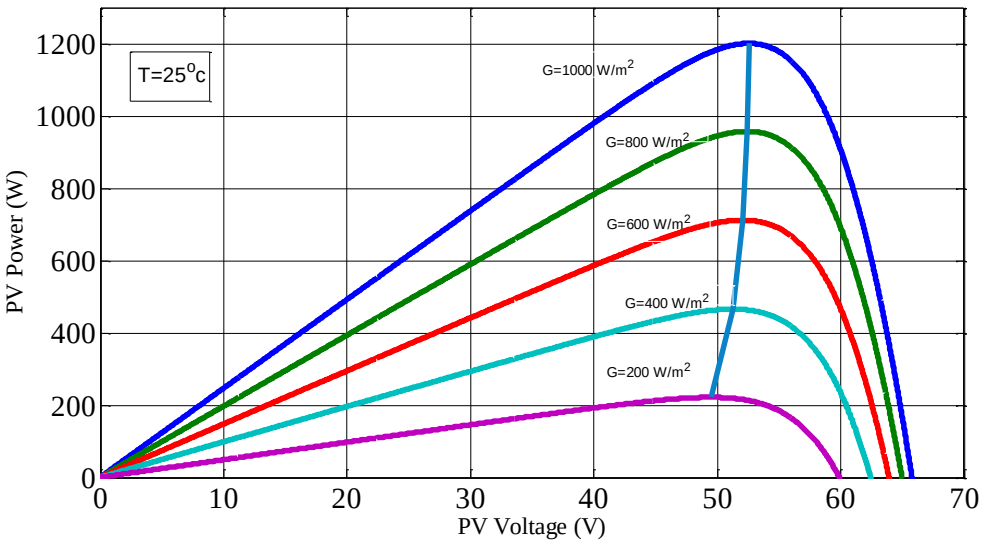

Figure (2.15) P-V Characteristics of PV array at constant temperature and varying irradiance

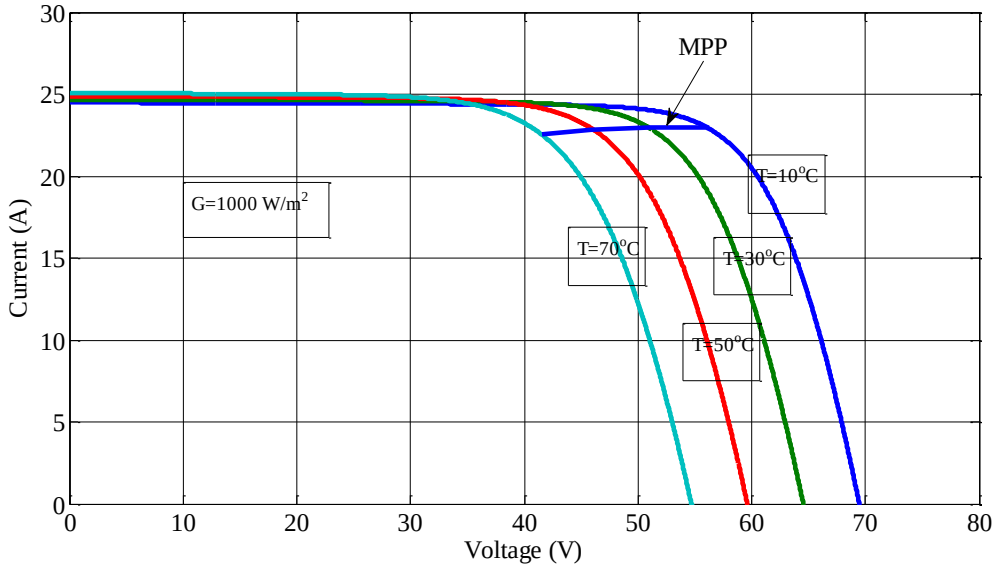

Figure (2.16) I-V Characteristics of PV array at varying temperature and constant irradiance

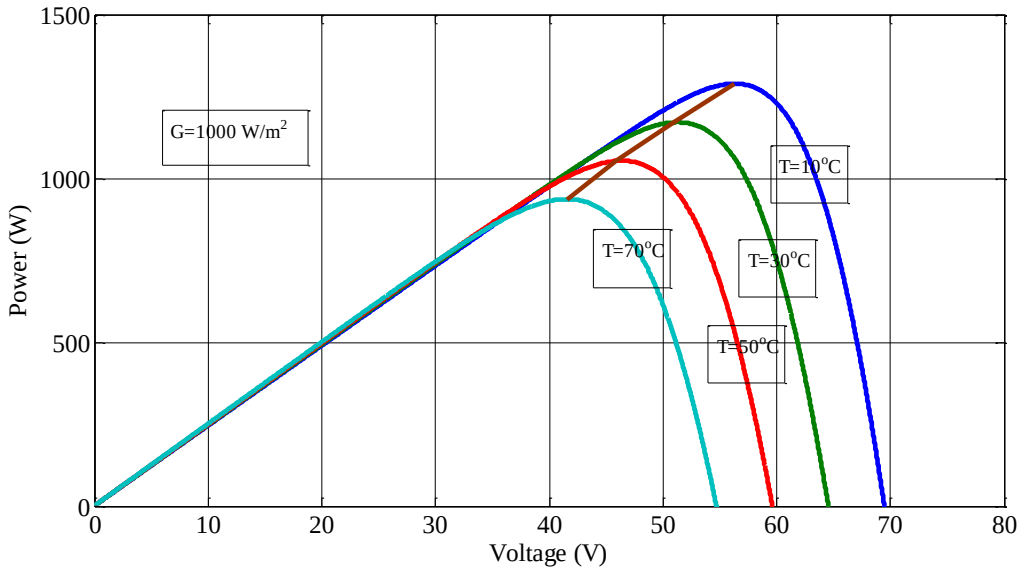

Figure (2.17) P-V Characteristics of PV array at varying temperature and constant irradiance

CHAPTER (3)

MAXIMUM POWER POINT TRACKER

CHAPTER (3)

MAXIMUM POWER POINT TRACKER

3.1 Introduction

PV systems have been rapidly used in many electrical power applications. The main drawbacks of PV systems are high fabrication cost and low energy-conversion efficiency, which is partly caused by their nonlinear and temperature-dependent V–I and P–I characteristics. To overcome these drawbacks, three essential approaches can be followed [39]:

- Enhance processes of manufacturing of solar arrays.
- By using sun-tracking solar collectors as shown in figure (3.1) [40,41], to track the position of the sun which varies during the day.
- By using MPPT: to ensure operation of the PV array at its MPP, regardless of atmospheric conditions and load variations.

Figure (3.1) sun tracking PV module

This chapter discusses the I-V characteristics of PV module with load, matching between them, and need of MPPT including the use of DC-DC converters and pulse width

modulation (PWM) as a means of MPPT. Finally application of PV water pumping system is described.

3.2 Direct coupling of PV system

When a PV module is directly coupled to a load, the system operating point will be at the intersection of the I–V curve of the PV module and load line shown in figure (3.2). Where the operating point of PV can be any point in this curve [8,42].

In general, the operating point is not at the PV module MPP. Thus, in a direct coupled system, the PV module must usually be oversized to ensure that the load's power requirements can be supplied. This leads to an overly expensive system [43].

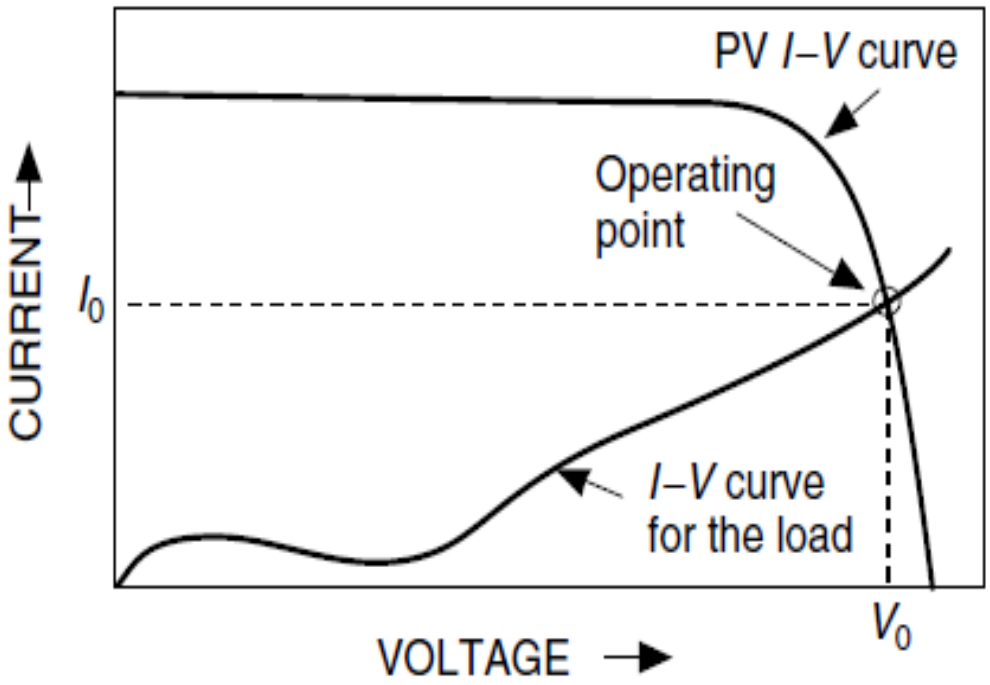

Figure (3.2) intersection point of the I-V curves for the load and PV

3.2.1 Resistive-Load Connection

To illustrate the importance and need for load curves, considering a variable resistive load (R) connected to a PV module as shown in figure (3.3). When plotting I-V curve, a straight line with a slope of 1/R is obtained and can be expressed by equation (3.1) [8]:

$$V = IR \qquad or \qquad I = \frac{1}{R}V \tag{3.1}$$

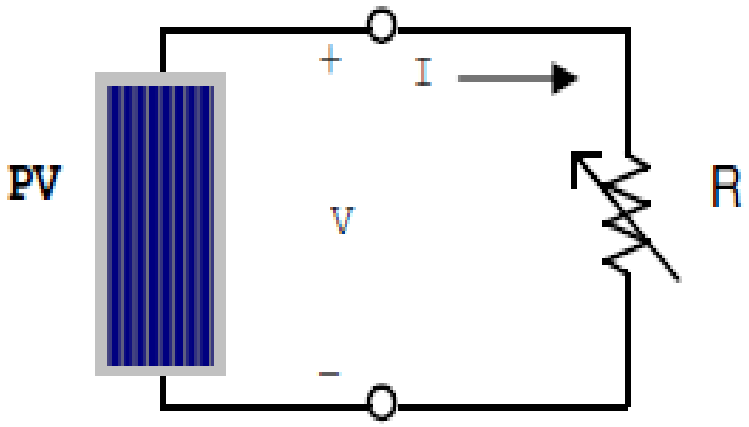

Figure (3.3) direct connection of PV to variable resistive load

As R increases, the operating point moves along the PV I-V curve from left to right as shown in figure (3.4). It can be observed that there is specific value of R called optimal resistance (R_{opt}), which operates at the MPP of the PV.

Since the delivered power to the load at MPP is equal to product of maximum current and voltage, then R_{opt} will be described as following [8]:

$$R_{opt} = \frac{V_{mp}}{I_{mp}} \tag{3.2}$$

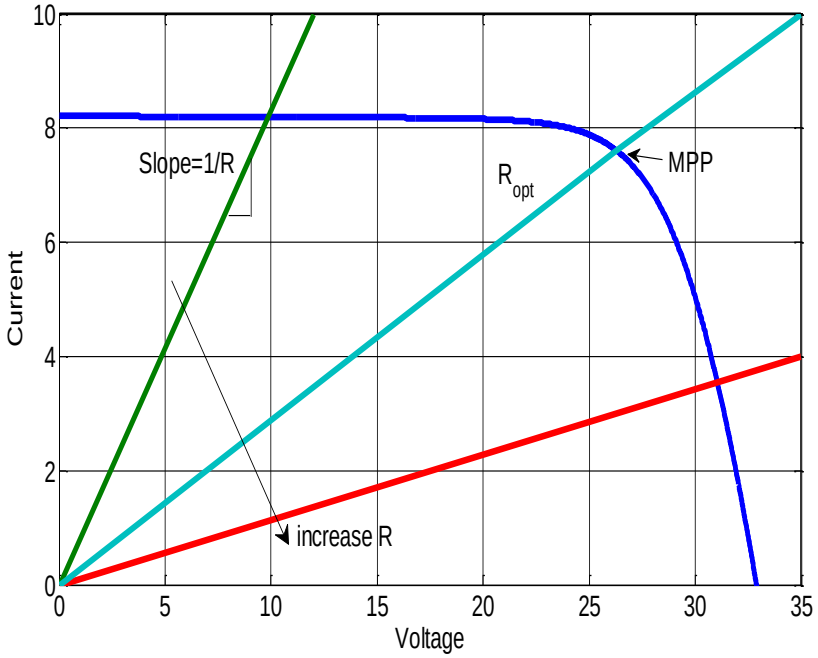

Figure (3.4) PV system operating points with varying resistive loads

Figure (3.5) shows that R_{opt} for irradiance 1000 W/m^2 and temperature 25^{o}C, is not the R_{opt} for other conditions. For example if there is change in irradiance conditions to be (800,600,400,200) W/m^2 then the operating point is far from MPP. This will lead to change load to satisfy R_{opt} of every change in environmental condition [8]. The MPPT system used to control the PV array's voltage or current independently of those of the load to ensure maximum power is extracted. A dc/dc converter acts as an interface between the load and the module [44,45].

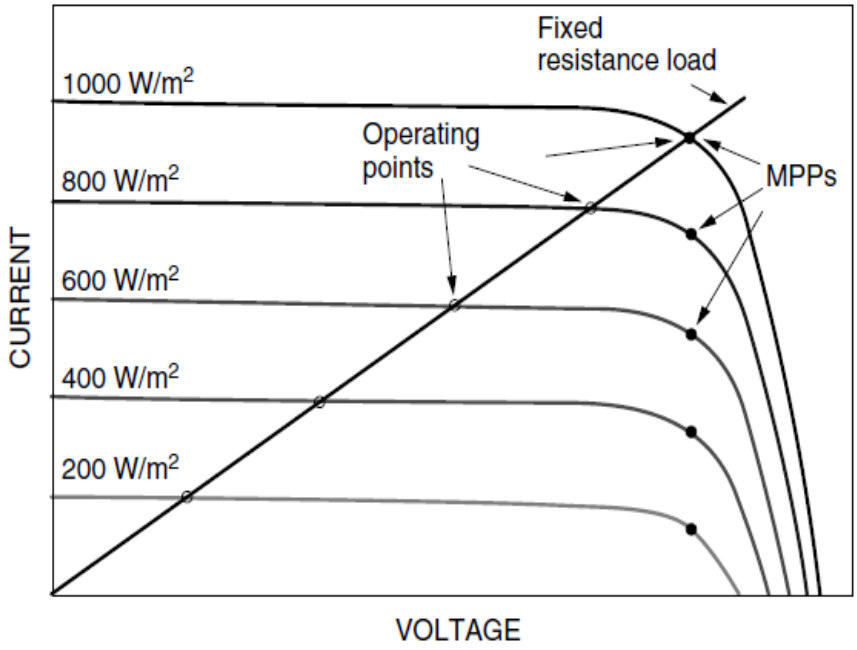

Figure (3.5) fixed load connected to PV at varying irradiance

3.3 DC/DC Converter

They are device that converts input dc voltage to a different output dc voltage level. Basic DC-DC converter topologies are the step-up or boost converter and the step-down or buck converter. Other designs such as Cuk and buck-boost converters are combinations of the two basic topologies [46,47]. In this thesis the work done by using boost converter.

3.3.1 Boost Converter

In this section the principles of boost converter is introduced and detail circuit is discussed in steady state. It consists of capacitors (C), an inductor (L), and a switch where values in appendix I. All these devices ideally do not consume any power, which is the

reason for the high efficiencies of switching converters. The switch is realized with a switched mode semiconductor device, which is a MOSFET. During the operation of the converter, the switch will be switched at a constant frequency (f_s) with an on-time (T_{on}) of DT_s, and an off-time (T_{off}) of $D'T_s$, where T_s is the switching period $1/f_s$, D is the duty ratio of the switch expressed by equation (3.3) and D' is (1 - D) as seen in figure (3.6) [46,47].

$$D = \frac{T_{on}}{T_s} = \frac{T_{on}}{T_{on} + T_{off}} \tag{3.3}$$

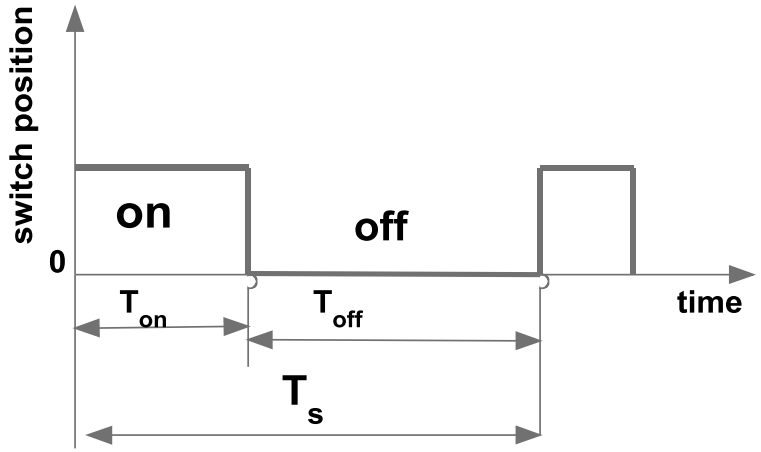

Figure (3.6) switching period

The equivalent circuit models of the boost converter along with its two states of the switch on and off are displayed in figures (3.7), (3.8), and (3.9) respectively

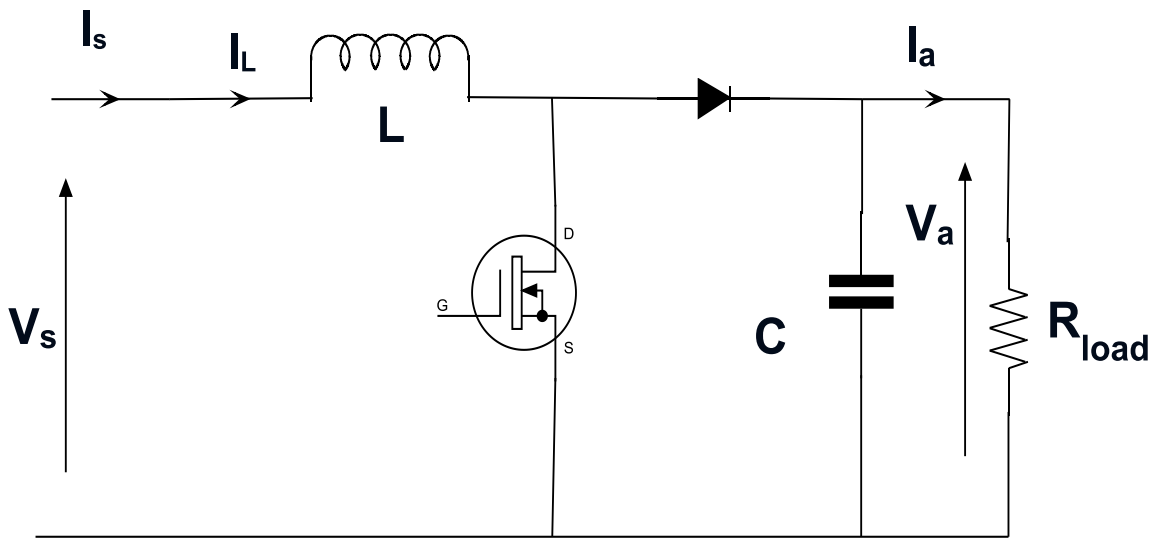

Figure (3.7) circuit diagram of boost converter

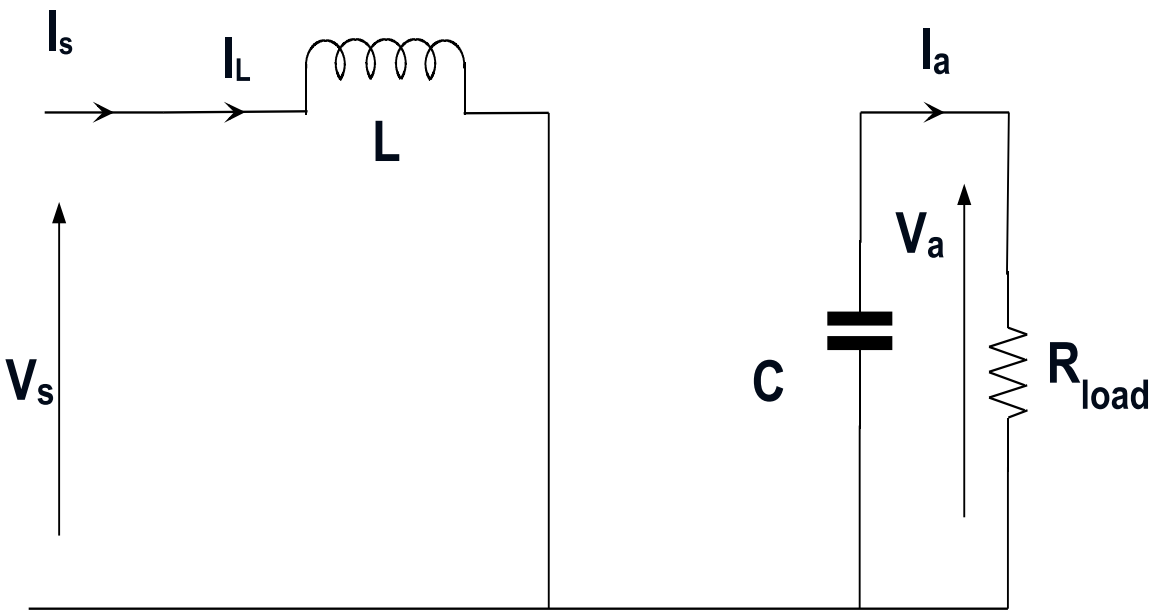

Figure (3.8) boost converter when switch is on

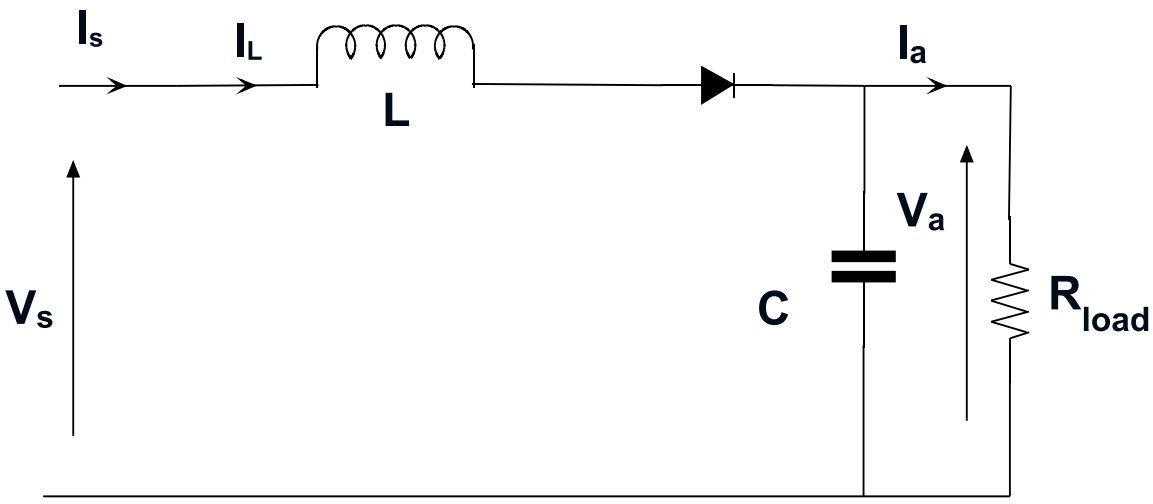

Figure (3.9) boost converter when switch is off

When the switch is in "on mode" and operating at $t = T_{on}$, the input current rises and flows through inductor L and the switch. The magnetic energy stored in the inductor can build up. The output stage is completely isolated because the diode is reverse biased, as shown in figure (3.8). When the switch is in "off mode", at $t = T_{off}$, the current flowing through the switch will now flow through towards the output stage because the diode becomes forward biased, as seen in figure (3.9). Moreover, the energy stored in the inductor will be released to the load [46].

3.3.2 Steady State Analysis

To investigate the boost converter and derive its steady-state transfer-functions, the equivalent circuit representation for the "on" and "off" states should be analyzed. the waveform of current and voltage are shown in shown figure (3.10), a set of the following equations can be derived from [46] assuming that current rises or falls linearly:

At time T_{on} inductor current rises linearly from I_1 to I_2,

$$V_s = L\frac{I_2 - I_1}{T_{on}} = L\frac{\Delta I}{T_{on}} \tag{3.4}$$

Where

- V_s is the input voltage of boost converter.

$$\Delta I = \frac{V_s T_{on}}{L} \tag{3.5}$$

At time T_{off} inductor current falls linearly from I_2 to I_1,

$$V_s - V_a = -L\frac{\Delta I}{T_{off}} \tag{3.6}$$

Where

- V_a is the output voltage of boost converter.

$$\Delta I = -\frac{(V_s - V_a)T_{off}}{L} \tag{3.7}$$

Where $\Delta I = I_2 - I_1$ is the peak to peak ripple current of inductor L, from equation (3.5) and (3.7)

$$\Delta I = \frac{V_s T_{on}}{L} = \frac{(V_s - V_a)T_{off}}{L} \tag{3.8}$$

By substituting $T_{on}= DT_s$ and $T_{off} = (1-D)*T_s$ in equation (3.8) then the average output voltage is equal to

$$V_a = V_s \frac{T}{T_{off}} = \frac{V_s}{(1-D)} \tag{3.9}$$

It can be seen from equation (3.9) that the output voltage increases as D increases. Then boost converter is capable of producing any output voltage greater than the input voltage.

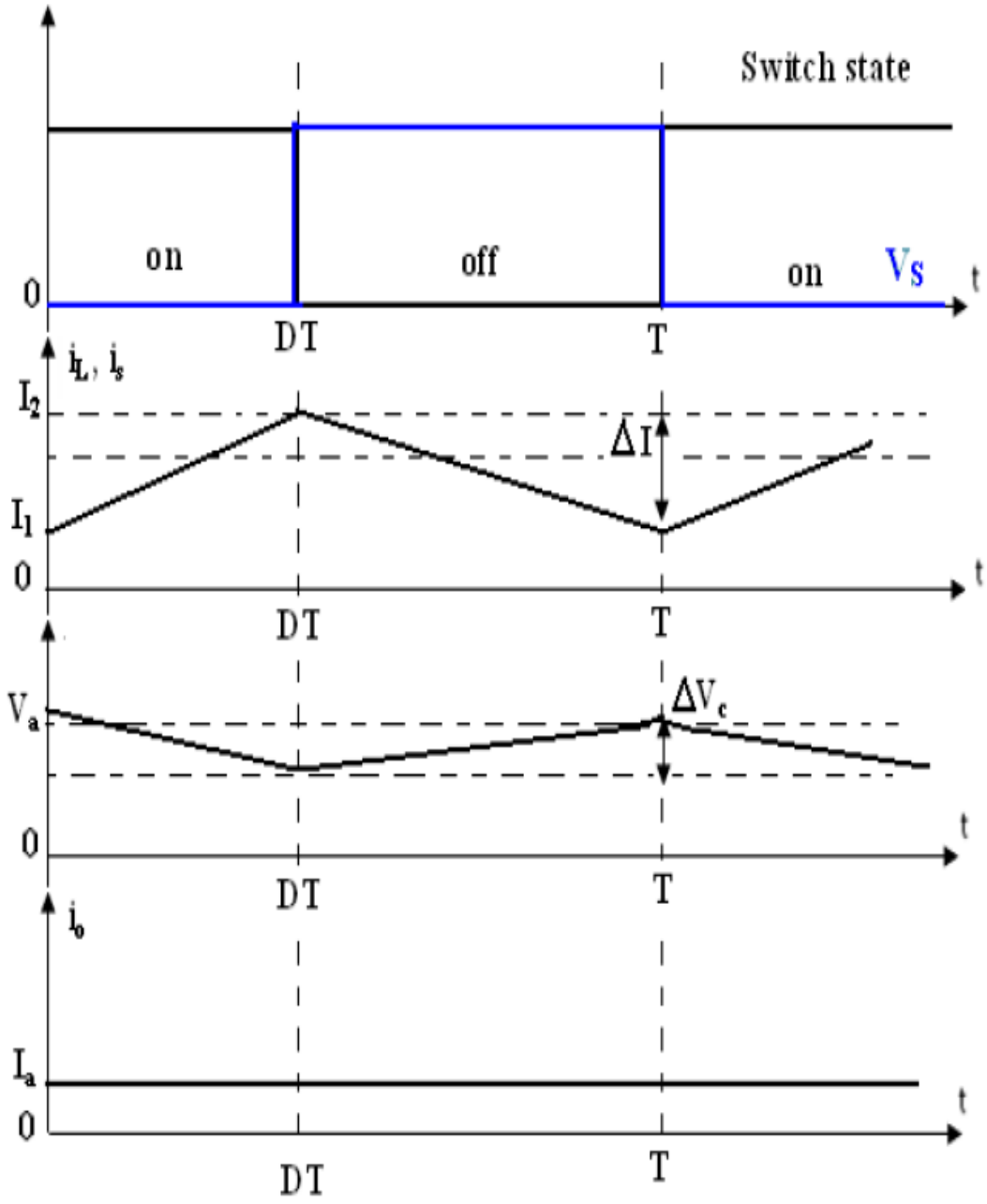

Figure (3.10) output waveform of boost converter

3.3.3 Continuous and discontinuous current mode

The DC-DC converters can have two distinct modes of operation [46,47]:

- Continuous current mode (CCM), inductor current never falls to zero in one switching cycle.
- Discontinuous current mode (DCM), the inductor current falls to zero before completing one switching cycle.

To make boost converter operates in CCM then the minimum value of the filter capacitance $C > C_{min}$:

$$C_{min} = \frac{D}{2R_{load}\mathrm{f}_s} \tag{3.10}$$

The minimum value of inductor is where $L > L_{min}$:

$$L_{min} = \frac{(1-D)^2\, DR_{load}}{2\mathrm{f}_s} \tag{3.11}$$

Where

- R_{load} is the load impedance (Ω).

3.4 Mechanism of Load Matching

As described in Section 3.2, when PV is directly coupled with a load, the operating point of PV is dictated by the load. DC/DC converter is used as an interface between the PV array and the load to perform the MPPT process and the load matching R_{load} is equal to R_{opt} of PV [44].

The following is an example of load matching using an ideal (loss-less) boost converter, then [44,46]:

$$I_s V_s = I_\mathrm{a} V_\mathrm{a} \tag{3.12}$$

Where

- I_a is the output current of the boost converter.

- I_s is the input current of the boost converter.

From equation (3.9) and (3.12) we can get

$$\frac{I_a}{I_s} = \frac{V_s}{V_a} = 1 - D \tag{3.13}$$

The input impedance (R_{in}) of boost converter is then:

$$R_{in} = \frac{V_s}{I_s} = (1-D)^2 \frac{V_a}{I_a} = (1-D)^2 R_{load} \tag{3.14}$$

As shown in figure (3.11), the impedance seen by PV is the input impedance of the converter (R_{in}). By changing the duty cycle, the value of R_{in} can be matched with that of R_{opt}. Therefore, the impedance of the load can be anything as long as the duty cycle is adjusted according to that as shown in figure (3.12).

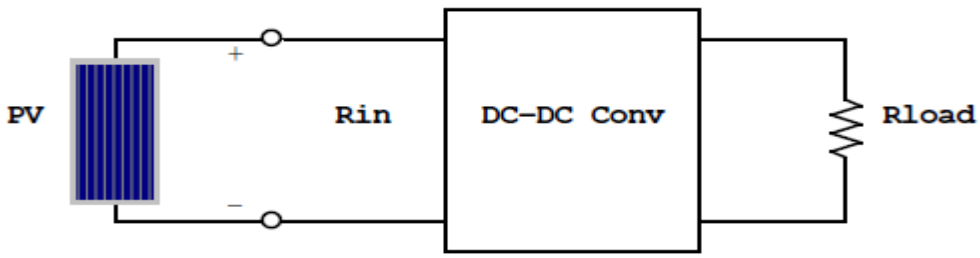

Figure (3-11) the impedance seen by PV is R_{in} that is adjustable by duty cycle

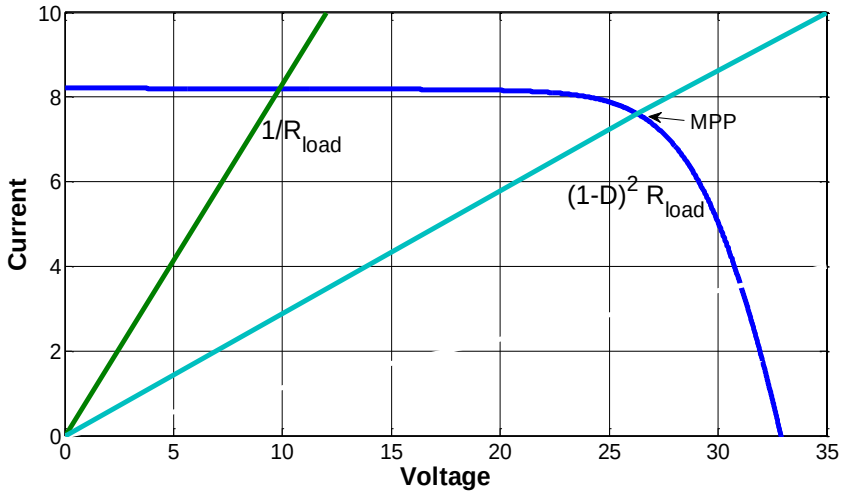

Figure (3.12) load resistance with and without boost converter

3.5 Pulse Width Modulation

The duty cycle D can be varied from 0 to 1 by varying T_{on}, T_s or f_s. Therefore controlling D can be controlled by [46]:

- Constant frequency operation: the converter, or switching f_s is kept constant and T_{on} is varied. Then width of the pulse is varied and this type known PWM. Therefore PWM waves are generated when a constant frequency signal (carrier signal) is compared with another signal (modulating signal) and the result is output as shown in figure (3.13). The output of MPPT algorithm is compared with the saw tooth waveform to generate a PWM signal for the boost converter to control D for load matching.
- Variable frequency operation: the converter, or switching, f_s is varied. Either T_{on} and T_{off} is kept constant. This called frequency modulation. This type of control would generate harmonics at unpredictable frequencies and filter design would be difficult.

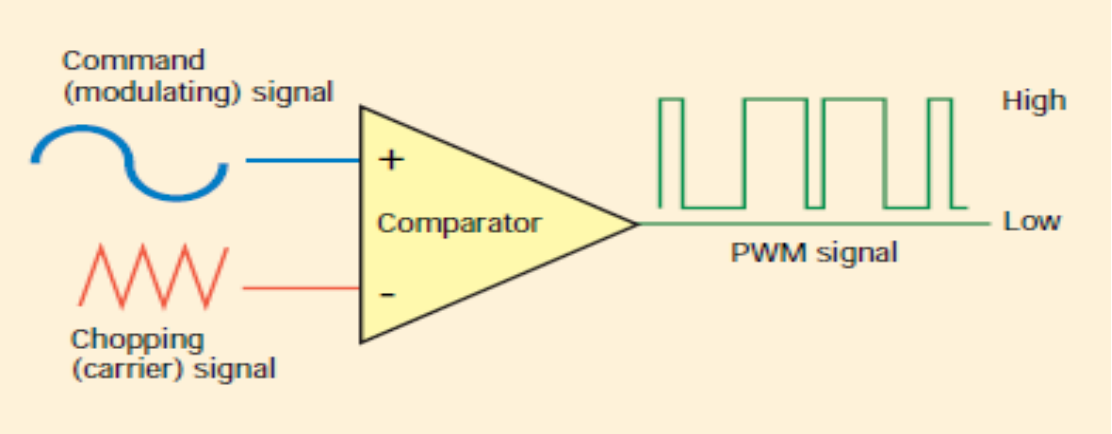

Figure (3.13) PWM diagram

3.6 PV Water Pumping System

While it is not often that a load would be an actual resistor, an application of dc motors, such as those often used in PV water pumping systems is studied. PV pumping system is used to ensure water supply in remote areas because no electricity supply is available.

A dc motor-pump set can be connected directly to the PV module as is the case with most commercial dc PV pumping systems. A comprehensive study for the starting and

steady state performance of dc motors (Permanent-Magnet, series and shunt) directly coupled to PV generators is given in [48]. In [49] it is concluded that a separately excited dc motor driving a centrifugal pump is the best candidate as far as better matching to the PV system.

In general, two types of pumps are commonly used for water-pumping applications. One is positive displacement pump and another is centrifugal pump. In displacement pumps, the water output is directly proportional to the speed of the pump, but almost independent of head. These pumps are used for solar water pumping from deep wells or bores. Centrifugal pumps are used for low-head applications, especially if they are directly interfaced with the solar panels. Centrifugal pumps are designed for fixed-head applications, and the pressure difference generated increases in relation to the speed of the pump. Centrifugal pumps also have relatively high efficiency and are capable of pumping a high volume of water [50].

3.6.1 System Configuration

In this thesis different configuration of PV water pumping system is studied:

- The first configuration is the directly coupled system, where a PV array is directly coupled to a DC motor and a pump.
- The second configuration is PV pumping system with DC motor using MPPT to improve the efficiency of the system as shown in figure (3.14).

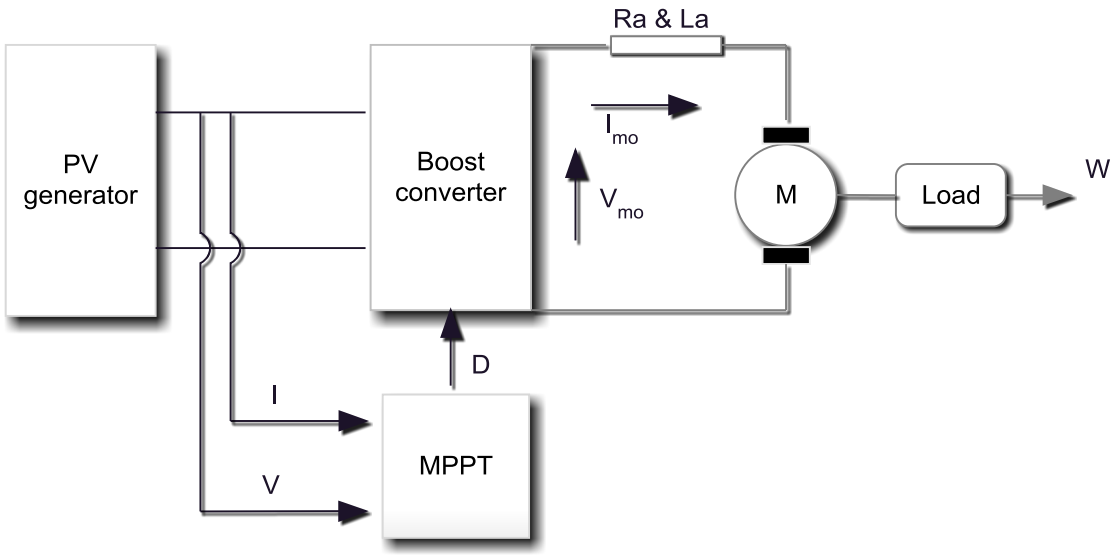

Figure (3.14) water pumping system with MPPT

3.6.2 DC motor & pump characteristic

Separately excited dc motor differential equations which describe the motor voltage and its torque are given as in equation (3.15) and (3.16) respectively. Also the centrifugal pump load equation is given as in (3.17) [49,51].

$$V_{mo} = I_{mo}R_{\mathrm{a}} + L_{\mathrm{a}}\frac{dI_{mo}}{dt} + K_3 w \tag{3.15}$$

$$T_m = A_3 + B_1 w + J\frac{dw}{dt} + T_{load} \tag{3.16}$$

$$T_{load} = A_2 + \in w^{1.8} \tag{3.17}$$

Where

- V_{mo} is armature voltage (V).
- I_{mo} is armature current (A).
- w is rotor speed (rpm).
- J is rotor inertia ($Kg.m^2$).
- R_a is armature resistance (Ω).
- L_a is armature inductance (H).
- K_3 is back emf constant ($Nm.A^{-1}$).
- A_3 motor friction (Nm).
- A_1 is load friction (Nm).
- B_1 is damping ($Nm.s.rad^{-1}$)
- $\in$ is load torque constant ($Nm.s.rad^{-1}$).
- T_m is motor torque (Nm).
- T_{load} is load torque (Nm).

The name-plate parameters of motor and pump are taken from [51] and found in appendix I.

CHAPTER (4)

FUZZY AND P&O ALGORITHMS

CHAPTER (4)

FUZZY AND P&O ALGORITHMS

4.1 Introduction

The field of fuzzy control developed by Lotfi Zadeh's dissatisfaction with the direction that control theory began to head during the 1950s and 1960s. He believed that, the control theory was becoming increasingly complex and mathematical, while neglecting the importance of practicality and applicability to real-world control problems. He suggested that his idea of fuzzy set theory, developed in 1965, might be useful in addressing his concerns about conventional control theory.

It offers a soft computing partnership with important concept of computing with words. It provides a technique to deal with imprecision and information granularity. The fuzzy theory provides a mechanism for representing linguistic constructs such as "many", "low", "medium", "often", "few". In general, the fuzzy logic provides an inference structure that enables appropriate human reasoning capabilities. On the contrary, the traditional binary set theory describes crisp events, events that either do or do not occur. It uses probability theory to explain if an event will occur, measuring the chance with which a given event is expected to occur [52].

Generally, in this chapter a brief discussion about FLC, the use of FLC algorithm to track MPP of PV and explanation of P&O algorithm with its advantage and disadvantage.

4.2 Advantage and Disadvantage of Using FLC

FLC offers several unique features that make it a particularly good choice for many control problems [53]:

- Fuzzy logic is conceptually easy to understand.
- Fuzzy logic is flexible.
- Fuzzy logic is tolerant of imprecise data.
- Fuzzy logic can model nonlinear functions of various complexity.
- Fuzzy logic can be blended with conventional control techniques.
- Fuzzy logic can be expressed by linguistic values.

- Fuzzy logic is based on natural language.

However , its disadvantage that their effectiveness depends a lot on the knowledge of the user or control engineer in choosing the right error computation and coming up with the rule base table [14].

4.3 Fuzzy logic Application Areas

Fuzzy systems have been used in a wide variety of applications in engineering, some potential application are [53,54]:

- Aircraft/spacecraft: Flight control, engine control, avionic systems, failure diagnosis, navigation, and satellite attitude control.
- Automated highway systems: Automatic steering, braking, and throttle control for vehicles.
- Automobiles: Brakes, transmission, suspension, and engine control.
- Manufacturing systems: Scheduling and deposition process control.
- Power industry: Motor control, power control/distribution, and load estimation.
- Process control: Temperature, pressure, and level control, failure diagnosis, distillation column control, and desalination processes.
- Robotics: Position control and path planning.

4.4 Classical Sets versus Fuzzy Sets

A classical (crisp) set is defined in such a way that all the individuals in a given universe can be divided into two classes: those who belong to the set, and those who do not belong to the set. This leads to the definition of a characteristic function $X_f(x)$ that expresses the membership of a given element x in the set F. If x is a member of F, then the characteristic function evaluated at x is exactly one; conversely, if x is not a member of F then the characteristic function evaluated at x is exactly zero. In mathematical terms, the characteristic function is expressed as [54]:

$$X_F(x) = \begin{cases} 1 & x \in F \\ 0 & x \notin F \end{cases} \quad (4.1)$$

The fundamental difference between classical set theory and fuzzy set theory is that instead of defining the elements x in the universal set X as being absolutely a member or

not a member of set A, fuzzy sets allow the elements to have a degree of membership in fuzzy set A. This is achieved by replacing the characteristic function $X_A(x)$ by a membership function, which is allowed to have values in the continuous range [0,1]. This membership function for a fuzzy set A is symbolized by $\mu_A(x)$, so that $\mu A(x_1) = 0$ denotes that x_1 is completely not a member of A, while $\mu_A(x_2) = 1$ denotes that x_2 is completely a member of A. The difference comes when it is expressed that $\mu_A(x_3) = 0.57$, which indicates that x_3 has partial membership in the fuzzy set A. This can be represented mathematically as follows:

$$\mu_A(x) \in [0,1] \qquad (4.2)$$

An example of a graphic for the membership function of a crisp set and fuzzy set is illustrated in figure (4.1).

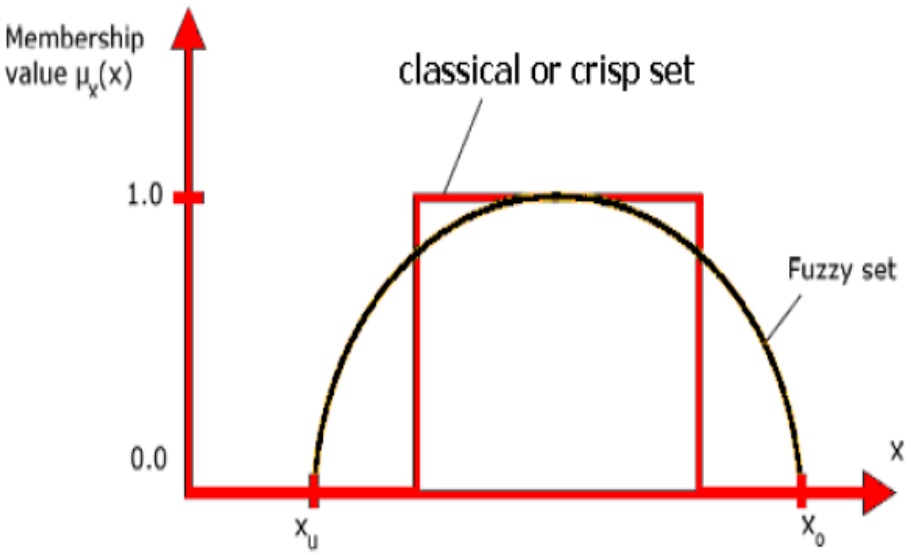

Figure 4.1 fuzzy and classical sets

4.4.1 Membership Function

Every fuzzy set can be represented by its membership function. The membership function could be defined as a graphical representation of the quantity of participation of the inputs. It associates a weighting with each of the inputs that are processed. The selection of a suitable shape of membership function for a fuzzy set is one of the most important activities in fuzzy logic. It is the responsibility of the user to select a function that is a best representation for the fuzzy concept to be modeled. Different shapes of

membership functions exist. Figure (4.2) shows the most common shapes used to describe the membership functions [54]:

- Triangular MF
- Trapezoidal MF
- Gaussian MF
- Generalized bell MF

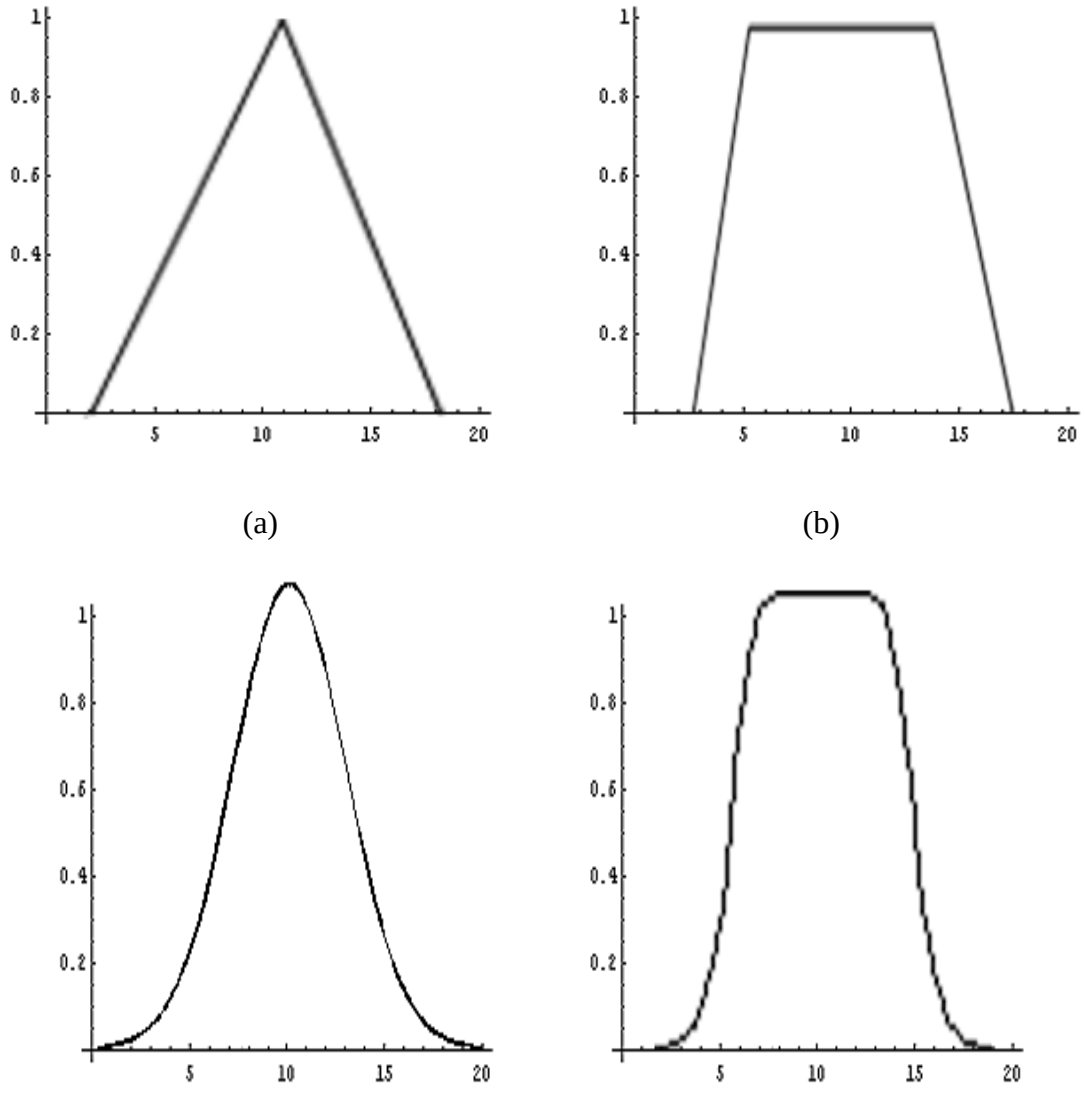

(a) (b)

(c) (d)

Figure (4.2) Different shapes of membership functions (a) triangular, (b) Trapezoidal, (c) Gaussian, (d) Generalized bell

4.5 Basic Operations

Basic operations of sets in classical set theory are the set complement, set intersection, and set union. Fuzzy set operations are very important because they can describe the relation between variables. For a given element X of the universe, the following function theoretic operations of fuzzy set for complement, intersection, and union are defined [55,56]:

4.5.1 Complement (NOT)

Consider a fuzzy set A in universe X. Its complement A as displayed in figure (4.3).

$$\mu_{\bar{A}}(x) = 1 - \mu_A(x) \tag{4.3}$$

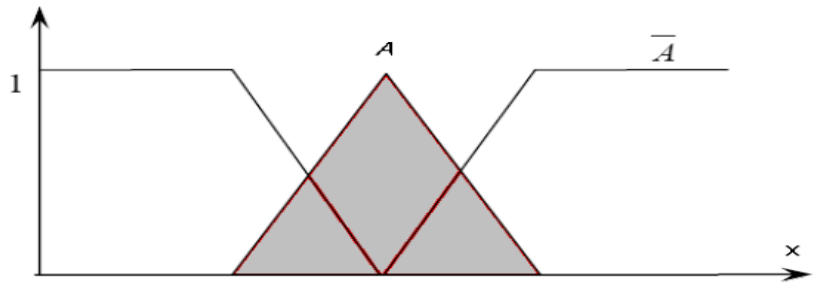

Figure (4.3) Complement of fuzzy sets A

4.5.2 Intersection (AND)

Consider two fuzzy sets A and B, as shown in figure (4.4), in the same universe X.

$$\mu_{A\cap B}(x) = \mu_A \cap \mu_B = min[\mu_A, \mu_B] \tag{4.4}$$

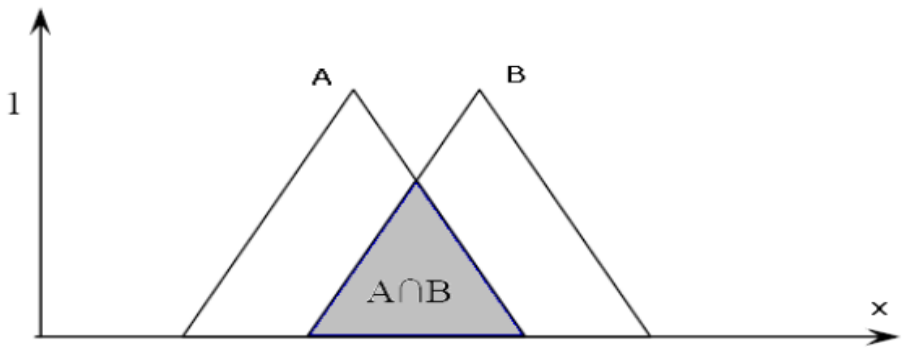

Figure (4.4) Intersection of fuzzy sets A and B

4.5.3 Union (OR)

Consider two fuzzy sets A and B in the same universe X. AU B is the whole area covered by the sets as shown in figure (4.5)

$$\mu_{AUB}(x) = \mu_A \cup \mu_B = max[\mu_A, \mu_B] \quad (4.5)$$

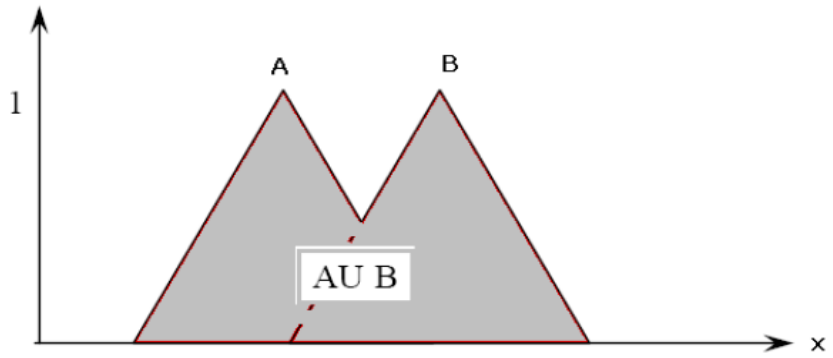

Figure (4.5) Union of fuzzy sets A and B

4.6 linguistic variables

In mathematics variables usually assume numbers as values. A linguistic variable is a variable that assumes linguistic values which are words (linguistic terms) [53]. For example, we have the linguistic variable "temperature", the linguistic values for it could be "cold", "warm", and "hot". These linguistic values possess a certain degree of uncertainty or vagueness that can be expressed by a membership function to a fuzzy set as shown in figure (4.6).

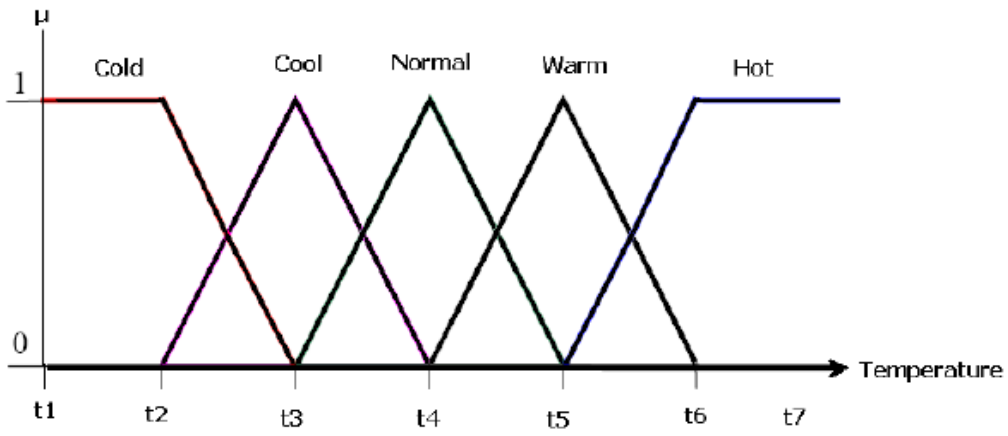

Figure (4.6) Universe of discourse for linguistic variable: temperature.

4.7 FLC Structure

FLC is composed of main three parts as shown in figure (4.7) [54,57]:

- Fuzzification interface
- Knowledge base and inference engine
- Defuzzification interface.

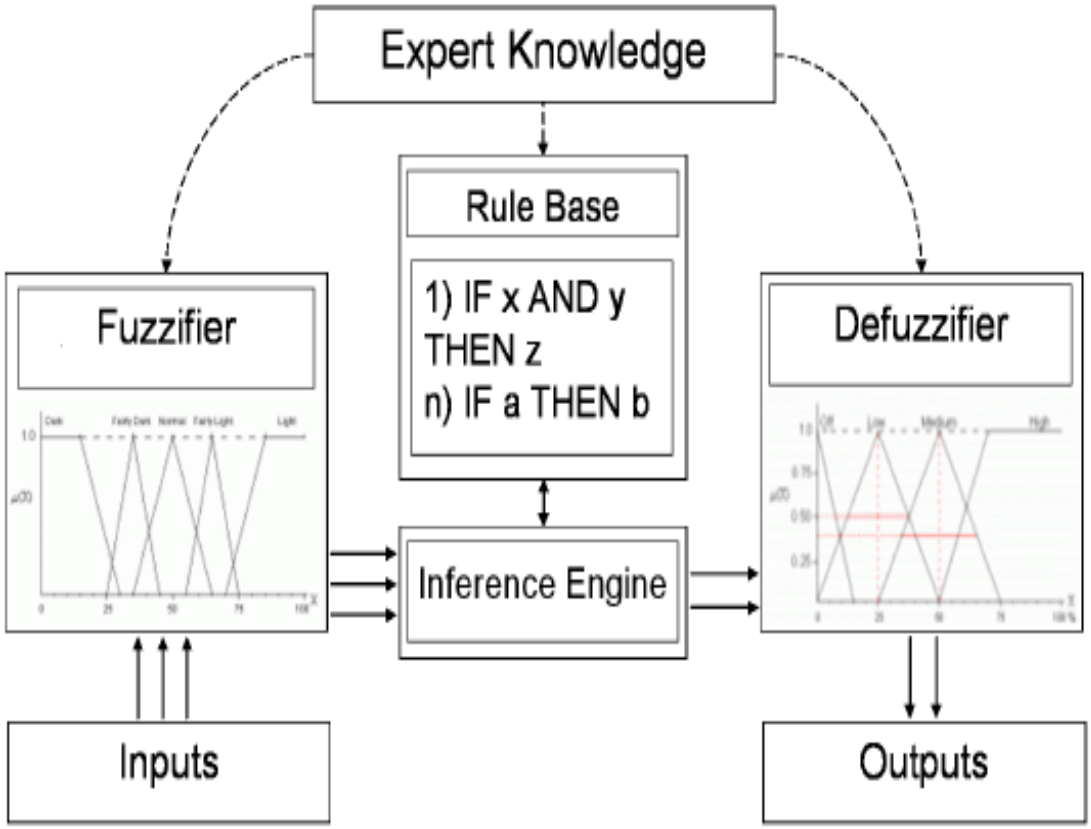

Figure (4.7) Basic parts of a Fuzzy Controller

4.7.1 FUZZIFICATION

The first step towards designing a FLC is choosing appropriate inputs which will be fed to the system. These input variables should be such that, they represent the dynamical system completely. Then the function of the fuzzifier comes into picture. As discussed before, instead of using numerical variables, fuzzy logic uses linguistic variables for processing information. This function of converting these crisp sets into fuzzy sets (linguistic variables) is performed by the fuzzifier. So fuzzification is the process of translating crisp input values into fuzzy linguistic values through the use of membership

functions. In other words, determining how much each discrete input value belongs to each input fuzzy set using the corresponding membership function [53].

4.7.2 Fuzzy Rule Base

In the field of artificial intelligence (machine intelligence) there are various ways to represent knowledge. Perhaps the most common way to represent human knowledge is to form it into natural language expressions of the type the IF–THEN rule-based form. If-then rule statements are used to formulate the conditional statements that comprise fuzzy logic [52]. A single fuzzy if-then rule assumes a form in the equation below:

if g is P then y is Q (4.6)

Where P and Q are linguistic values defined by fuzzy sets on the ranges (universes of discourse) g and Y, respectively. The if-part of the rule "x is A" is called the antecedent or premise, while the then-part of the rule "y is B" is called the consequent or conclusion. In general, one rule alone is not effective. Two or more rules that can be used are shown in table (4.1).

Table (4.1) the canonical form for a fuzzy rule base

Rule 1: IF condition C_1, THEN restriction R_1
Rule 1: IF condition C_2, THEN restriction R_2
.
.
.
.
Rule r: IF condition C_r, THEN restriction R_r

Where C_1,C_2,C_r are input conditions and R_1,R_2,R_r are the restrictions apply to the output actions. By using the basic properties and operations defined for fuzzy sets, any compound rule structure may be decomposed and reduced to a number of simple canonical rules; the

following illustrates the most common techniques for decomposition of linguistic rules involving multiple antecedents into the simple canonical [52,54].

(1) Multiple conjunctive antecedents:

This uses fuzzy intersection operation. Since it involves linguistic "AND" connective

$$\text{if g is } P_1 \text{ AND } P_2 \ldots\ldots \text{AND } P_n \text{ then y is Q} \tag{4.7}$$

Where the fuzzy set P_s is defined as

$$P_s = P_1 \cap P_2 \cap \ldots\ldots \cap P_n \tag{4.8}$$

Expressed by means of membership function

$$\mu_{p_s}(x) = mim\left[\mu_{p_1}(x), \mu_{p_2}(x), \ldots\ldots \mu_{p_n}(x)\right] \tag{4.9}$$

(2) Multiple disjunctive antecedents:

This uses fuzzy union operations. Since It involves linguistic "OR" connections

$$\text{if g is } P_1 \text{ OR } P_2 \text{ OR } \ldots\ldots \text{OR } P_n \text{ then y is Q} \tag{4.10}$$

Where the fuzzy set P_s is defined as

$$P_s = P_1 \cup P_2 \cup \ldots\ldots \cup P_n \tag{4.11}$$

Expressed by means of membership function

$$\mu_{p_s}(x) = max\left[\mu_{p_1}(x), \mu_{p_2}(x), \ldots\ldots \mu_{p_n}(x)\right] \tag{4.12}$$

(3) Conjunctive system of rules:

In the case of a system of rules that must be jointly satisfied, the rules are connected by ''and'' connectives. In this case, the aggregated output may be found by the fuzzy intersection of all individual rule consequents.

$$Q = Q_1\ AND\ Q_2\ AND\ \ldots\ldots AND\ Q_n \tag{4.13}$$

Then the membership function is defined as

$$\mu_Q(Q) = mim\left[\mu_{Q_1}(Q), \mu_{Q_2}(Q), \ldots\ldots \mu_{Q_n}(Q)\right] \tag{4.14}$$

(4) Disjunctive system of rules:

The rules that are connected by "OR" connectives satisfies the disjunctive system of rules. In this case, the aggregated output may be found by the fuzzy union of all individual rule consequents.

$$Q = Q_1\ OR\ Q_2\ OR\ \ldots\ldots OR\ Q_n \tag{4.15}$$

Then the membership function is defined as

$$\mu_Q(Q) = Max\left[\mu_{Q_1}(Q), \mu_{Q_2}(Q), \ldots\ldots \mu_{Q_n}(Q)\right] \tag{4.16}$$

4.7.2.1 Fuzzy Inference Engine

Fuzzy inference is the process of formulating the mapping from a given input to an output using fuzzy logic. The mapping then provides a basis from which decisions can be made, or patterns discerned. The process of fuzzy inference involves all of the pieces that are Membership Functions, Logical Operations and If-Then Rules. The most important two types of fuzzy inference method are [52,54]:

- Mamdani fuzzy inference method
- Sugeno fuzzy inference method.

Mamdani fuzzy inference method is the most commonly seen fuzzy methodology. Mamdani method was among the first control systems built using fuzzy set theory. It was proposed by Mamdani (1975) as an attempt to control a steam engine and boiler combination by synthesizing a set of linguistic control rules obtained from experienced human operators.

Mamdani fuzzy inference can be represented by two methods:

- A max–min inference method.
- A max–product inference method.

Figure (4.8) show an example of graphical representation for max-min Mamdani inference system. To compute the output of this fuzzy inference given the inputs, six steps have to be followed [52,54]:

- Determining a set of fuzzy rules. (As we can see in figure (4.8) we have two rules)
- Fuzzifying the inputs using the input membership functions. (To take the input1 and input 2 and determine the degree to which they belong to each of the appropriate fuzzy sets via membership functions which are A1, A2, B1, B2).
- Combining the fuzzified inputs according to the fuzzy rules to establish a rule strength. (Appling Logical Operations (or, and) to the input as rules, the two rules here use and operation)
- Finding the output of the rule by combining the rule strength and the output membership function. (The output is reshaped to min value according to input combination rule to get C1,C2)
- Combining the consequences to get an output distribution (by combining output by mean of max operation)
- Defuzzifying the output distribution (this step will be discuss in next paragraph)

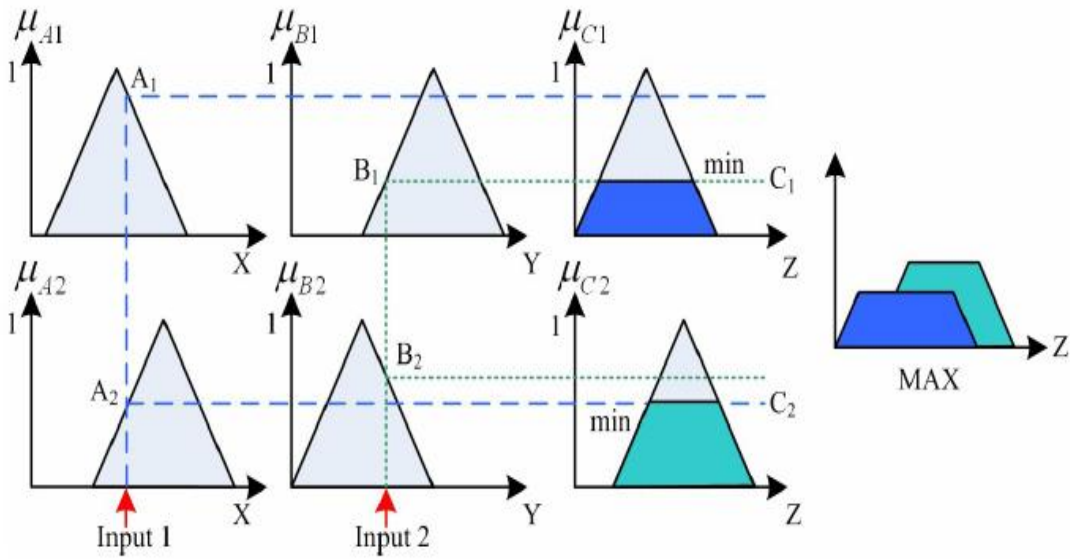

Figure (4.8) max-min Mamdani Model Example

4.7.3 Defuzzification

A defuzzifier performs the exact opposite function of a fuzzifier. It transforms the fuzzy variables (which are obtained as output after processing of the inputs) to crisp sets. The defuzzifier is necessary because in the real world the crisp values can only be taken as inputs to the other systems. Even though the fuzzy sets resemble the human thought process, their functionality is limited only to the above processes [52].

There are many methods that have been proposed in the literature in recent years, these methods are:

(1) Centroid method.

(2) Max-membership principle.

(3) Weighted average method.

(4) Mean-max membership.

(5) Centre of sums.

(6) Centre of largest area.

(7) First of maxima or last of maxima.

One of the most popular methods for defuzzification is centroid method. This method has been used in our modeling and simulation.

4.7.3.1 Centroid Method

This method can be called as center of gravity or center of area method. Figure (4.9) Show the graphical representation of method and it can be defined by the algebraic expression:

$$Z^* = \int \frac{\mu_c(z) z \, dz}{\mu_c(z) dz} \tag{4.17}$$

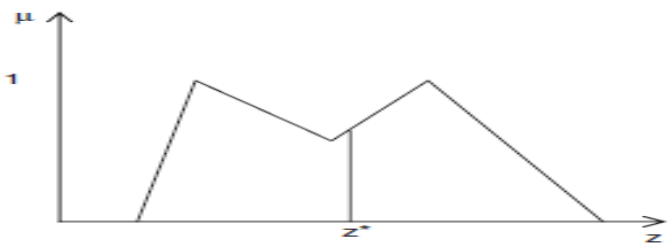

Figure (4.9) example of Centroid Method

Where Z* is the defuzzified value and $\int$ is used for algebraic integration

4.8 FLC MPPT

Recently fuzzy logic controllers have been introduced in the tracking of the MPP in PV systems. They have the advantage to be robust and relatively simple to design. Since they do not required the knowledge of an accurate plant model. On the other hand, the designer needs expert knowledge of the PV system working [58,59,60].

The proposed FLC is shown in figure (4.10); it consists of two inputs and one output. The two FLC input variables are E, CE and the output (U) is compared with the saw tooth waveform to generate a PWM signal for the D of boost converter.

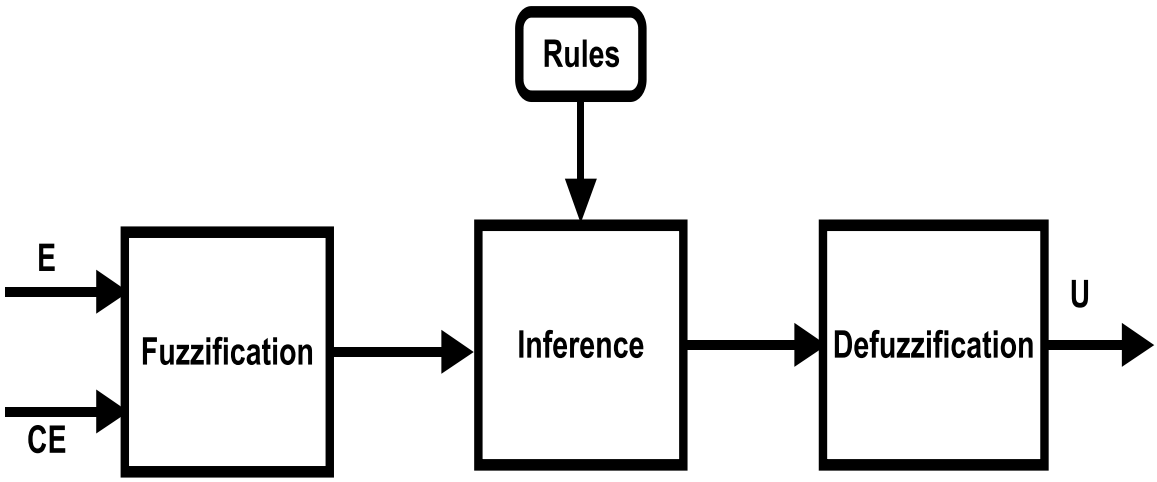

Figure (4.10) fuzzy MPPT input and output variables

Where the inputs of FLC can be expressed by equation

$$E = \frac{p(k) - p(k-1)}{v(k) - v(k-1)} \tag{4.18}$$

$$CE = E(k) - E(k-1) \tag{4.19}$$

Where P, V are the PV power and voltage respectively at instant k. E is equal to zero at MPP, so E shows load operating point at instance k if it is located at left or right or at MPP

on P-V characteristic cure of PV, on other hand change of error is used to express the moving direction of this point.

4.8.1 FUZZIFICATION MPPT

The fuzzification process converts the system actual inputs values E and CE into linguistic fuzzy sets using fuzzy triangular and trapezoidal membership functions as shown in figure (4.11). These linguistic variables are expressed in terms of five linguistic variables.

- Positive big (PB).
- Positive small (PS).
- Zero (ZE).
- Negative small (NS).
- Negative big (NB).

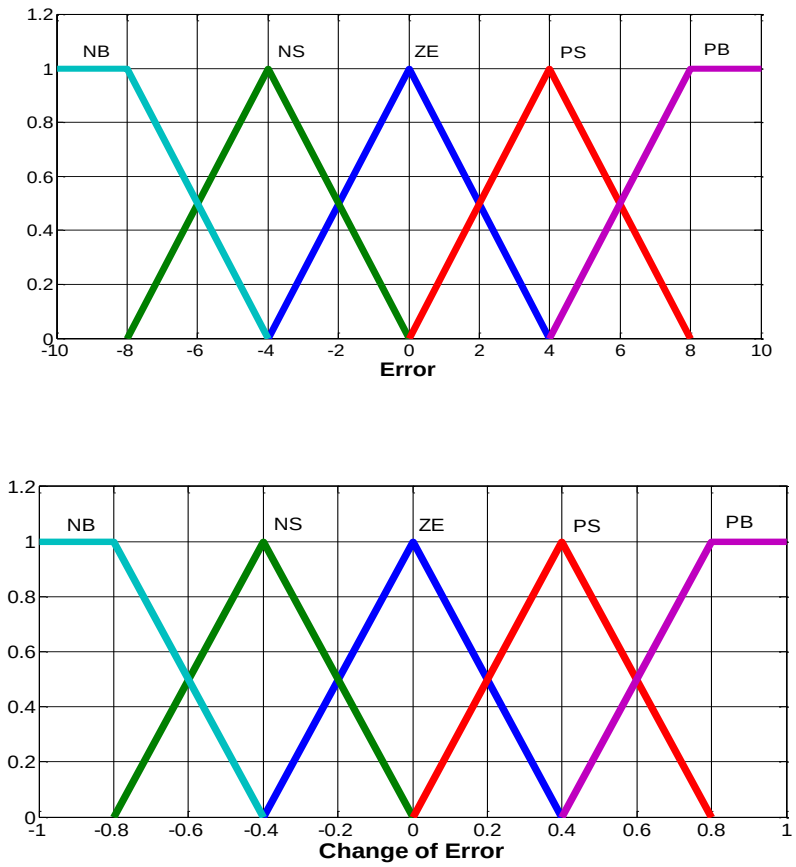

Figure (4.11) Membership function of E, CE

4.8.2 Fuzzy Inference Engine MPPT

Fuzzy rule base is a collection of if-then rules that contain all the information for the controlled parameters. It is set according to professional experience and the operation of the system control. The fuzzy rule algorithm includes 25 fuzzy control rules listed below in table (4.2).

Table (4.2) FLC Rules base

E \ CE	NB	NS	ZE	PS	PB
NB	ZE	ZE	PB	PB	PB
NS	ZE	ZE	PS	PS	PS
ZE	PS	ZE	ZE	ZE	NS
PS	NS	NS	NS	ZE	ZE
PB	NB	NB	NB	ZE	ZE

In this thesis Mamdani's fuzzy inference method, with Max-Min operation fuzzy combination has been used.

4.8.3 Defuzzification MPPT

Defuzzification of the inference engine, which evaluates the rules based on a set of control actions for a given fuzzy inputs set. This operation converts the inferred fuzzy control action into a numerical value at the output by forming the union of the outputs resulting from each rule. The center of area algorithm is used for defuzzification. Figure (4.12) shows member ship of output U.

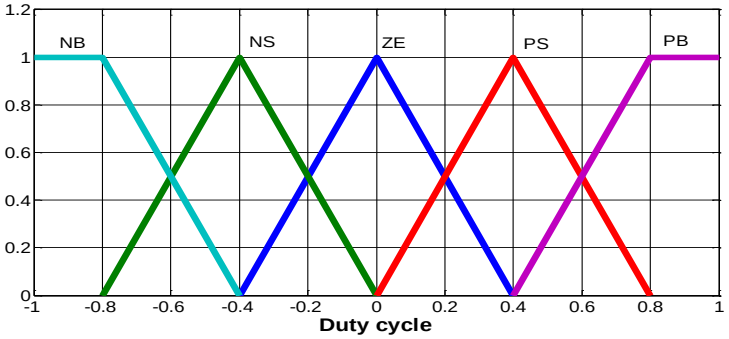

Figure (4.12) Membership function U

i.e If E is NB and CE is ZE then crisp U is PB, it means that if the operating point is far away from the MPP by the right side, and the variation of the slope of the curve is almost Zero; then increase the duty cycle.

4.9 P&O MPPT

P&O algorithm, also known as the "hill climbing" method, is very popular and the most commonly used in practice because of its simplicity in algorithm and the ease of implementation.

It can be seen From P-V curve in figure (4-13) that incrementing (decrementing) the voltage by change duty cycle of boost converter, increases (decreases) the power when operating on the left of the MPP and decreases (increases) the power when on the right of the MPP. Therefore, if there is an increase in power, the subsequent perturbation should be kept the same to reach the MPP and if there is a decrease in power, the perturbation should be reversed [61]. Figure (4-14) shows the flowchart of this algorithm.

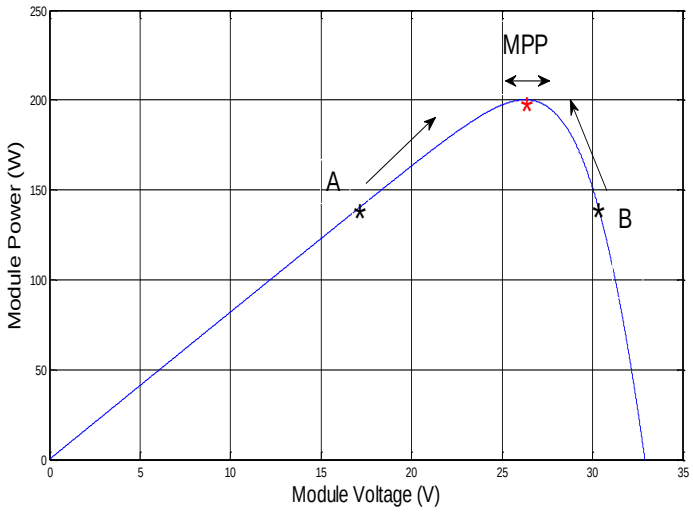

Figure (4.13) P-V curve of KC200GTS PV module at 1000 W/m^2 and 25^{o}C

There are some limitations that reduce its MPPT efficiency. First, it cannot determine when it has actually reached the MPP. Instead, it oscillates the operating point around the MPP after each cycle and slightly reduces PV efficiency under the constant irradiance condition. Second, it can fail under in cases of rapidly changing atmospheric conditions as a result of moving clouds [14,62].

The cause of this problem can be explained using figure (4.15) with a set of P-V curves with varying irradiance. Assume starting from an operating point A, if atmospheric conditions stay approximately constant, a perturbation will bring the operating point to B and the perturbation will be reversed due to a decrease in power. However, if the irradiance increases and shifts the power curve from P1 to P2 within one sampling period, the operating point will move from A to C. This represents an increase in power and the perturbation is kept the same. Consequently, the operating point diverges from the MPP and will keep diverging if the irradiance steadily increases [14].

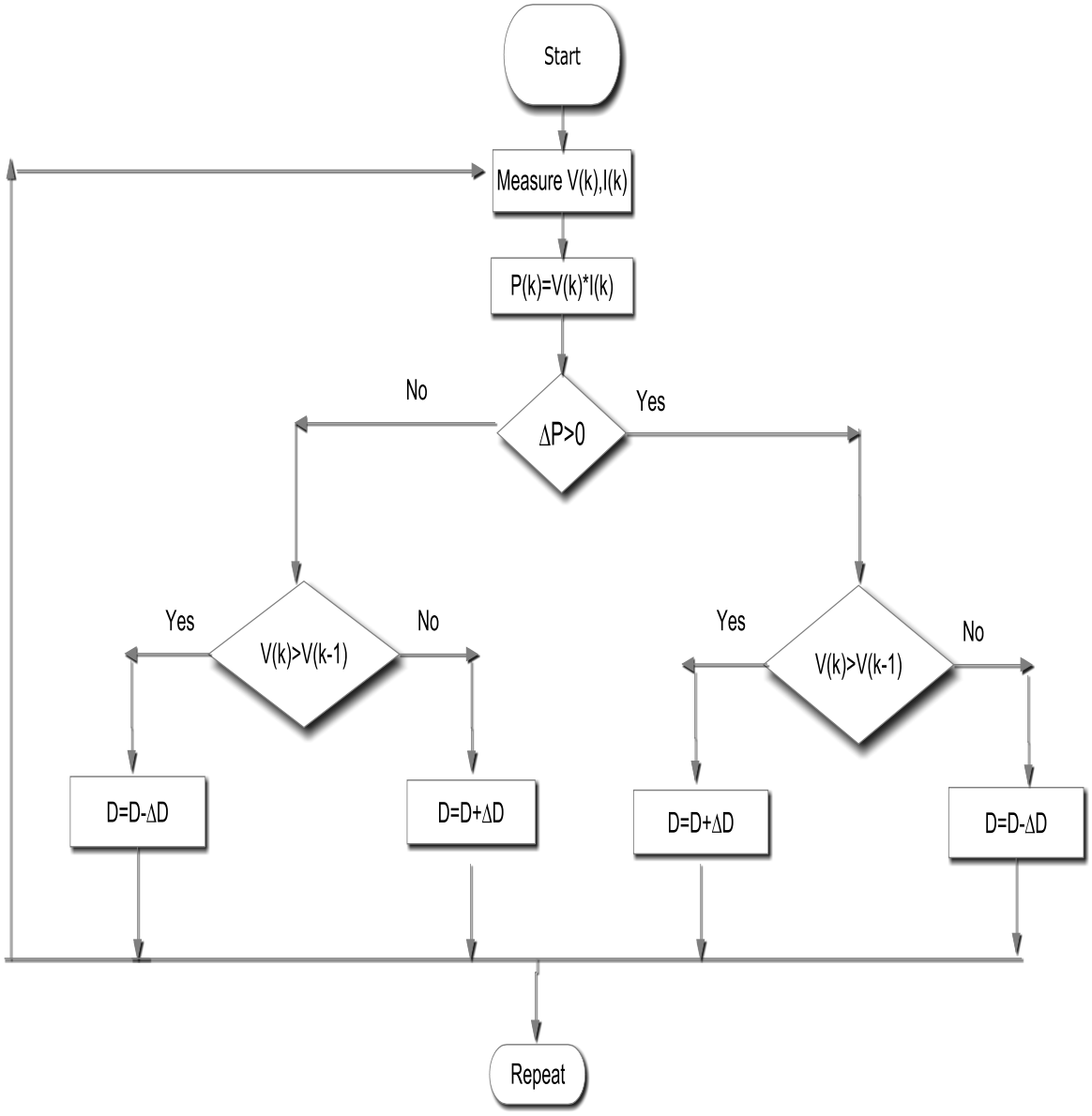

Figure (4.14) P&O flowchart

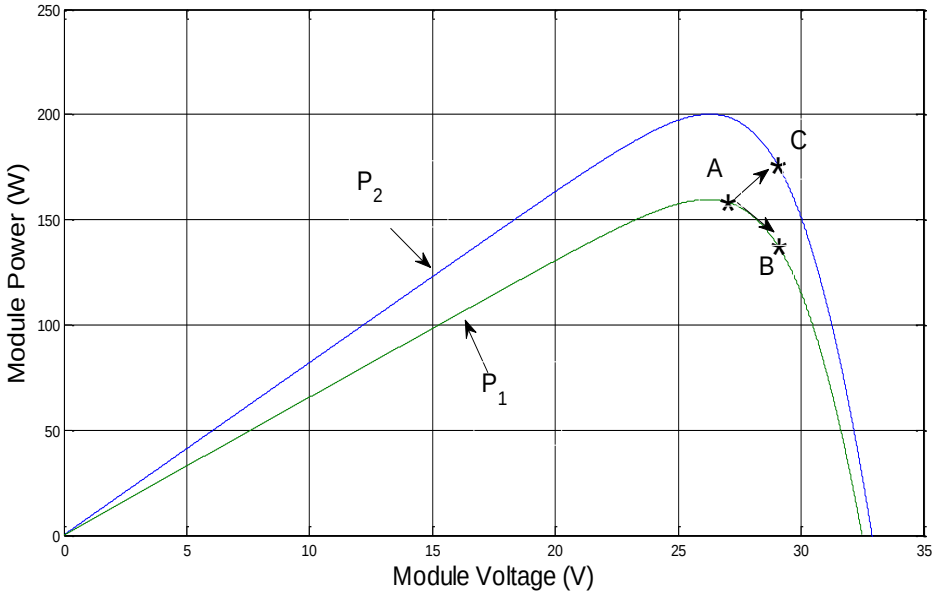

Figure (4.15) Divergence P&O from MPP

The performance of the algorithm is affected by the choice of the magnitude (ΔD) of the converter switching duty cycle. Large perturbations cause large output power fluctuations around the MPP while small perturbations slow down the algorithm [3,59].

CHAPTER (5)

SIMULATION AND RESULTS

CHAPTER (5)

SIMULATION AND RESULTS

5.1 Simulation results

This chapter presents MATLAB simulations perform comparative tests between the P&O, fuzzy MPPT algorithm and direct coupling of PV system. Simulations also verify the functionality of MPPT with a resistive load and then with the DC pump motor load. Some selected results are presented which show the simulation results of PV and load operating point at different irradiance and temperature levels.

Figure (5.1) shows simulink circuit diagram of direct coupling of PV array to dc motor pump. Figure (5.2) shows simulink circuit diagram of MPPT system which consist of PV array, boost converter, MPPT controller, PWM block and dc motor pump.

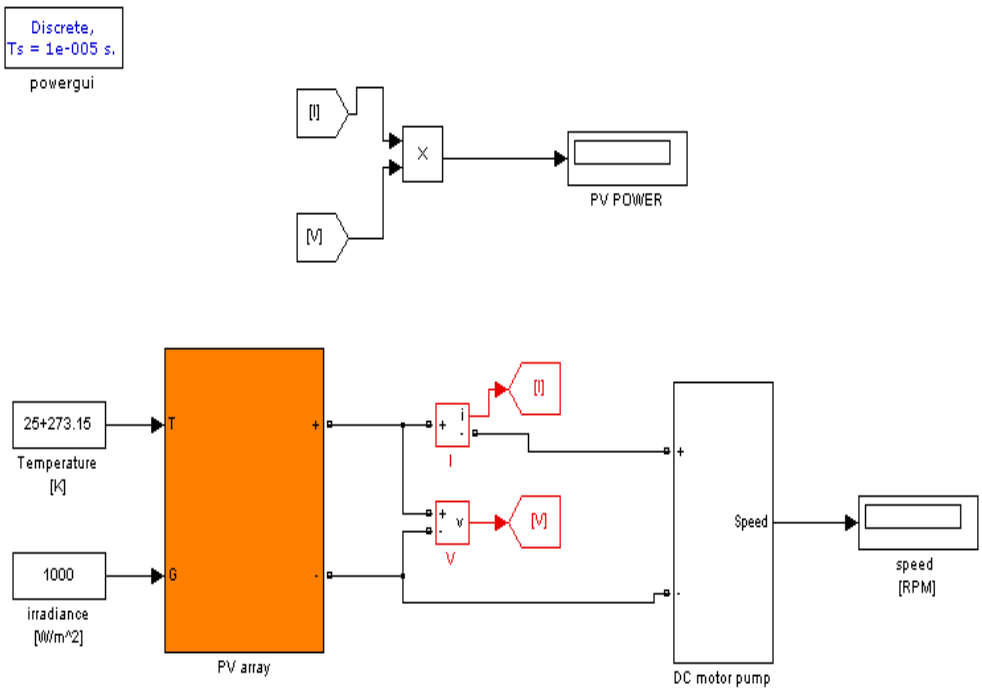

Figure (5.1) simulink of PV array direct coupled to Dc motor pump load

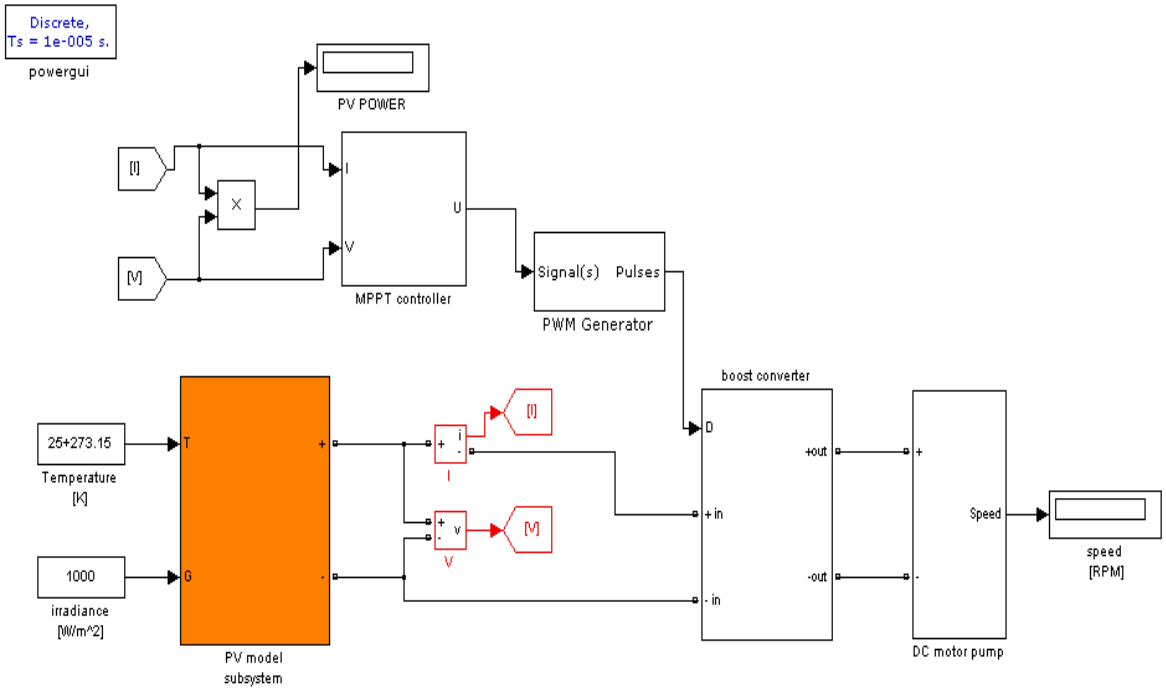

Figure (5.2) simulink of PV MPPT system with DC motor pump load

5.2 Simulation of Resistive load under Varying Irradiance

Extensive simulation for cases, direct coupling and MPPT for KC200GT PV model connected to resistive load is implemented under varying irradiance and keeping temperature constant. Figure (5.3) shows the simulation of decreasing and increasing of irradiance form/to 200, 600, 1000 W/m^2 on PV model at constant temperature 25^{o}C, which is indication of variation in the sunlight during the daytime.

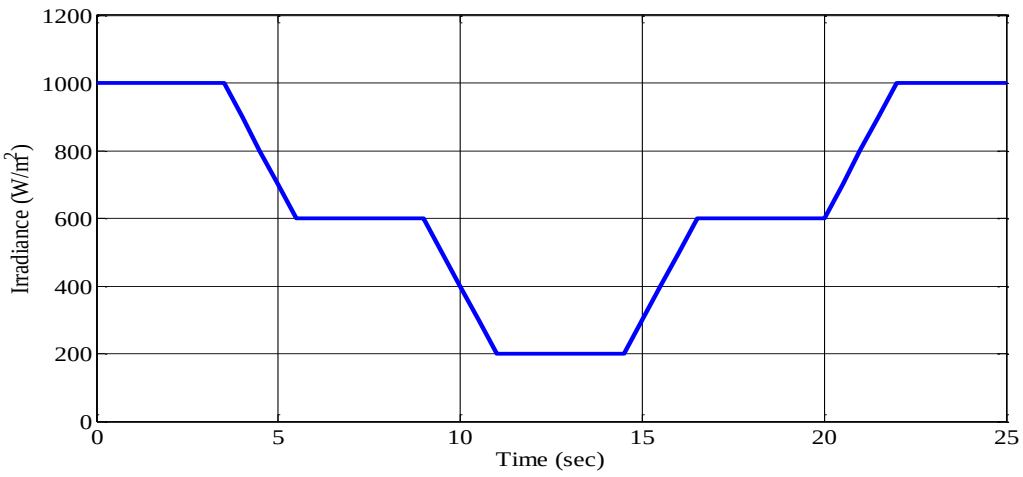

Figure (5.3) changing irradiance at 25^{o}C for resistive load

Figure (5.4) shows PV output power under changing irradiance, it can be observed that using MPPT algorithms succeed to track MPP of PV model. It can be seen also fuzzy algorithm is smoother than P&O algorithm. It is cleared that using MPPT increase output power of the PV especially at high irradiance levels up to 81%.

Figure (5.5) (a), (b), (c) shows sample of performance of MPPT of PV power using fuzzy and P&O at 1000, 600, 200 W/m^2 respectively, which show fuzzy is less oscillating and better stable operating.

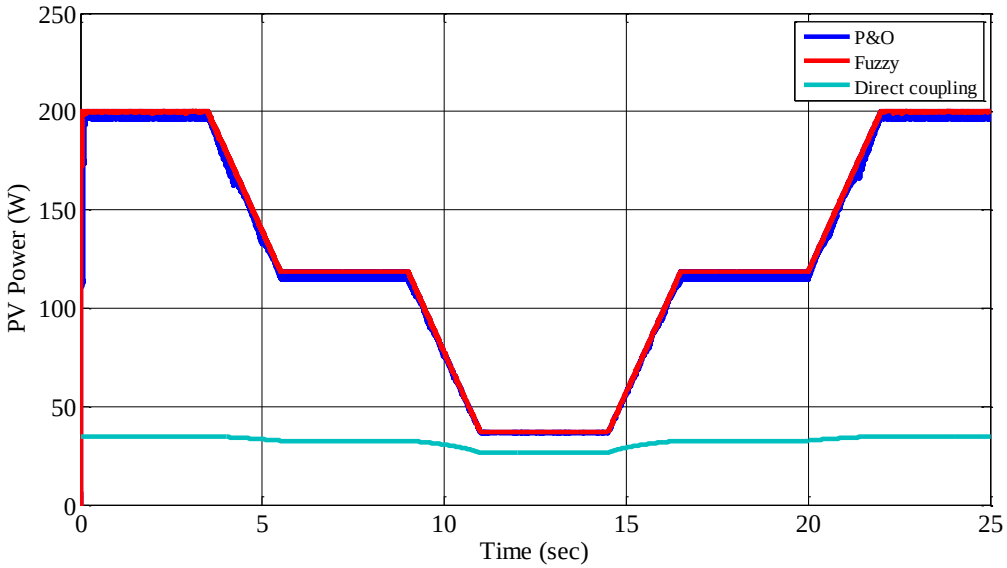

Figure (5.4) PV output power under changing irradiance at 25^{o}C for resistive load

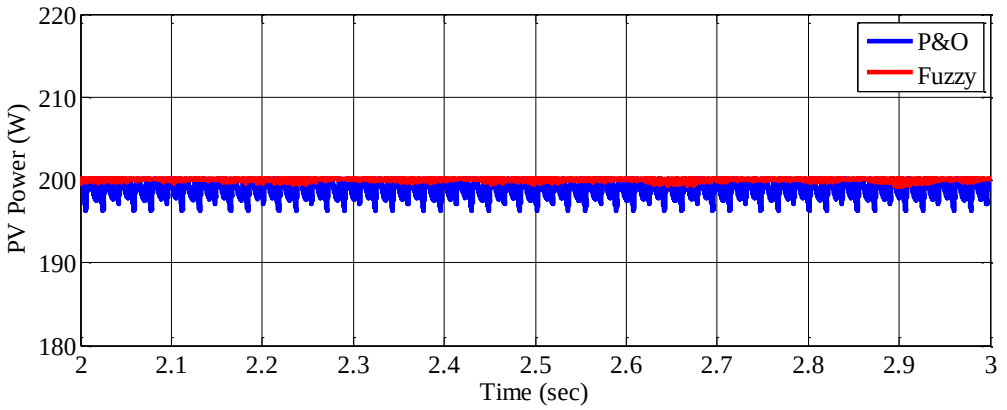

(a) At 1000 W/m^2

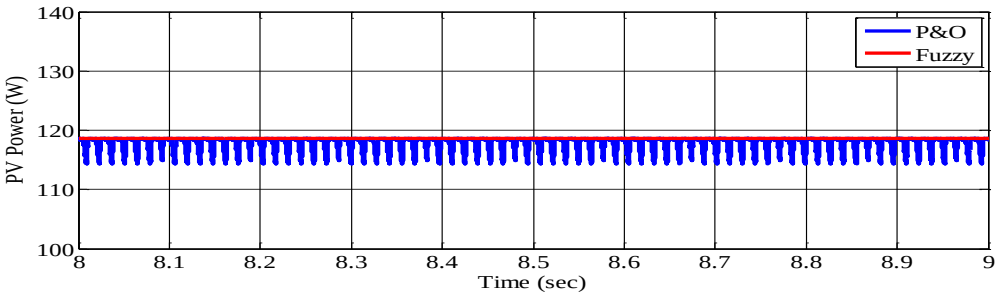

(b) at 600 W/m^2

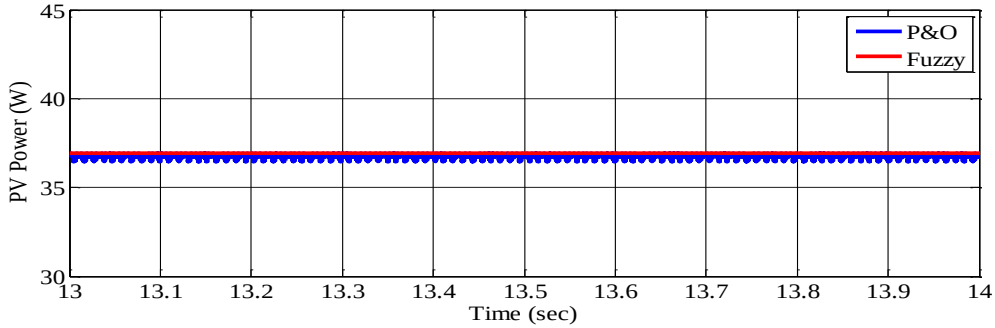

(c) at 200 W/m^2

Figure (5.5) performance of MPPT of PV output power under fixed irradiance at 25^{o}C for resistive load

Figure (5.6) shows the duty cycle of the converter of both MPPT algorithms and the change occur due to change in irradiance to track MPP. P&O shows more oscillation than fuzzy.

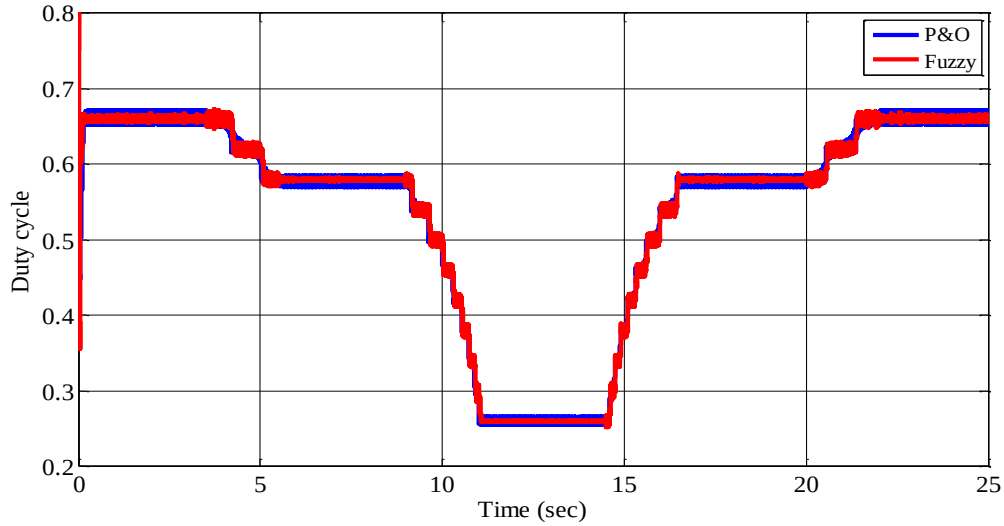

Figure (5.6) duty cycle of converter under changing irradiance at 25^{o}C for resistive load

Figure (5.7), (5.8) shows the load voltage and current respectively, by using MPPT and direct coupling.

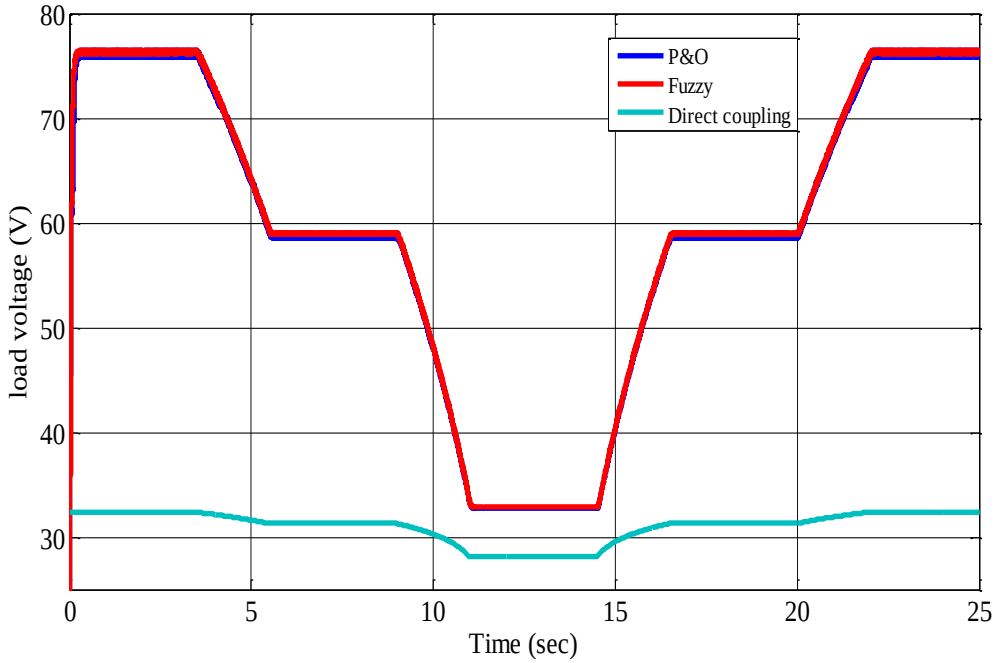

Figure (5.7) resistive load voltage under changing irradiance at 25°C

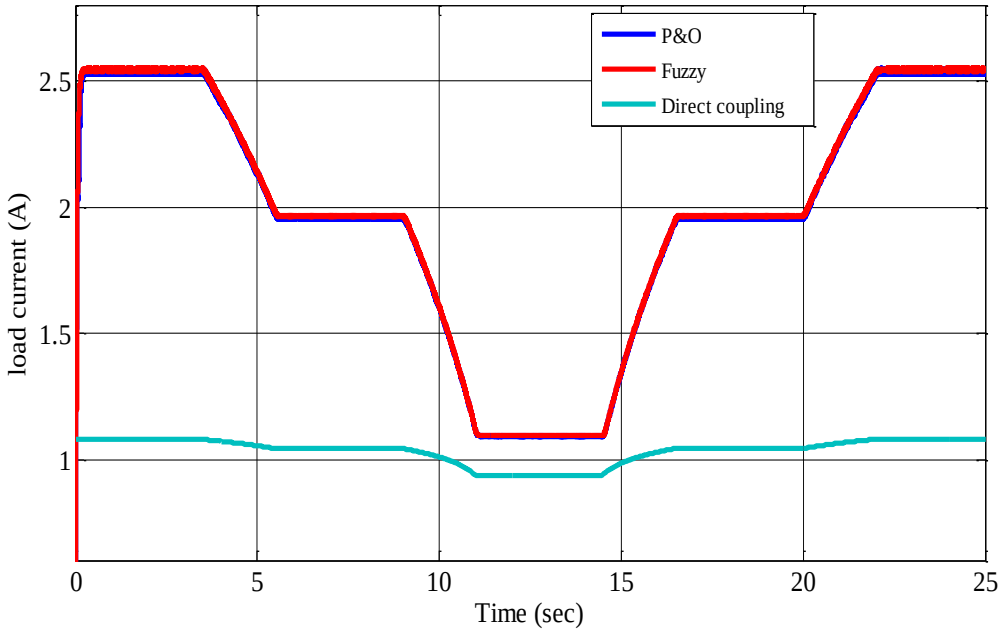

Figure (5.8) resistive load current under changing irradiance at 25°C

5.3 Simulation of Resistive load under Varying Temperature

A simulation for direct coupling and MPPT for KC200GT PV model connected to resistive load is implemented under varying temperature and constant irradiance. Figure (5.9) shows the simulation of decreasing and increasing of temperature form/to 25, 70 ^{o}C on PV model at constant irradiance 800 W/m^2.

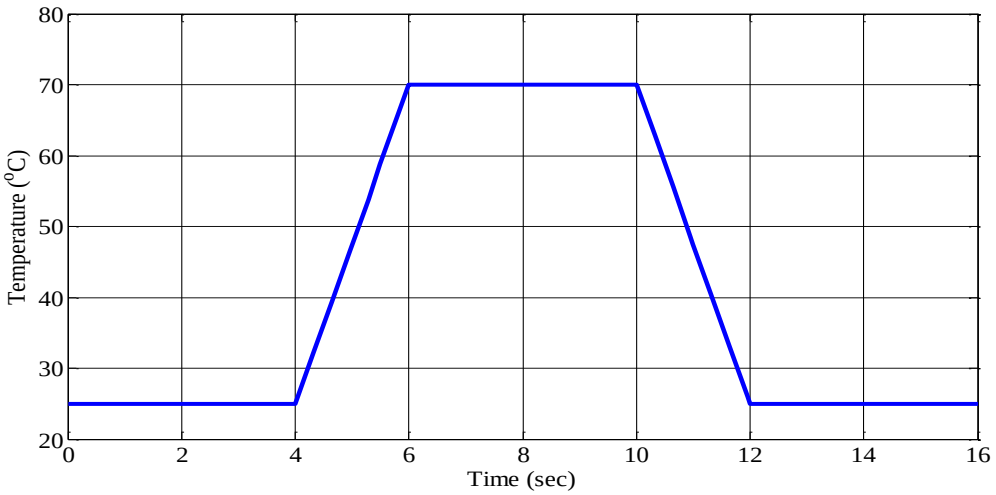

Figure (5.9) changing temperature at 800 W/m^2 for resistive load

Figure (5.10) shows PV output power under changing temperature for MPPT and direct coupling, which show that even change of temperature, can be tracked by MPPT algorithms. It can be noticed that output power decreases as temperature increases.

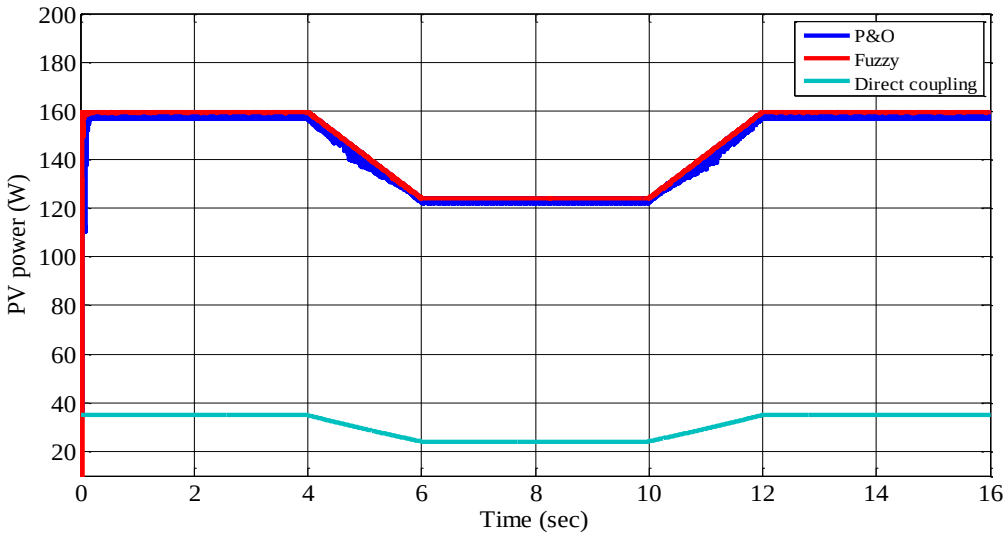

Figure (5.10) PV output power under changing temperature at 800 W/m^2 for resistive load

Figure (5.11) (a), (b) shows the sample of performance of MPPT of PV power using fuzzy and P&O at 25, 70 ^{o}C respectively.

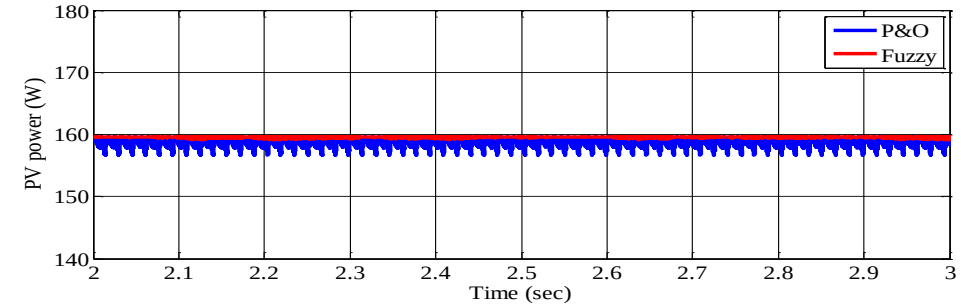

(a) at 25 ^{o}C

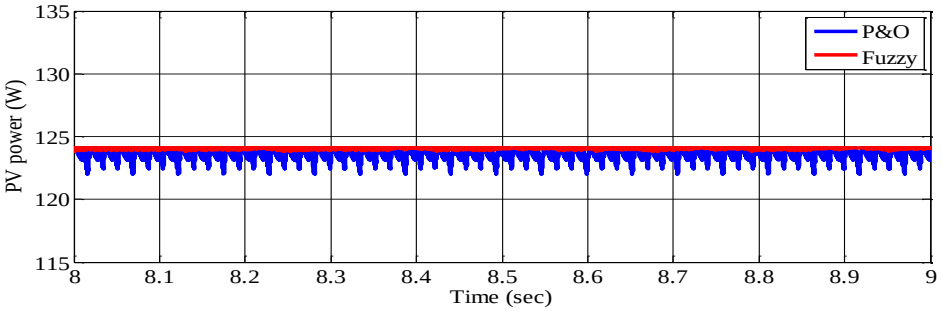

(b) at 70 ^{o}C

Figure (5.11) performance of MPPT of PV output power under fixed temperature at 800 W/m^2 for resistive load

Figure (5.12) shows duty cycle of the converter of both MPPT algorithms and the change occurs due to change in temperature to track MPP.

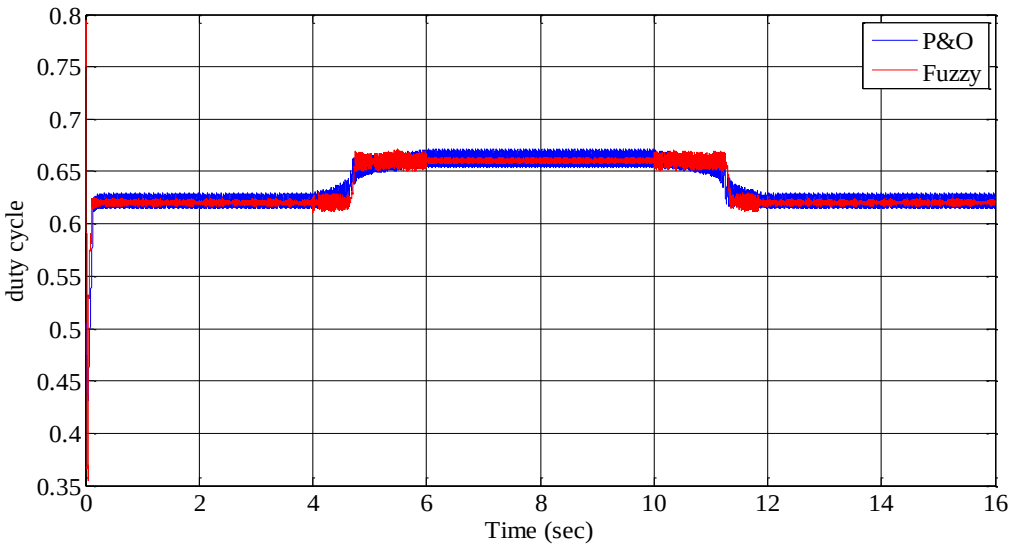

Figure (5.12) duty cycle of converter under changing temperature at 800 W/m^2 for resistive load

Figure (5.13), (5.14) shows the load voltage and current respectively, by using MPPT and direct coupling.

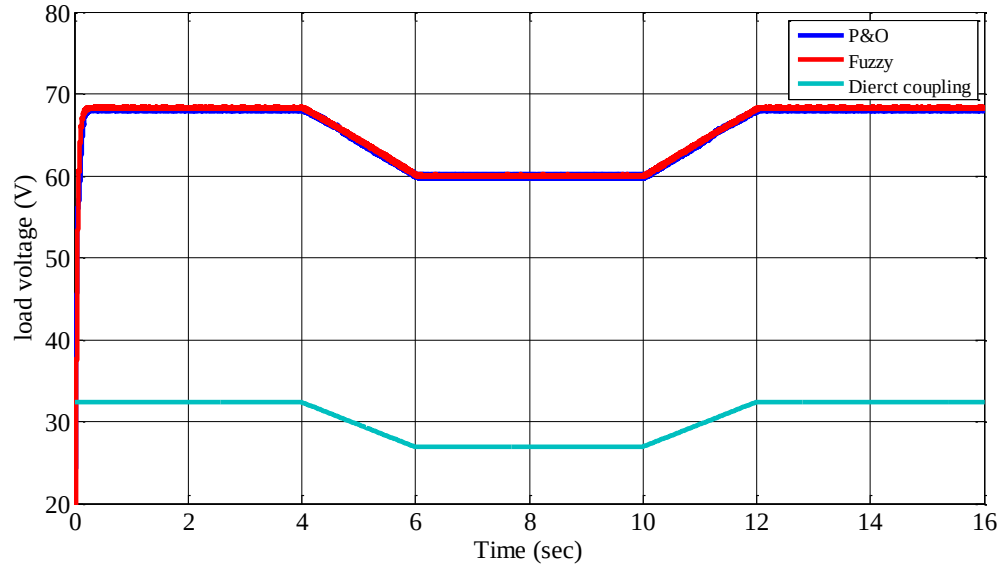

Figure (5.13) resistive load voltage under changing temperature at 800 W/m^2

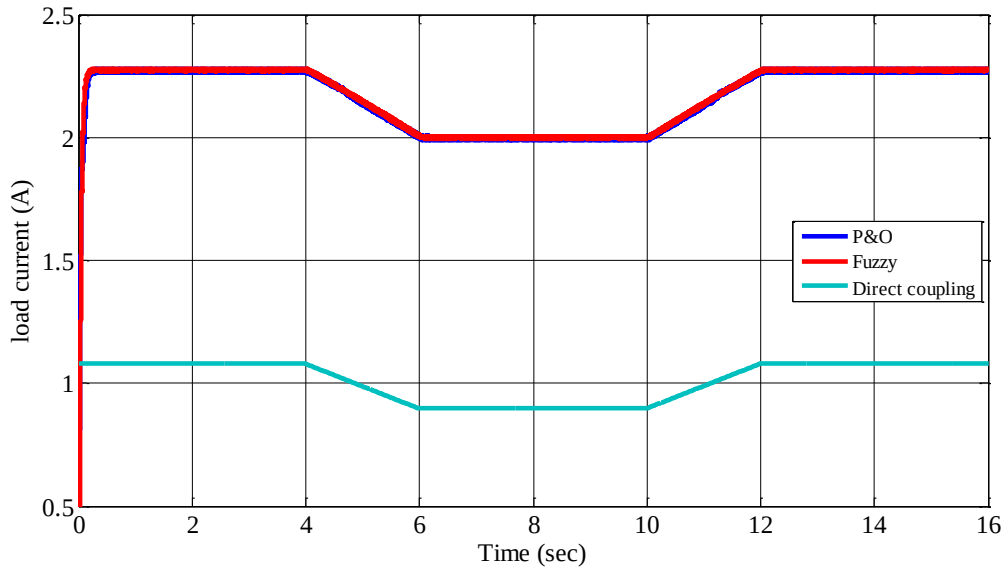

Figure (5.14) resistive load current under changing temperature at 800 W/m^2

5.4 Simulation of DC Motor Pump under Varying Irradiance

Replacing the resistive load by DC motor pump. A simulation for direct coupling and MPPT for KC200GT PV array which consist of N_{ser}=2 and N_{par}=3 modules connected to DC motor pump load is implemented under varying irradiance and constant temperature. Figure (5.15) shows the simulation of decreasing and increasing of irradiance form/to 200, 600, 1000 W/m^2 on PV model at constant temperature 25^{o}C.

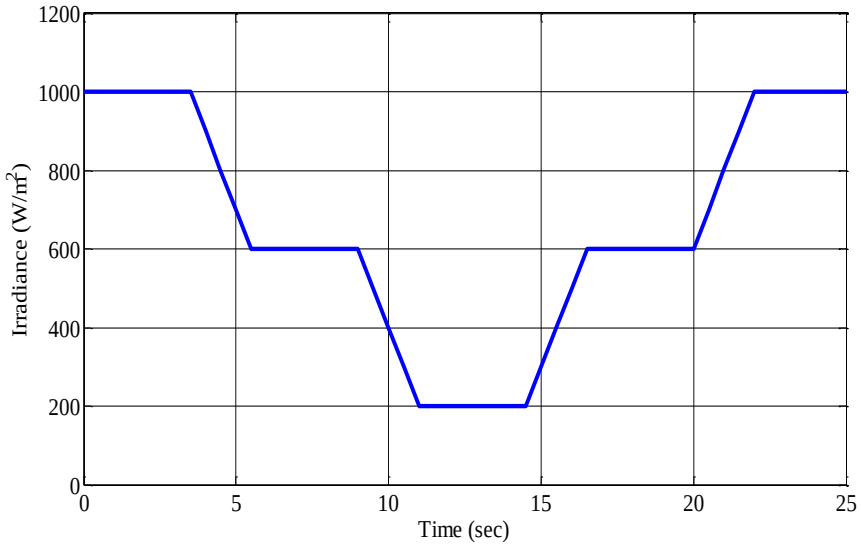

Figure (5.15) changing irradiance at 25^{o}C for DC motor pump

Figure (5.16) shows the PV output power under changing irradiance, it can be observed that MPPT algorithms succeed to track MPP of PV array even with changing load.

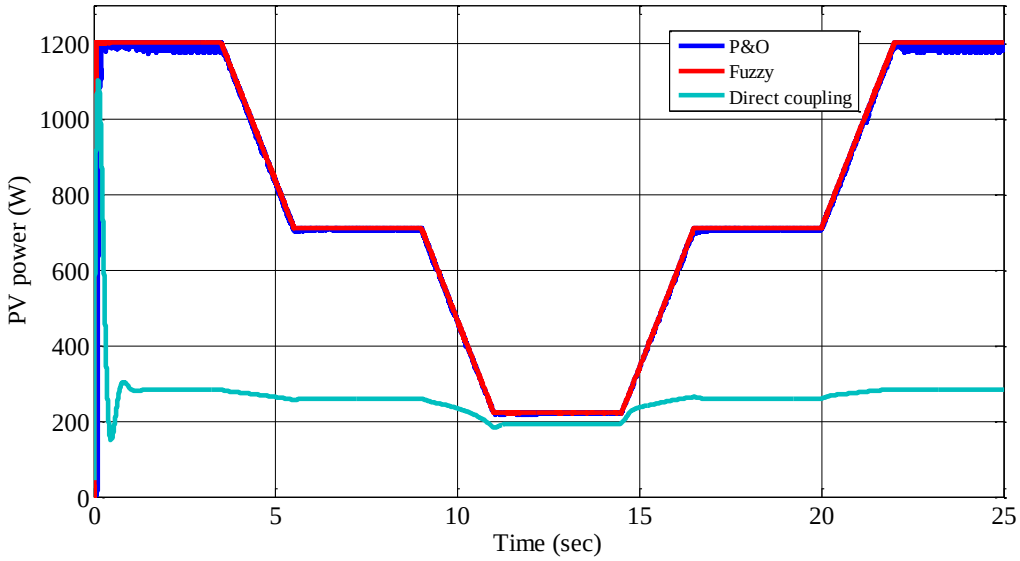

Figure (5.16) PV output power under changing irradiance at 25^{o}C for DC motor pump

Figure (5.17) (a), (b), (c) shows the sample of performance of MPPT of PV power using fuzzy and P&O at 1000, 600, 200 W/m^2 respectively.

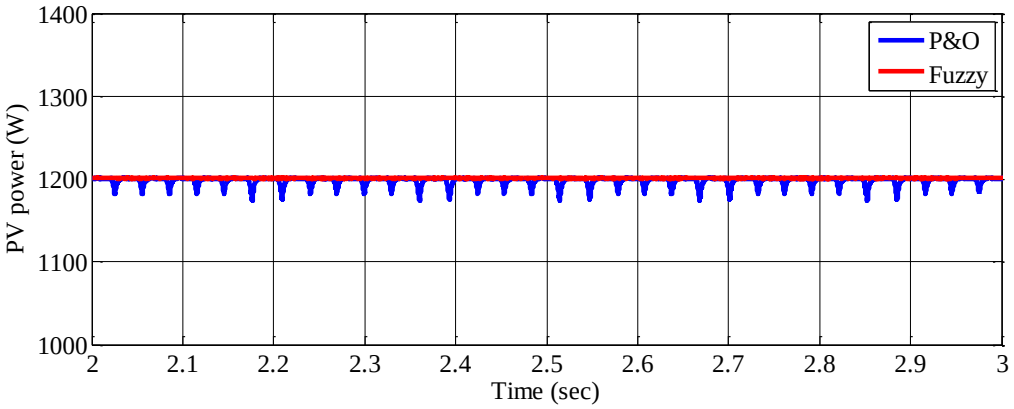

(a) at 1000 W/m^2

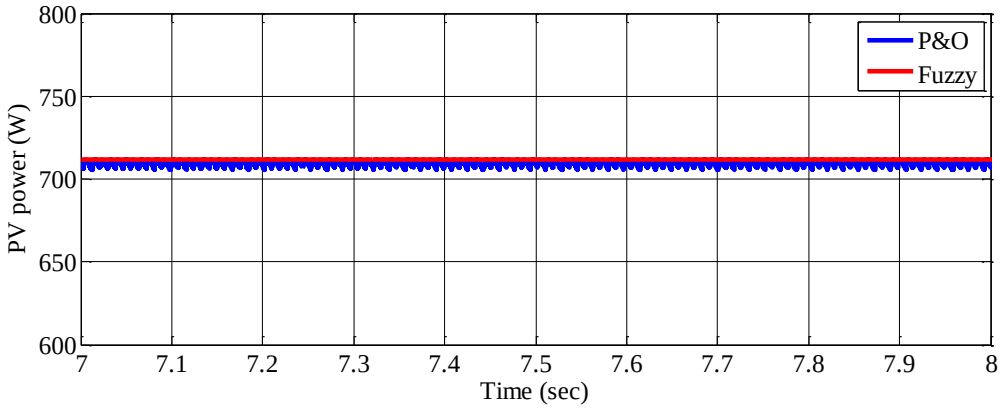

(b) at 600 W/m^2

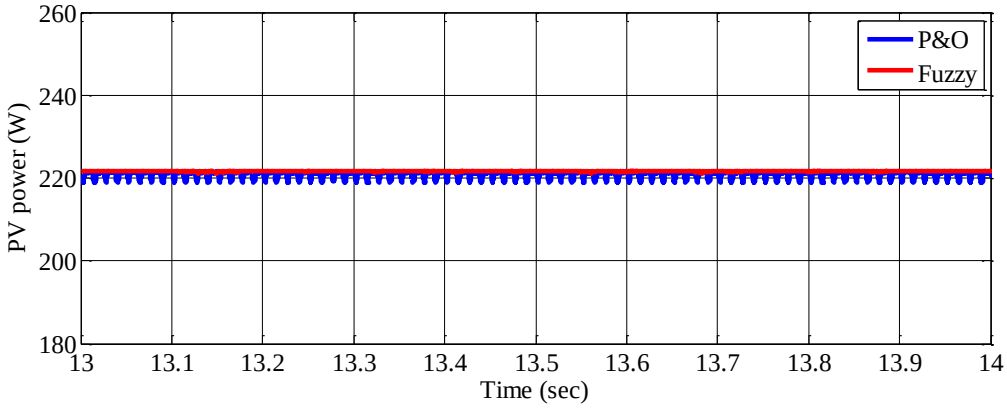

(c) at 200 W/m^2

Figure (5.17) performance of MPPT of PV output power fixed irradiance at 25^{o}C for DC motor pump.

Figure (5.18) shows duty cycle of the converter of both MPPT algorithms and the change occurs due to change in irradiance to track MPP.

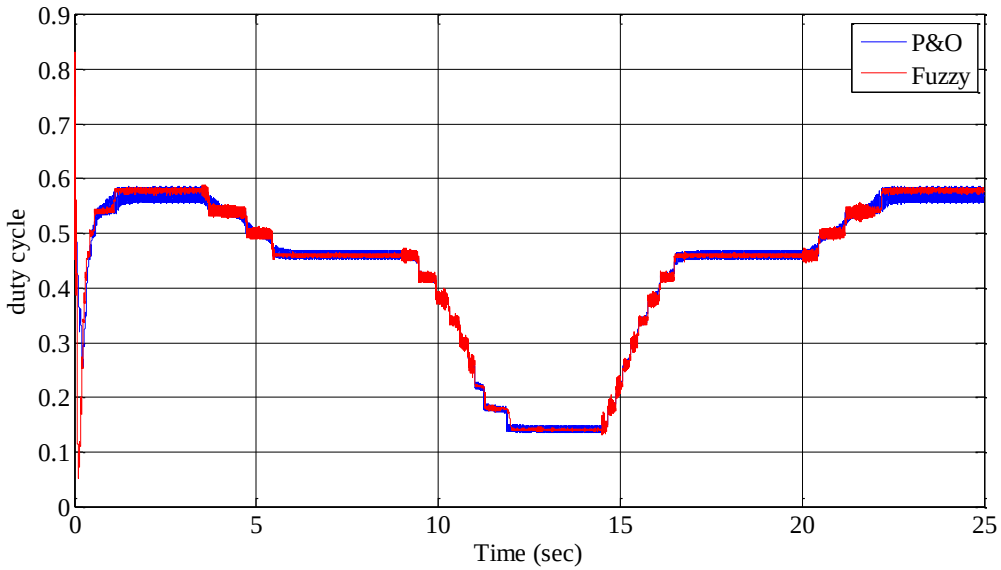

Figure (5.18) duty cycle of converter under changing irradiance at 25°C for DC motor pump

Figure (5.19), (5.20), (5.21) shows the load voltage, current and speed respectively, by using MPPT and direct coupling.

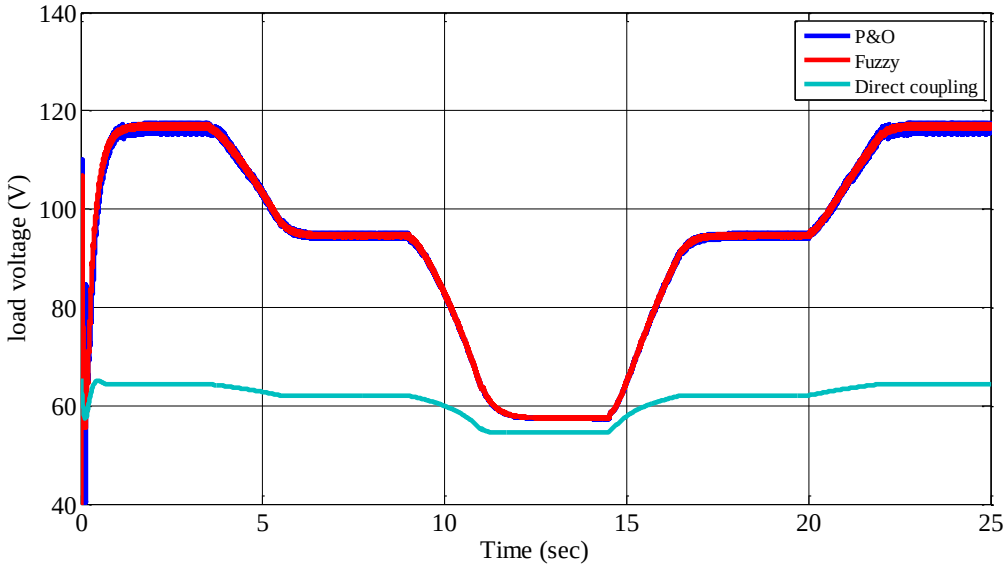

Figure (5.19) DC motor voltage under changing irradiance at 25°C

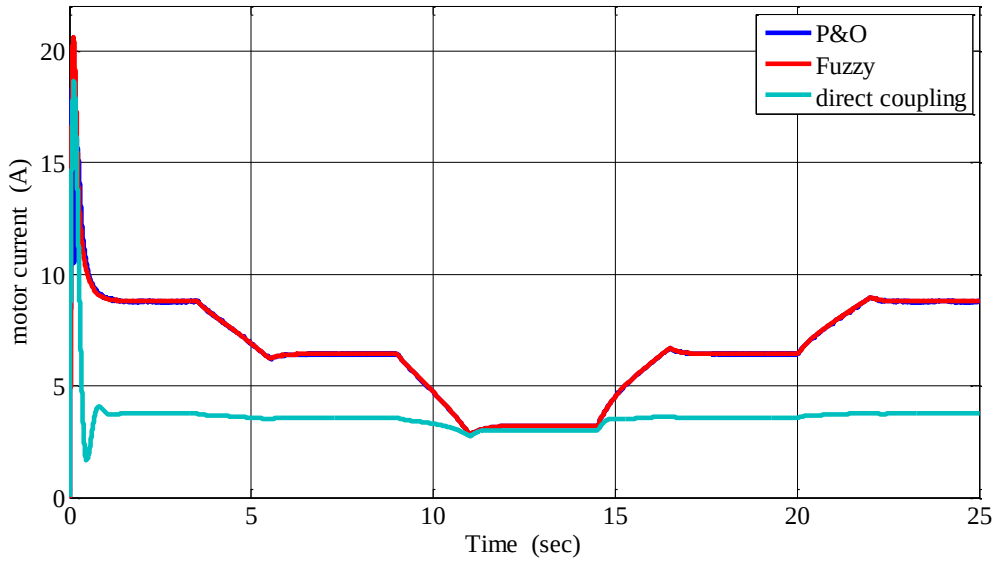

Figure (5.20) DC motor current under changing irradiance at 25°C

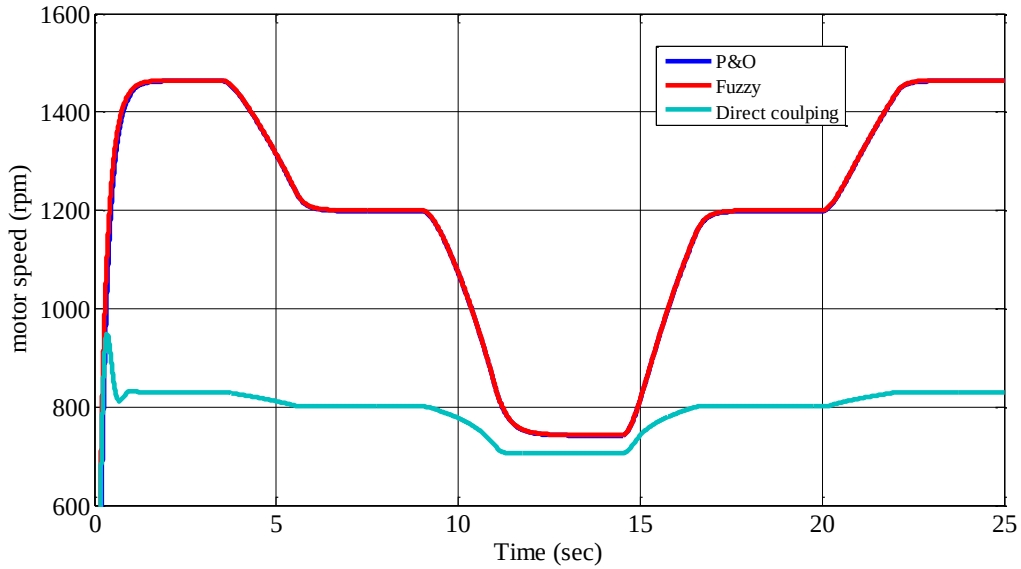

Figure (5.21) DC motor speed under changing irradiance at 25°C

Figure (5.22) (a), (b), (c) shows the sample of performance of MPPT of dc motor speed using fuzzy and P&O at 1000, 600, 200 W/m^2 respectively, fuzzy have faster rotational speed which will lead to much pumping of water as in centrifugal pump depend on motor speed.

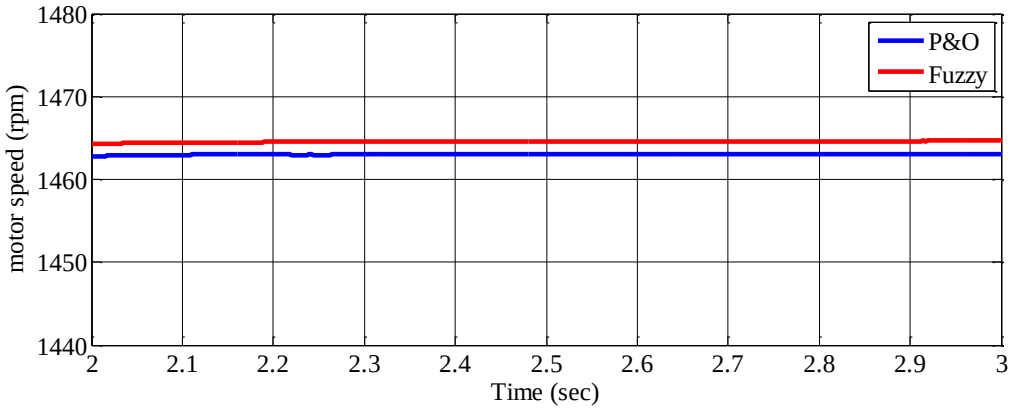

(a) at 1000 W/m^2

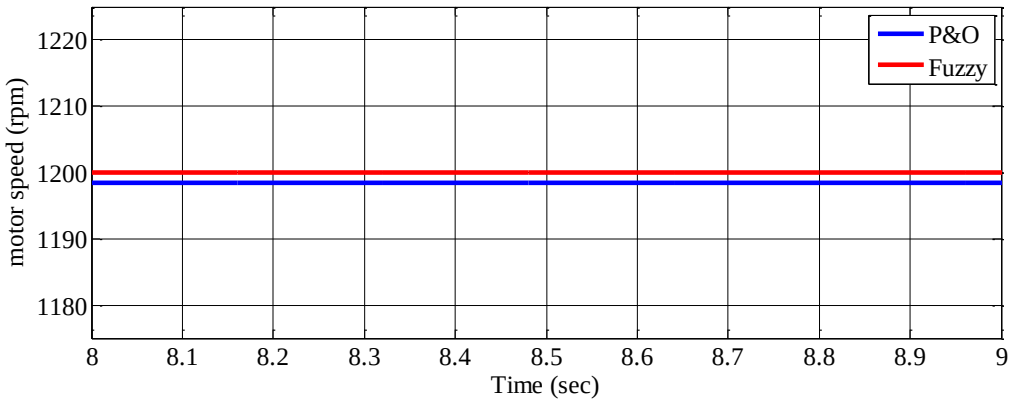

(b) at 600 W/m^2

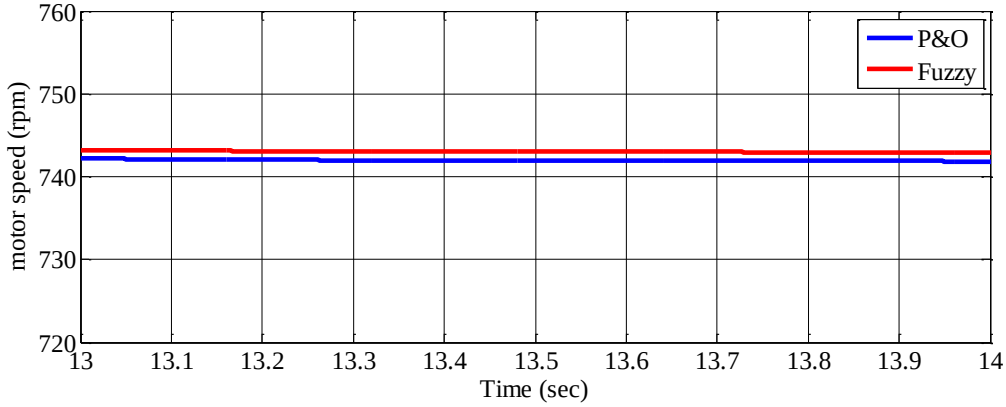

(c) at 200 W/m^2

Figure (5.22) performance of MPPT of motor speed under fixed irradiance at 25^{o}C for DC motor pump

5.5 Simulation of DC Motor Pump under Varying Temperature

A simulation for direct coupling and MPPT for KC200GT PV array connected to dc motor pump load is implemented under varying temperature and constant irradiance. Figure (5.23) shows the simulation of decreasing and increasing of temperature form/to 25, 70 ^{o}C on PV model at constant irradiance 400 W/m^2.

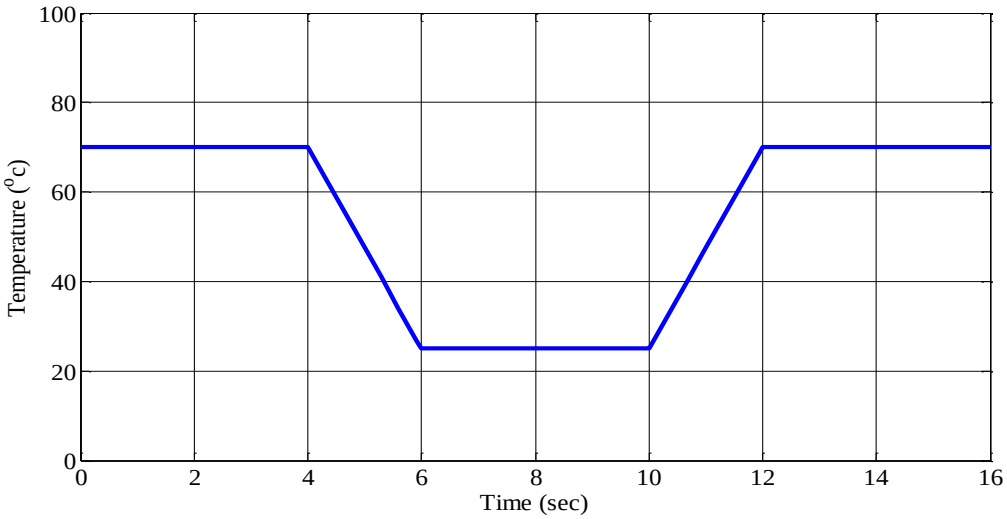

Figure (5.23) changing temperature at 400 W/m^2 for DC motor pump

Figure (5.24) shows the PV output power under changing temperature for MPPT and direct coupling.

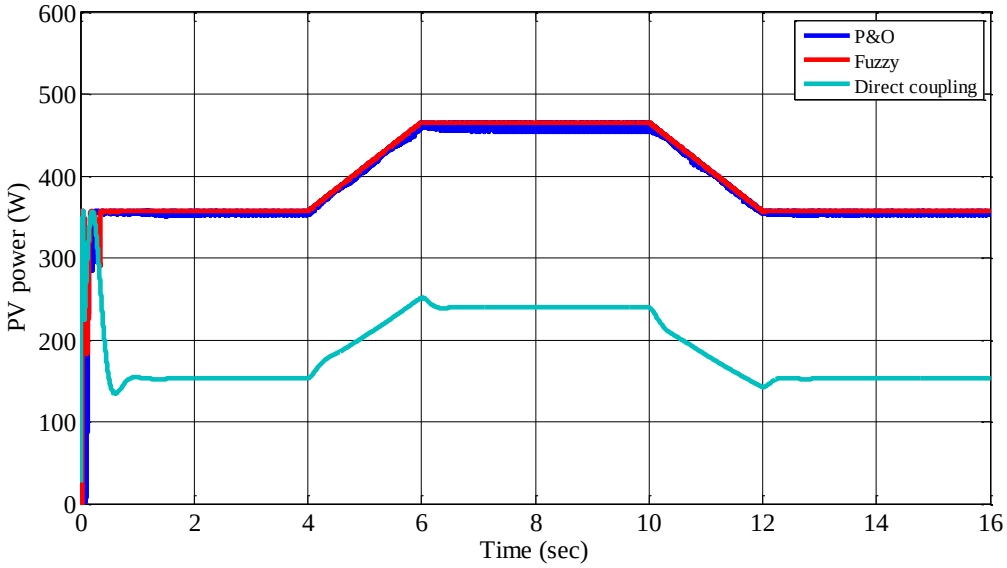

Figure (5.24) PV output power under changing temperature at 400 W/m^2 for DC motor pump load

Figure (5.25) (a), (b) shows the sample of performance of MPPT of PV power using fuzzy and P&O at 70,25 ^{o}C respectively.

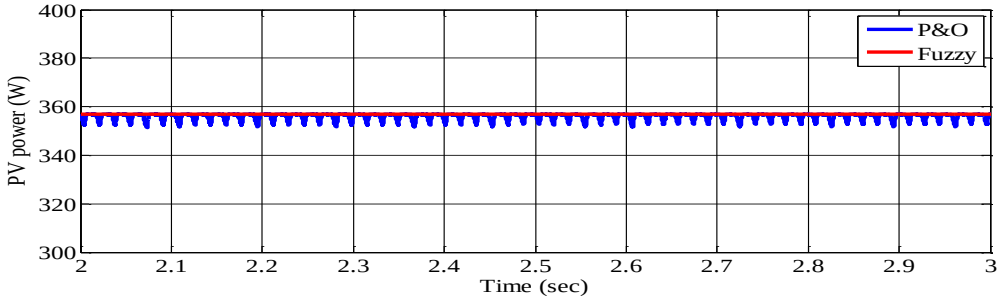

(a) at 70 ^{o}C

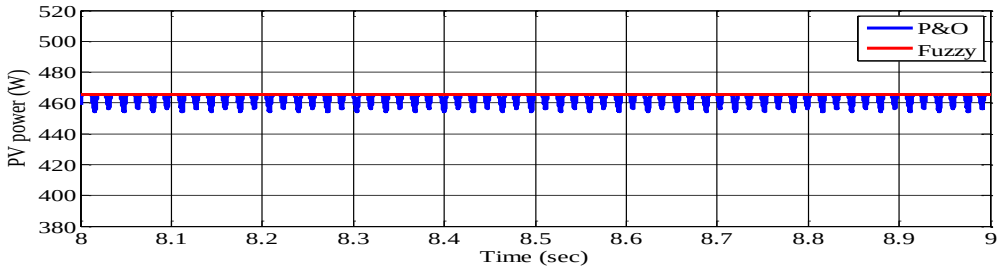

(b) at 25 ^{o}C

Figure (5.25) performance of MPPT of PV output power under fixed temperature at 400 W/m^2 for DC motor pump.

Figure (5.26) shows duty cycle of the converter of both MPPT algorithms and the change that occurs due to change in temperature to track MPP for dc pump load.

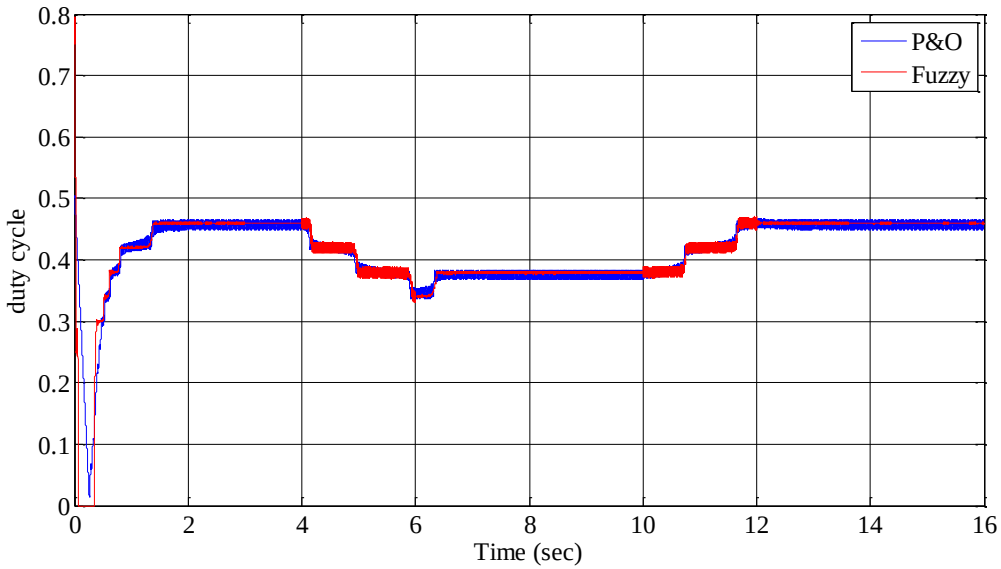

Figure (5.26) duty cycle of converter under changing temperature at 400 W/m^2 for DC pump load

Figure (5.27), (5.28), (5.29) shows the load voltage, current and speed respectively, by using MPPT and direct coupling.

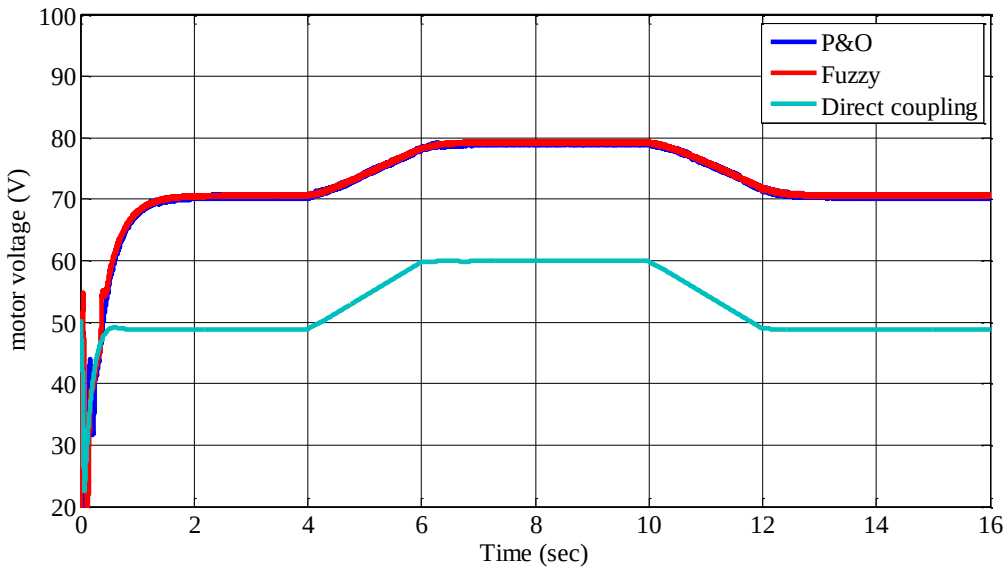

Figure (5.27) DC motor voltage under changing temperature at 400 W/m^2

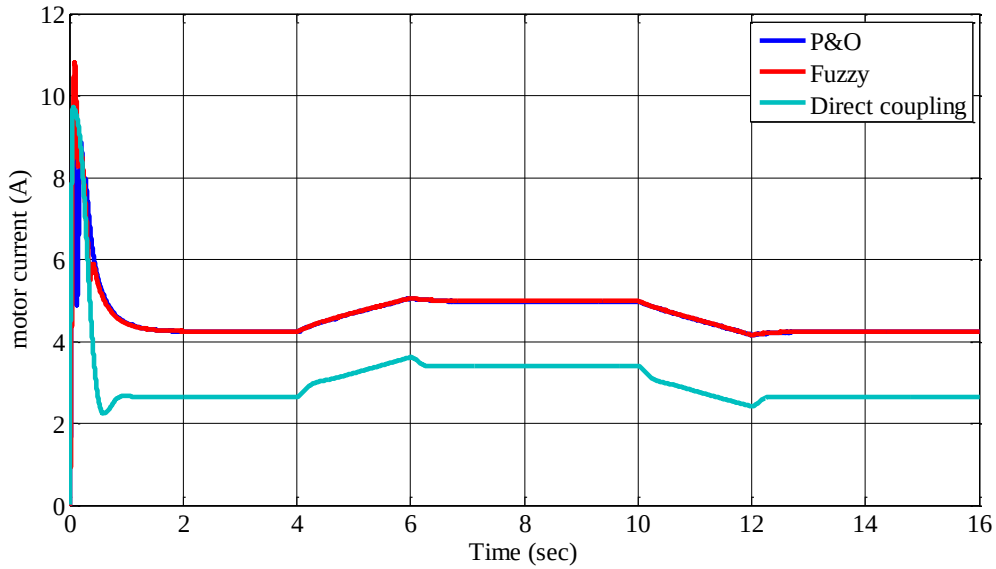

Figure (5.28) DC motor current under changing temperature at 400 W/m^2

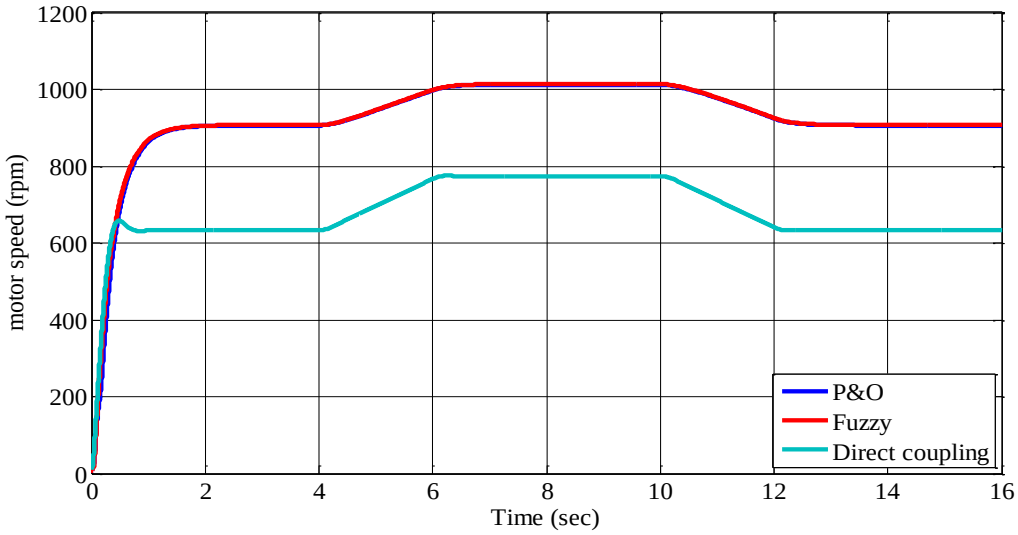

Figure (5.29) DC motor speed under changing temperature at 400 W/m^2

Figure (5.30) (a), (b) shows the sample of performance of MPPT of dc motor speed using fuzzy and P&O at 70,25 ^{o}C respectively

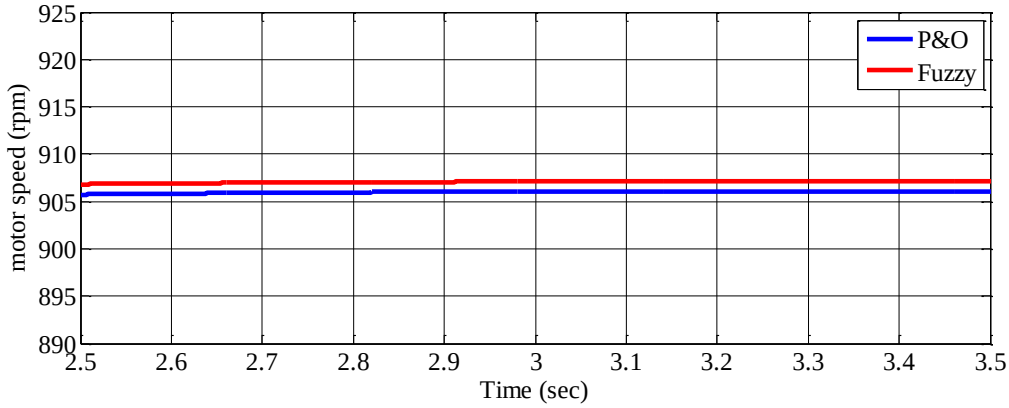

(a) at 70 ^{o}C

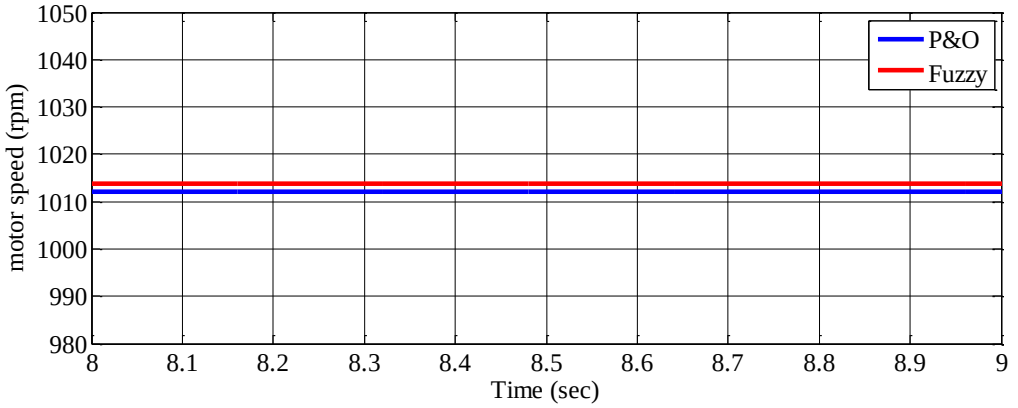

(b) at 25 ^{o}C

Figure (5.30) performance of MPPT of motor speed under fixed temperature at 400 W/m^2 for DC motor pump

CHAPTER (6)

CONCLUSION AND FUTURE SCOPE

CHAPTER (6)

CONCLUSION AND FUTURE SCOPE

6.1 Conclusion

This thesis presents a study of MPPT for PV systems and its different applications for different loads under varying irradiation and temperature conditions. The modeling of the PV module based on a simplified version of the single exponential model achieves good matching with data sheet information.

Simulation of the PV system with resistive load and DC motor pump has been implemented with MPPT vs. direct coupling system by MATLAB. The comparison shows that the PV system without MPPT has poor efficiency due to mismatching between the PV module and the load. On the other hand, it shows that the MPPT techniques increase in solar output power about 23% to 81% more than direct coupling.

The MPPT ensure impedance matching between the PV and the load for maximum power transfer by controlling the duty cycle of the DC-DC boost converter.

Different types of MPPT algorithms have been reviewed. Two MPPT algorithms are simulated to achieve maximum power transfer; P&O algorithm and Fuzzy algorithm. Fuzzy algorithm shows better performance in terms of efficiency compared to the P&O algorithm. It also shows smother power tracking; less oscillating and better stable operation. A further comparison has been made in terms of speed of motor shows that the system with fuzzy algorithm can pump more water than P&O algorithm. Even a small improvement of efficiency could bring substantial savings if the system is large.

After examining the PV system, it can be said that the proposed MPPT is a feasible method of maximizing the energy received from solar cells. In this thesis, the fuzzy logic control demonstrates good performance. Furthermore, fuzzy logic offers the advantage of faster design, and emulation of human control strategies. Also fuzzy control worked well for nonlinear systems and shows higher efficiency over the conventional controllers. The fuzzy logic control required complete knowledge of the operation of the system by the designer.

6.2 Future work

In this thesis, the MPPT has been carried out based on FLC and P&O methods for dc motor pump load. In future the MPPT study can be carried out for AC motor pump load. Also a good area of research is using optimization method to reduce the rules of the controller such as using Genetic Algorithm with fuzzy controllers. They can be used in the control algorithm to tune the membership functions so that the inexact reasoning characteristics of the FLC are sufficient to control a system that requires precise control actions.

PUBLICATION:

1- H.E.A.Ibrahim and Mahmoud Ibrahim, 2012. Comparison between fuzzy and P&O control for MPPT for photovoltaic system using boost converter. Journal of energy technologies and policy, 2 (6), 1-11.

2- H.E.A.Ibrahim and Mahmoud Ibrahim, 2013. MPPT using fuzzy controller for photovoltaic pumping system. IEEE international conference on control engineering and communication technology (ICCECT), 150-155.

Reference

[1] Chen-Chi Chu and Chieh-Li Chen, 2009. Robust maximum power point tracking method for photovoltaic cells: A sliding mode control approach. Elsevier solar energy, 83 (8), 1370-1378.
[2] M. Abdulkadir, A. S. Samosir, A. H. M. Yatim and S. T. Yusuf, 2013. A new approach of modeling simulating of MPPT for photovoltaic system in simulink model. ARPN journal of engineering and applied sciences, 8 (7), 488-494.
[3] Ali Nasr Allah Ali, Mohamed H. Saied, M. Z. Mostafa and T. M. Abdel- Moneim, 2012. A survey of maximum PPT Techniques of PV Systems. IEEE energy Tech, 1-17.
[4] A.Dolara, R.Faranda and S.Leva, 2009. Energy comparison of seven MPPT techniques for PV systems. Journal of electromagnetic analysis and applications, 1 (3), 152-162.
[5] Mohammed Ali Elgendy, Bashar Zahawi and David John Atkinson, 2010. Comparison of directly connected and constant voltage controlled photovoltaic pumping systems. IEEE transactions on sustainable energy, 1 (3), 184–192.
[6] Renewable Energy Policy Network For The 21st Century, Renewables 2012 Global Status Report.
[7] Volker Quaschning, 2005. Understanding renewable energy systems. UK and USA: Earthscan. ISBN: 1844071286.
[8] Gilbert M. Masters, 2004. Renewable and efficient electric power systems. Canada: John Wiley & Sons, Inc. ISBN: 0471280607.
[9] Paul A. Lynn, 2010. Electricity from sunlight: An introduction to photovoltaics. United Kingdom: John Wiley & Sons, Ltd. ISBN: 9780470745601.
[10] Deutsche Gesellschaft Fur Sonnenenergie, 2008. Planning and installing photovoltiac systems : a guide for installers, architects and engineers. UK and USA: Earthscan. ISBN: 9781844074426.
[11] Tarak Salmi, Mounir Bouzguenda, Adel Gastli and Ahmed Masmoudi, 2012. Matlab/Simulink based modelling of solar photovoltaic cell. International journal of renewable energy research, 2 (2), 213-218.
[12] Solar energy International, 2004. Photovoltaics: design and installation manual. Canada: Fourth Printing. ISBN: 0865715203.
[13] Dominique Bonkoungou1, Zacharie Koalaga and Donatien Njomo, 2013. Modelling and simulation of photovoltaic module considering single-diode equivalent circuit model in MATLAB. International journal of emerging technology and advanced engineering, 3 (3), 493-502.
[14] Trishan Esram and Patrick L. Chapman, 2007. Comparison of photovoltaic array maximum power point tracking techniques. IEEE Transactions on Energy Conversion, 22 (2), 439-449.
[15] J. Surya Kumari and Ch. Sai Babu, 2011. Comparison of maximum power point tracking algorithms for photovoltaic system. International journal of advances in engineering & technology, 1 (5), 133-148.
[16] J.Surya Kumari, Ch. Sai Babu and J. Yugandhar, 2011. Design and investigation of ahort circuit current based maximum power point tracking for photovoltaic system. International journal of research and reviews in electrical and computer engineering, 1 (2), 63-68.
[17] M.Lokanadham and K.Vijaya Bhaskar, 2012. Incremental conductance based maximum power point tracking (MPPT) for photovoltaic system. International journal of engineering research and applications (IJERA), 2 (2), 1420-1424.

[18] S.Gomathy, S.Saravanan and Dr. S. Thangavel, 2012. Design and implementation of maximum power point pracking (MPPT) algorithm for a standalone PV system. International journal of scientific & engineering research, 3 (3), 1-7.
[19] S. Karthik, P. Rathika and D. Devaraj, 2013. Fuzzy logic based maximum power point tracking designed for 10kW solar photovoltaic system. International journal of computer science and management research, 2 (2), 1421-1427.
[20] Chao Zhang and Dean Zhao, 2009. MPPT with asymmetric fuzzy control for photovoltaic system. Industrial electronics and applications ICIEA 4th IEEE Conference, 2180-2183.
[21] Pongsakor Takun, Somyot Kaitwanidvilai and Chaiyan Jettanasen, 2011. Maximum power point tracking using fuzzy logic control for photovoltaic systems. Proceeding of the international multiconference of engineering and computer scientists (IMECS), 2, 986-990.
[22] Yuen-Haw Chang and Chia-Yu Chang, 2010. A maximum power point tracking of PV system by scaling fuzzy control. Proceeding of the international multiconference of engineering and computer scientists (IMECS), 2, 1212-1216.
[23] A. Chouder, F. Guijoan and S. Silvestre, 2008. Simulation of fuzzy-based MPP tracker and performance comparison with perturb & observe method. Revue des energies renouvelables, 11 (4), 577-586.
[24] M. Masoum and M. Sarvi, 2005. A new fuzzy-based maximum power point tracker for photovoltaic applications. Iranian journal of electrical & electronic engineering, 1, 28-35.
[25] Ramos Hernanz, JA., Campayo Martín, J.J., Zamora Belver, I., Larrañaga Lesaka, J., Zulueta Guerrero, E. and Puelles Pérez, E., 2010. Modelling of photovoltaic module. Proceedings of the international conference on renewable energies and power quality, (ICRERPQ'10).
[26] Huan-Liang Tsai, Ci-Siang Tu, and Yi-Jie Su, 2008. Development of generalized photovoltaic model using MATLAB/SIMULINK. Proceedings of the world congress on engineering and computer science (WCECS), 846-851.
[27] Luis Castafier and Santiago Silvestre, 2002. Modelling photovoltaic systems using pSpice. England: John Wiley & Sons Ltd. ISBN: 0470845279.
[28] Antonio Luque and Steven Hegedus, 2003. Handbook of photovoltaic science and engineering. England: John Wiley & Sons Ltd. ISBN: 0471491969.
[29] M. R. AlRashidi, K. M. El-Naggar and M. F. AlHajri, 2013. Parameters estimation of double diode solar cell model. World academy of science, engineering and technology, 100-103.
[30] G.H. Yordanov, O.M. Midtgård and T.O. Saetre, 2010. Two diode model revisited: parameters extraction from semi-log plots of I-V data. 25th european photovoltaic solar energy conference and exhibition/5th world conference on photovoltaic energy conversion, 4156-4163.
[31] P. Rodrigues, J. R. Camacho and F. B. Matos, 2011. The application of trust region method to estimate the parameters of photovoltaic modules through the use of single and double exponential models**.** Proceedings of the international conference on renewable energies and power quality, (ICRERPQ'11).
[32] ADEL EL SHAHAT, 2010. PV cell module modeling & ANN simulation for smart grid application. Journal of theoretical & applied information technology, 16 (2), 9-20.
[33] M. G. Villalva, J. R. Gazoli and E. Ruppert F., 2009. Modeling and circuit-based simulation of photovoltaic arrays. Barzilian journal of power electronics, 14 (1), 35-45.

[34] Basil M. Hamed and Mohammed S. El-Moghany, 2012. Fuzzy controller design using FPGA for photovoltaic maximum power point tracking. International journal of advanced research in artificial intelligence (IJARAI), 1 (3), 14-21.
[35] KC200GT solar cell data sheet.
[36] Marcelo Gradella Villalva, Jonas Rafael Gazoli, and Ernesto Ruppert Filho, 2009. Comprehensive approach to modeling and simulation of photovoltaic arrays. IEEE transactions on power electronics, 24 (5), 1198-1208.
[37] Furkan Dinçer and Mehmet Emin Meral, 2010. Critical factors that affecting efficiency of solar cells. smart grid and renewable energy, 1 (1), 47-50.
[38] G. N. Tiwari and Swapnil Dubey, 2010. Fundamentals of Photovoltaic Modules and Their Applications. United Kingdom: The Royal Society of Chemistry. ISBN: 9781849730204.
[39] Mohammad A. S. Masoum, Hooman Dehbonei, and Ewald F. Fuchs, 2002. Theoretical and experimental analyses of photovoltaic systems with voltage and current based maximum power-point tracking. IEEE transactions on energy conversion, 17 (4), 514-522.
[40] J. Rizk, and Y. Chaiko, 2008. Solar tracking system: more efficient use of solar panels. World academy of science engineering and technology, 41, 313-315.
[41] Hossein Mousazadeh, Alireza Keyhani, Arzhang Javadi , Hossein Mobli, Karen Abrinia and Ahmad Sharifi, 2009. A review of principle and sun-tracking methods for maximizing solar systems output. Elsevier renewable and sustainable energy reviews, 13 (8), 1800-1818.
[42] M.S. Aït Cheikh, C. Larbes†, G.F. Tchoketch Kebir and A. Zerguerras, 2007. Maximum power point tracking using a fuzzy logic control scheme. Revue des Energies Renouvelables, 10 (3), 387-395.
[43] D. P. Hohm and M. E. Ropp, 2003. Comparative study of maximum power point tracking algorithms. Progress in photovoltaic: research and application, 11 (1), 47-62.
[44] Joe-Air Jiang, Tsong-Liang Huang, Ying-Tung Hsiao and Chia-Hong Chen, 2005. Maximum power tracking for photovoltaic power systems. Tamkang journal of science and engineering, 8 (2), 147-153.
[45] J.M. Enrique, E. Dura, M. Sidrach and J.M. Andu, 2007. Theoretical assessment of the maximum power point tracking efficiency of photovoltaic facilities with different converter topologies. Elsevier solar energy, 81 (1), 31-38.
[46] Muhammad. H. Rashid, 2004. Power Electronics Circuits Devices and Applications, New Jersey: Pearson Education, Inc, 3rd edition, ISBN 0131228153.
[47] Muhammad. H. Rashid, 2011. Power Electronics Handbook, United State of America: Elsevier Inc, 3rd edition, ISBN 978-0-12-382036-5.
[48] M. S. Widyan, A. I. Al Tarabsheh, Issa Y. Etier and Rolf E. Hanitsch,2010. Transient analysis and output characteristics of DC motors fed by photovoltaic systems. Jordan journal of mechanical and industrial engineering, 4 (1),193–204.
[49] Ahmed Hussein, Kotaro Hirasawa, Jinglu Hu and Junichi Murata, 2002. The dynamic performance of photovoltaic supplied DC motor fed from DC-DC converter and Controlled by neural networks. IJCNN '02. Proceedings of the 2002 International joint IEEE Conference on, 1, 607-612.
[50] N. Chandrasekaran1, B. Ganeshprabu and K. Thyagarajah, 2012. MATLAB based comparative study of photovoltaic fed DC motor and PMDC motor pumping system. ARPN journal of engineering and applied Sciences, 7 (5), 543-547.

[51] Ahmed Hussein, Kotaro Hirasawa and Jinglu Hu, 2003. Online identification and control of a PV supplied DC motor using universal learning networks. European symposium on artificial neural networks, 173-178.
[52] Timothy J. Ross, 2004. Fuzzy logic with engineering application, England: John Wiley & Sons Ltd, 2nd Edition, ISBN 047086074.
[53] Chennakesava R. Alavala, 2008. Fuzzy logic and neural networks basic concepts and applications, New Delhi: New Age International Pvt Ltd Publishers, ISBN 8122421822.
[54] S. N. Sivanandam, S. Sumathi and S. N. Deepa, 2007. Introduction to Fuzzy Logic using MATLAB, Berlin Heidelberg: Springer, ISBN 3540357807.
[55] Ahmad M. Ibrahim, 2004. Fuzzy Logic For Embbeded Systems Applications, USA: Elsevier Science, ISBN 075067699.
[56] Jan Jantzen, 2007. Foundations of Fuzzy Control, England: John Wiley & Sons Ltd., ISBN 0470029633.
[57] Mehmet Karakose and Erhan Akin, 2010. Block Based Fuzzy Controllers. International journal of research and reviews in applied sciences (IJRRAS), 3 (1), 100-110.
[58] C. Larbes, S.M. Ait Cheikh, T. Obeidi and A. Zerguerras, 2009. Genetic algorithms optimized fuzzy logic control for the maximum power point tracking in photovoltaic system, Elsevier Renewable Energy, 34, 2093‑2100
[59] Mayssa Farhat and Lassâad Sbita, 2011. Advanced Fuzzy MPPT Control Algorithm for Photovoltaic Systems, Science Academy Transactions on Renewable Energy Systems Engineering and Technology, 1 (1), 29-36.
[60] Aurobinda Panda, M.K.Pathak and S.P.Srivastava, 2011. Fuzzy Intelligent Controller for the Maximum Power Point Tracking of a Photovoltaic Module at Varying Atmospheric Conditions, Journal of Energy Technologies and Policy, 1 (2), 18-27.
[61] C. Liu, B. Wu and R. Cheung, 2004. Advanced Alogrithn For MPPT Control of Photovoltaic Systems, Canadian Solar Buildings Conference Montreal
[62] Mahmoud A. Younis, Tamer Khatib, Mushtaq Najeeb and A Mohd Ariffin, 2012. An Improved Maximum Power Point Tracking Controller for PV Systems Using Artificial Neural Network, PRZEGLĄD ELEKTROTECHNICZNY (Electrical Review), 116-121.

APPENDIX I

Boost Specifications

L=15 mH

C=2200 μF

R_{load}=30 ohm

f_s=5 kHZ

ΔD=0.0001

Machine Specifications:

V_{mo}=120 volt; I_{mo}=9.2 A.; w=1500 rpm; J=0.02365 Kg.m_2; R_a =1.5 Ω; L_a=0.2 H; K_3=0.67609 Nm.A^{-1}; motor friction A_3=0.2 Nm; A_1=0.3 Nm; B=0.002387 Nm.s.rad^{-1}; ∈=0.00059 Nm.s.rad^{-1}.

المستخلص:

تعتبر الطاقة الشمسية الكهروضوئي مصدر لتوليد الطاقة الجديدة والمتجددة. وللحصول على أكبر قدرة كهربية منها يتم تعقب نقطة التشغيل العظمي والتي عادة ما تتغير بتغير مستوى الإشعاع وتغير درجة الحرارة. وقد تم في هذه الرسالة توصيل الألواح الشمسية مباشرة إلى الحمل الكهربائي, وقد وجد ان الطاقه التي يتم استخدامها ليس هى الأمثل .وبالتالي، فإن تعقب القدره العظمى ضروري لتحقيق أقصى قدر من الكفاءة.

تقدم هذه الرسالة دراسة فى كيفية تعقب القدره العظمى للنظام الكهروضوئي. وتشمل الدراسة على مناقشة أنواع مختلف من الخوارزميات فى تعقب القدرة العظمى مع مقارنة بين اثنين منهما و هى أولاً خوارزميات منطق التحكم الغامض وثانياً الاضطراب والمراقبة تحت اختلاف مستويات الاشعاع ودرجة الحرارة. و قد تم استخدم نوعنين من الأحمال الكهربائية أحدهما يمثل بمقاومة بمحاكاة لمولد كهروضوئي مع محول تيار مستمر/ تيار مستمر وأخر نظام ضخ مياه باستخدام محرك ذو مغناطيس دائم مرتبط بمضخة طرد مركزي.

أثبتت النتائج تحسن أداء أنظمة تحكم للسيطرة على مسار تعقب نقاط القدرة العظمي. وباستعمال تقنية منطق التحكم الغامض تعمل بكفاءة عالية وأكبر من غيرها من الطرق السابقه.